Arctic Sea Level Reconstruction

Peter Limkilde Svendsen
PhD Thesis
April 2015

Abstract

Reconstruction of historical Arctic sea level is very difficult due to the limited coverage and quality of tide gauge and altimetry data in the area. This thesis addresses many of these issues, and discusses strategies to help achieve a stable and plausible reconstruction of Arctic sea level from 1950 to today.

The primary record of historical sea level, on the order of several decades to a few centuries, is tide gauges. Tide gauge records from around the world are collected in the Permanent Service for Mean Sea Level (PSMSL) database, and includes data along the Arctic coasts. A reasonable amount of data is available along the Norwegian and Russian coasts since 1950, and most published research on Arctic sea level extends cautiously from these areas. Very little tide gauge data is available elsewhere in the Arctic, and records of a length of several decades, as generally recommended for sea-level reconstruction, are completely absent outside the Norwegian and Russian sectors.

Since the early 1990s, altimetric satellite missions have provided more spatially complete observations of sea level. This allows extraction of the primary variation patterns, which can be used as calibration for a reconstruction method. For oceanographic purposes, the altimetric record over the Arctic Ocean is inferior in quality to that of moderate latitudes, but nonetheless an invaluable set of observations. During this project, newly processed Arctic altimetry from the ERS-1/-2 and Envisat missions has become available, allowing analysis in greater detail, though much early progress on the project was based on ocean model data.

Like other published sea level reconstructions, this project is based on the combination of tide gauge records and altimetry patterns. It is found that while it

is possible to reconstruct the timestep differences and cumulate these to obtain a reconstructed sea-level record, this approach may yield widely variable results and is difficult to stabilize due to the many gaps in the data. A more robust approach, as described by Ray and Douglas (2011), takes into account the entirety of each tide gauge record and makes the reconstruction much less prone to drifting away over time.

Unfortunately, many of the Russian-sector tide gauge records end around 1990, leaving a fairly sparse record after this. This project examines the effect of introducing a subset of the altimetric dataset as "virtual tide gauges" to remedy this sparsity, and appears to further stabilize the reconstruction. As Arctic sea level changes are particularly concentrated in the Beaufort Gyre area, this also introduces observations in an important area. However, this approach to some extent relies on relatively stationary conditions before the altimetric era, though previous research indicates largely stationary amounts of freshwater until the 1980s.

This project initially aimed to obtain a robust reconstruction through the use of alternative decompositions, rather than the commonly used empirical orthogonal functions (EOFs), for the calibration. While one alternative decomposition, maximum autocorrelation factors (MAFs), is investigated, it is found that preprocessing and handling of gaps (through appropriate method choice) in the tide gauge record is the primary concern for obtaining robust sea level reconstructions in the Arctic area.

The reconstructions obtained in this project concern the period 1950 to 2010 using monthly data. The spatial coverage is all ocean areas above 68°N, limited to the north depending on the calibration dataset used (90°N for Drakkar-calibrated reconstructions, 82°N for altimetry-based reconstructions).

Resumé

Rekonstruktion af historisk arkisk havniveau er meget vanskeligt på grund af den begrænsede dækning og kvalitet af data fra tidevandsstationer og altimetri i området. Denne afhandling omhandler mange af disse problemer, og diskuterer strategier til at opnå en stabil og plausibel rekonstruktion af arktisk havniveau fra 1950 til i dag.

Den primære kilde til data om historisk havniveau, i hvert fald i størrelsesordenen årtier til århundreder, er tidevandsstationer. Observationer fra tidevandsstationer verden over indsamles i databasen Permanent Service for Mean Sea Level (PSMSL), og inkluderer data langs de arktiske kyster. En rimelig mængde data er tilgængeligt langs de norske og russiske kyster fra ca. 1950 og frem, og de fleste publicerede resultater har hidtil holdt sig nær disse. Kun ganske lidt data fra tidevandsstationer andre steder er tilgængeligt, og tidsserier med en længde på flere årtier, sådan som det generelt anbefales til havniveaurekonstruktion, er slet ikke tilgængelige uden for de norske og russiske sektorer.

Siden begyndelsen af 1990'erne har altimetri-satellitmissioner givet observationer af havniveau med mere spatielt komplet dækning. Dette gør det muligt at udtrække de primære variationsmønstre, hvilket kan bruges som kalibrering for en rekonstruktionsmetode. Til oceanografiske formål er altimetridataene over det Arktiske Ocean ikke af så god kvalitet som på lavere breddegrader, men udgør ikke desto mindre en uvurderlig datakilde. I løbet af dette projekt er nyprocesseret arktisk altimetri blevet tilgængeligt, hvilket muliggør mere detaljerede analyser. Meget af det tidlige arbejde med projektet har dog været baseret på data fra havmodeller som substitut for altimetrien.

Ligesom andre publicerede havniveaurekonstruktioner er dette projekt baseret

på kombinationen af data fra tidevandsstationer og mønstre fra altimetri. Det viser sig, at selv om det er muligt at rekonstruere differenserne mellem hvert tidsskridt og kumulere disse for at få et rekonstrueret havniveaudatasæt, så kan denne metode give vidt forskellige resultater og er svær at stabilisere pga. de mange huller i dataene. En mere robust metode, beskrevet i Ray og Douglas (2011), tager højde for hele tidsrækken for hver tidevandsstation og er væsentligt mindre tilbøjelig til at drive væk vertikalt.

Desværre stopper mange optegnelser fra russiske tidevandsstationer omkring 1990, hvorefter antallet af tilgængelige tidevandsstationer er temmelig begrænset. I dette projekt undersøges virkningen af at introducere en del af altimetridatasættet som "virtuelle tidevandsstationer" for at imødegå denne mangel på data, og dette lader til at stabilisere rekonstruktionen yderligere. Dog er denne tilgang i et vist omfang afhængig af et relativt stationært havniveau før altimetriæraen, men tidligere resultater indikerer at mængderne af ferskvand i området har været nogenlunde stationære indtil 1980'erne.

Det var oprindeligt hensigten i dette projekt at opnå en robust rekonstruktion ved brug af alternative dekompositionsteknikker som erstatning for de almindeligt brugte empiriske ortogonale funktioner (EOF'er) til kalibreringen. Om end en alternativ dekomposition (maksimal-autokorrelationsfaktorer, MAF'er), er blevet undersøgt, så viser det sig at præprocessering og håndtering af huller i data (gennem omhyggeligt metodevalg) er den primære udfordring mht. at opnå robuste havniveaurekonstruktioner i det arktiske område.

Rekonstruktionerne i dette projekt dækker perioden 1950 til 2010 med månedlige data. Alle havområder nord for 68°N indgår (op til 90°N med Drakkar-kalibrering, og op til 82°N med altimetrikalibrering).

Preface

This thesis is submitted in fulfilment of the requirements for obtaining the PhD degree at DTU Space. The research was carried out at DTU Space, National Space Institute, Technical University of Denmark, under the supervision of Ole Baltazar Andersen and Allan Aasbjerg Nielsen.

I would like to thank my supervisors, Ole Baltazar Andersen and Allan Aasbjerg Nielsen, for their support and guidance throughout the project, as well as the rest of DTU Space for their friendly help and support.

A special thank you should go to John Church and Neil White of CSIRO Marine and Atmospheric Research, Hobart, Australia, for being kind hosts of my external research stay, and for providing invaluable suggestions and feedback to my project.

Last but not least, I want to thank my family and my girlfriend Marie for supporting me through the entire project.

List of publications

During the course of the project, twelve publications have been made in addition to the present thesis. The posters and articles are enclosed in appendix A.

- "Acceleration of the GrIS mass loss as observed by GRACE". Poster presented at EGU General Assembly, Vienna, Austria, 2012.

- "Sea level reconstruction from satellite altimetry and tide gauge data". Poster presented at EGU General Assembly, Vienna, Austria, 2012.

- "Sea level reconstruction: Exploration of methods for combining altimetry with other data to beyond the 20-year altimetric record". Poster/conference proceedings for 20 years of Progress in Radar Altimetry, Venice, Italy, 2012.

- "Exploring methods for combining altimetry with other data to extend the 20-year altimetric record onto a 50 year timescale". Poster presented at AGU Fall Meeting, San Francisco, United States, 2012.

- "Acceleration of the Greenland ice sheet mass loss as observed by GRACE: Confidence and sensitivity". Peer-reviewed journal article in *Earth and Planetary Science Letters*, 2013.

- "Confidence and sensitivity of sea-level reconstructions". Oral presentation/conference proceedings for CLIVAR WGOMD/SOP Workshop on Sea Level Rise, Ocean/Ice Shelf Interactions and Ice Sheets, Hobart, Australia, 2013.

- "Using leverages for objective analysis of PSMSL tide gauges in Arctic Ocean sea level reconstruction". Poster presented at PSMSL 80th Anniversary Workshop on Sea Level Science, Liverpool, United Kingdom, 2013.

- "Analysis of sea-level reconstruction techniques for the Arctic Ocean". Poster presented at AGU Fall Meeting, San Francisco, United States, 2013.

- "Influence analysis of Arctic tide gauges using leverages". Poster presented at EGU General Assembly, Vienna, Austria, 2014.

- "Arctic sea-level reconstruction analysis using recent satellite altimetry". Oral presentation given at EGU General Assembly, Vienna, Austria, 2014.

- "Analysis and robustness of Arctic sea level reconstructions". Poster presented at AGU Fall Meeting, San Francisco, United States, 2014.

- "Statistical selection of tide gauges for Arctic sea-level reconstruction". Peer-reviewed journal article in *Advances in Space Research*, 2015.

- "60-year Nordic and Arctic sea level reconstruction based on a reprocessed two-decade altimetric sea-level record and tide gauges". Poster presented at EGU General Assembly, Vienna, Austria, 2015.

Nomenclature

ADT   absolute dynamic topography

AMO   Atlantic Multidecadal Oscillation

AO   Arctic Oscillation

AR4   Fourth Assessment Report by IPCC

AR5   Fifth Assessment Report by IPCC

CMSL coastal mean sea level

DORIS Doppler Orbitography and Radiopositioning Integrated by Satellite

ENSO El Niño–Southern Oscillation

EOF   empirical orthogonal function

GIA   glacial isostatic adjustment

GMSL global mean sea level

GRACE Gravity Recovery And Climate Experiment

IB   inverse barometer

IBC   inverse barometer correction

IPCC   Intergovernmental Panel on Climate Change

LGM   Last Glacial Maximum

MAF   minimum/maximum autocorrelation factors

MDT   mean dynamic topography

MSL   mean sea level

MSS   mean sea surface

NAO   North Atlantic Oscillation

OcM   ocean mass

OI   optimal interpolation

PCA   principal component analysis

PDO   Pacific Decadal Oscillation

PGR   post-glacial rebound, see GIA

PSMSL   Permanent Service for Mean Sea Level

RLR   Revised Local Reference

RSL   relative sea level

RSOI   reduced-space optimal interpolation

SLP   sea-level pressure

SOI   Southern Oscillation Index

SSH   sea-surface height

SST   sea-surface temperature

SVD   singular value decomposition

TAR   Third Assessment Report by IPCC

Contents

CHAPTER 1

Introduction

1.1 Structure of the thesis

The present thesis represents an attempt to obtain the best possible reconstruction of Arctic sea level for the period 1950 to today. The project was initially planned to achieve this by adapting existing reconstruction methods with a variety of decompositions (EOF and MAF, possibly more) for the calibration data, and systematically comparing the results and uncertainties. However, it turned out that without careful method consideration, tide-gauge-based reconstructions of Arctic sea level are less robust than expected, producing highly implausible trends and precluding meaningful systematic comparisons.

It was found that careful handling of the spatial and temporal gaps in the tide gauge data was of greater importance in terms of stabilizing the reconstruction and obtaining results that are merely plausible. Thus, focus shifted towards procedures for rejecting inappropriate tide gauges, using empirical criteria and the statistical notion of leverage. The study of these inclusion/rejection criteria formed the basis for the article "Statistical selection of tide gauges for Arctic sea-level reconstruction", see appendix A.11.

Finally, further progress in stabilizing the reconstruction was made by introducing a datum-fit approach for the tide gauges rather than using cumulated

timestep differences, and additional robustness was achieved by introducing altimetry-based "virtual tide gauges".

Until an appropriate altimetry dataset became available, EOF (and MAF) patterns were obtained from ocean model data to avoid dealing with missing data in the initial experiments. The SODA was briefly tried and then dismissed due to its lack of MSL trend, and replaced by the Drakkar model for many analyses. The Drakkar data were found to have conspicuously high sea level trends, and the altimetry dataset appears more useful for validation of the reconstruction.

The reconstructions in this project cover areas north of 68°N, as the early experiments used ocean model data which might have assimilated altimetry data up to 66°N; it was desired to avoid any artifacts from such assimilation, and this latitude threshold has been retained for consistency.

The present thesis is divided into an introduction (Chapter 1), introducing the motivation for the project and some terminology, Chapter 2 describing the available data in the Arctic, Chapter 3 discusses the geophysical signals typically appearing in sea-level data, Chapter 4 describes theory behind sea-level reconstructions, Chapter 5 presents the results of different reconstruction approaches in the Arctic, and overall conclusions are given in Chapter 6. The structure of the results chapter reflects the development in methodology in the project, with relatively thorough analyses made using Drakkar ocean model data and cumulated timestep differences, done before the introduction of altimetry data and the datum-fit approach.

The journal article "Acceleration of the Greenland ice sheet mass loss as observed by GRACE: Confidence and sensitivity" (appendix A.5), published in February 2013, has limited subject connection with the present PhD project; it is a continuation of my previous master thesis work, but written entirely within the PhD period, and thus included here.

1.2   Context

As an indicator of a changing climate system, sea level change has received considerable attention in recent decades. The development in global mean sea level over the last century is now relatively well-described (see e.g. Church et al. (2013)), and since the early 1990s, near-global images of sea level have been continually obtained using satellite altimetry.

Prior to the altimetry era, however, consistent and repeated observations of sea

level are available only from tide gauges. Reconstructions of historical sea level for the last decades to century thus rely on tide gauges, possibly in conjunction with variability patterns from altimetry.

While there is both tide gauge and altimetry data available for the Arctic Ocean, the quality of either is generally inferior to that of more moderate latitudes, with both spatial and temporal coverage often being patchy. The primary purpose of this project has been, through understanding of existing sea-level reconstruction methods, to adapt these methods to work well in the Arctic area.

1.3   Sea level reconstructions

The basic approach used in many sea-level reconstruction studies (such as Berge-Nguyen et al. (2008); Calafat et al. (2014); Church and White (2011); Hamlington et al. (2011); Jevrejeva et al. (2014); Llovel et al. (2009); Meyssignac et al. (2012)) originates in that of Church et al. (2004). The paper describes an approach in which a set of spatial patterns are determined by the leading empirical orthogonal functions (EOFs) of satellite altimetry, and thus constitute the empirical patterns that maximize the explained variance of the altimetry data. The altimetry dataset thus constitutes a calibration part of the method, and the resulting patterns are then fitted to a historical tide gauge record. For each timestep in the reconstruction period, a linear combination of these patterns is determined in the way that is most consistent with the available tide gauge data, subject to regularization. Thus, a spatially complete sea level reconstruction is obtained.

In the approach of Church et al. (2004), it is assumed that while the EOF patterns account for the variability of sea level, an overall trend (and/or changes in global mean sea level) are present and should be captured using a spatially uniform pattern. As described in a comparative study by Christiansen et al. (2010), the inclusion of a spatially uniform pattern ("EOF0" in the terminology of Church et al.) is crucial to an accurate reconstruction of GMSL.

In Church et al. (2004), the problem of unknown vertical datums for each tide gauge is addressed by considering sea level *changes* between each timestep and cumulating these to obtain the complete reconstruction. This is reasonable when the tide gauge records used are long and free of gaps, but the situation is more precarious in the Arctic. As noted in Ray and Douglas (2011), errors may accumulate over time using this approach, as nothing forces the reconstructed sea level back towards reality. Instead, they suggest an approach that considers the entire time series for each gauge and solves for the gauge datums as part of

the solution. This thesis discusses the approach of Ray and Douglas (2011) as a viable option for Arctic sea level reconstruction.

1.4   Sea-surface terminology

In a context of high-precision geodesy, it is necessary to be very specific regarding choice of reference systems and terminology. Statements like "sea level is rising" are not very meaningful without specifying relative to what.

The shape of the Earth is approximated in a geometrically convenient way by the *reference ellipsoid*. This is simply a best-fit ellipsoid shape. A more refined approximation is the *geoid*, an equipotential surface where the gravitational potential is constant. On Earth, the geoid height (relative to the ellipsoid) varies between approximately ± 100 m, see Fig. 1.1. The geoid does not quite coincide with the actual mean sea surface, due to — among other things — variations in sea water density.

The difference in height between the geoid and the sea surface is called the *dynamic topography*. The position of the mean sea surface is then given by the *mean dynamic topography*, when added to the geoid. Due to different water densities (primarily caused by the different mean temperatures across the globe), the MDT is between approximately ± 1.6 m. The exact MDT must always be specified along with the time interval it covers, as it is affected by climate variability; so is the geoid, but to a much smaller extent. See Fig. 1.2 for an illustration of these terms.

For this project, we will attempt to reconstruct dynamic topography anomalies relative to an arbitrary MDT, as the focus has been on studying trends obtained with various methods. Establishing an absolute vertical reference for the reconstruction has not been prioritized, but the reconstruction may be fitted to a given MDT as a post-processing step (by minimizing each pixel's misfit over the MDT's time interval). Alternatively, if if using the datum-fit approach of Ray and Douglas (2011) and "virtual tide gauges" from extracts of altimetry datasets, these altimetry time series may be set as absolutely vertically referenced while the vertical datums of the actual tide gauges can be considered unknown and treated as such. A detailed discussion on Arctic mean dynamic topography/mean sea surface is given in Andersen and Knudsen (2009).
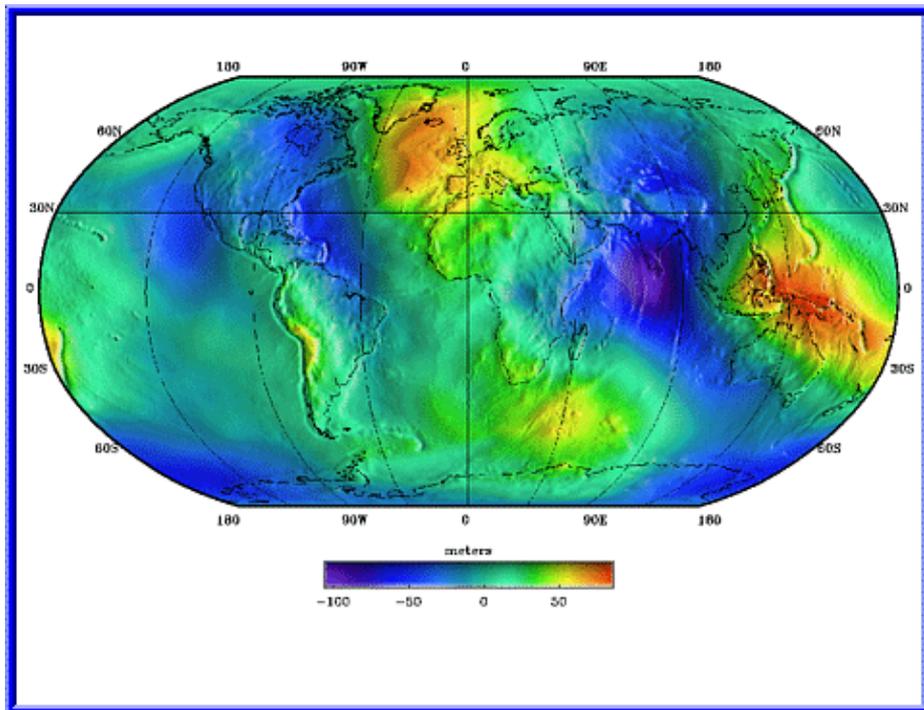
Figure 1.1: Geoid heights (in the EGM96 model) around the Earth. Image credit: J. Frawley, NASA GSFC
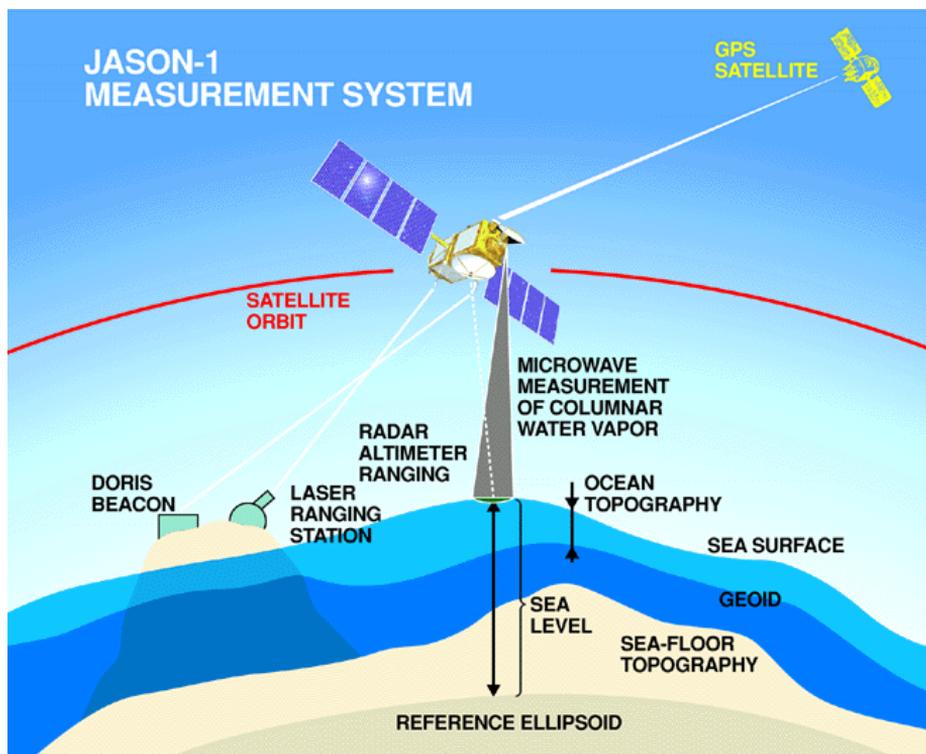
Figure 1.2: Relevant surfaces in the context of sea level, and infrastructure for altimetric measurements. Image credit: NASA/JPL

1.5   Global sea level changes

Using altimetry, the global mean sea level trend from 1993 to 2010 is well-established at $3.2 \pm 0.4 \, \mathrm{mm/yr}$ (Church et al., 2013). Church and White (2011) found a trend of $1.7 \pm 0.2 \, \mathrm{mm/yr}$ for the period 1900–2009, and a statistically significant acceleration of $0.009 \pm 0.004 \, \mathrm{mm/yr^2}$ in sea level since 1900. The global mean rate of rise since 1950 has been estimateed at $1.8 \pm 0.3 \, \mathrm{mm/yr}$ (Church et al., 2004; Nerem et al., 2006).

The possibility of 60-year oscillations in global mean sea level has been studied in Chambers et al. (2002) and Chambers et al. (2012); they found that while such an oscillation appears to be present in most of the world's oceans, the tide gauge data was too limited to conclusively prove the existence of such and oscillation.

1.6   Arctic Ocean characteristics

The Arctic Ocean, surrounding and including the North Pole, is a Mediterranean sea (see e.g. Tomczak and Godfrey (2005)). That is, it has limited water exchange with the large oceans of the world; the only major connection with a large ocean is the Fram Strait between Greenland and Svalbard, connecting it to the North Atlantic Ocean. This isolation causes the currents of the Arctic Ocean to be driven mostly by thermohaline forcing, rather than wind, which is the primary driver of currents in major ocean basins.

However, it is found in Volkov and Landerer (2013); Volkov (2014) that non-seasonal variations in Arctic Ocean mass (OcM) is mostly explained by wind forcing. Note that those studies are based on observations of mass (rather than sea level) as obtained from the Gravity Recovery And Climate Experiment (GRACE) satellites. Interestingly for sea level studies, Volkov (2014) find a strong correlation between mass observations (from GRACE) and altimetry.

For reference, a labelled map of the Arctic Ocean is provided in Fig. 1.3. A bathymetric map (showing ocean depths) is provided in Fig. 1.4; it is seen that the shelf is generally wide (several hundred kilometres), in particular in the Russian sector.

Figure 1.3: Labelled topographic map of the Arctic. Image credit: United States Naval Research Laboratory, Marine Meteorology Division.
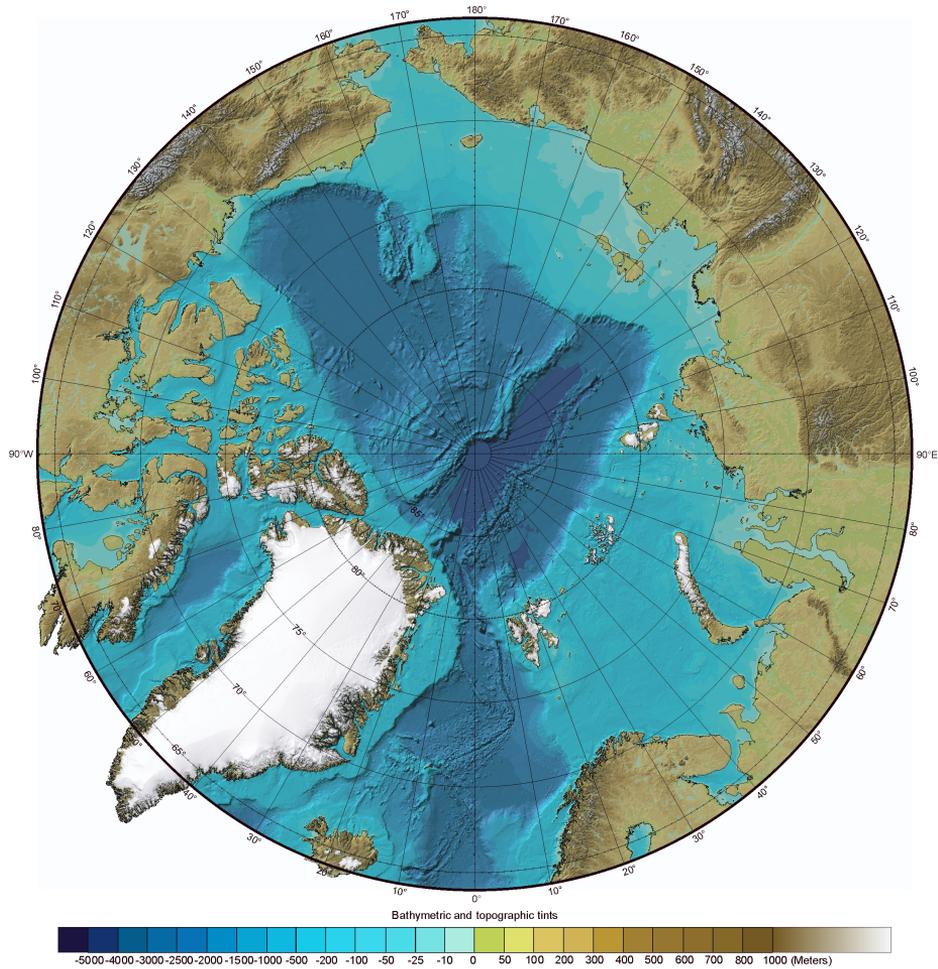
Figure 1.4: Bathymetric map of the Arctic. Image credit: United States Naval Research Laboratory, Marine Meteorology Division.

1.6.1 Currents

The two major current patterns of the Arctic Ocean are the Beaufort Gyre and the Transpolar Drift. The Beaufort Gyre is a wind-driven circulation in the western part of the Arctic Ocean. Several studies have revealed an increasing accumulation of freshwater in the area; Giles et al. (2012) found, using satellite altimetry, a trend of up to +2 cm/yr in the area for the period 1995–2010.

As established in Proshutinsky et al. (2002), the Beaufort Gyre accumulates freshwater during anticyclonic regimes and releases it during cyclonic regimes. The gyre thus acts as a "flywheel" for wind energy in the Arctic.

1.6.2 Sea level variability and trends

Pavlov (2001) found an increasing trend in sea level variability for the Russian sector between 1950 and 1990. Modelling results in that study, in the form of decadal means, show an increase in coastal sea level of about 5 cm between the Taymyr Peninsula and the Bering Strait from the 1970s to the 1980s, while a deepening of approx. 10–15 cm is obtained north of the Laptev sea for the same period.

1.6.3 Norwegian sector

The Norwegian-sector coastal mean sea level exhibits a slight downward trend from 1950 until 1975–1980, after which an upward trend is seen (Henry et al., 2012).

Focusing on future projections, Simpson et al. (2012) note that there are currently few detailed studies of the Norwegian tide gauge records. They estimate sea-level rates, both relative and GIA-corrected, for 18 tide gauges along the Norwegian coast. For the period 1980–2010, the GIA-corrected sea level rates lie between +2.6 mm/yr and +4.4 mm/yr except one outlier (Kabelvåg, at +1.4 mm/yr).

1.6.4 Russian sector

The sea level of the Russian sector of recent decades, based on tide gauge data, has been extensively described in the work of Andrey Proshutinsky (see e.g.

Proshutinsky et al. (2001, 2004)). In Proshutinsky et al. (2004), it is estimated that Russian-sector sea level rose by 1.85 mm/yr for the period 1954-1989 (after GIA correction; 1.23 mm/yr before GIA correction). The study attributes the rise to steric effects (35%), barometric contribution (30%), wind action (10%), and changing ocean mass (approx. 25%).

According to Proshutinsky et al. (2007), observations show that for the Kara, Laptev and East Siberian seas, sea level rose by 2.50 mm/yr for the period 1954–2006. The sea level is noted to correlate well with the Arctic Oscillation (AO) until 2000; however, the AO is at a stable low for the period 2000–2006, corresponding to a high Arctic pressure (and thus low sea level); even so, sea level rose in that period.

1.6.5   Canadian sector

Very limited tide gauge data from Arctic coasts are available in the Canadian sector. Plag (2000) noted that Canada has shut down all its Arctic tide gauges except Churchill (which is located in the Hudson Bay). Altimetry data indicate a sea level rise of approx. 2 cm/yr in the Beaufort Gyre area for the period 1995–2010 (Giles et al., 2012), by far the dominant feature in sea level change for that period, correlating with a change of wind curl.

1.6.6   Previous reconstructions of Arctic sea level

In a study of the Norwegian and Russian sectors, Henry et al. (2012) found mean sea level to be largely stable until 1980, after which an increasing trend appears, with a rate of approx. 4 mm/yr after 1995. Their study also attempted to include as much data as possible around the entire Arctic, using 62 tide gauge records in Norway and Russia.

The trend in the MONARCH-A reconstruction by Henry et al. (for the period 1958–2006, covering the Norwegian and Russian sectors) is dominated by rise in the area south of the Denmark Strait, around the Taymyr peninsula and in the East Siberian Sea, see Fig. 1.6. The mean sea level as reconstructed in MONARCH-A is shown in Fig. 1.5. The trends for various timespans are listed in Table 1.1; it is clear that there is an acceleration in sea level rise for the entire period, beginning around 1980. While the trend from 1993 onwards may seem extreme, it should be noted that the sea level seems to be in a "low" phase in 1993.

The MONARCH-A reconstruction is based on Drakkar data, and the western Arctic Ocean has been omitted due to difficulties in getting plausible results there (Benoit Meyssignac, personal communication).

Period	Trend (mm/yr)
1958–2006 (entire period)	1.82 ± 0.49
1958–1980	-0.56 ± 1.36
1980–2006	2.43 ± 1.25
1993–2006	6.26 ± 2.76

Table 1.1: Trends for various time periods of the MONARCH-A dataset above 68°N.
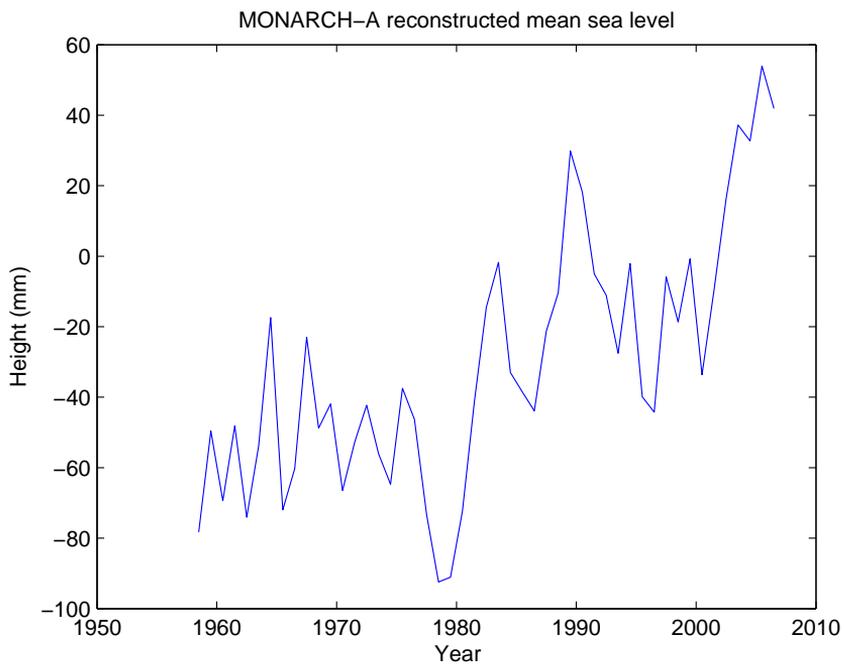
Figure 1.5: Mean sea level in the MONARCH-A reconstruction for the period 1958–2006, 40°W to 180°E, 68°N to 82°N.
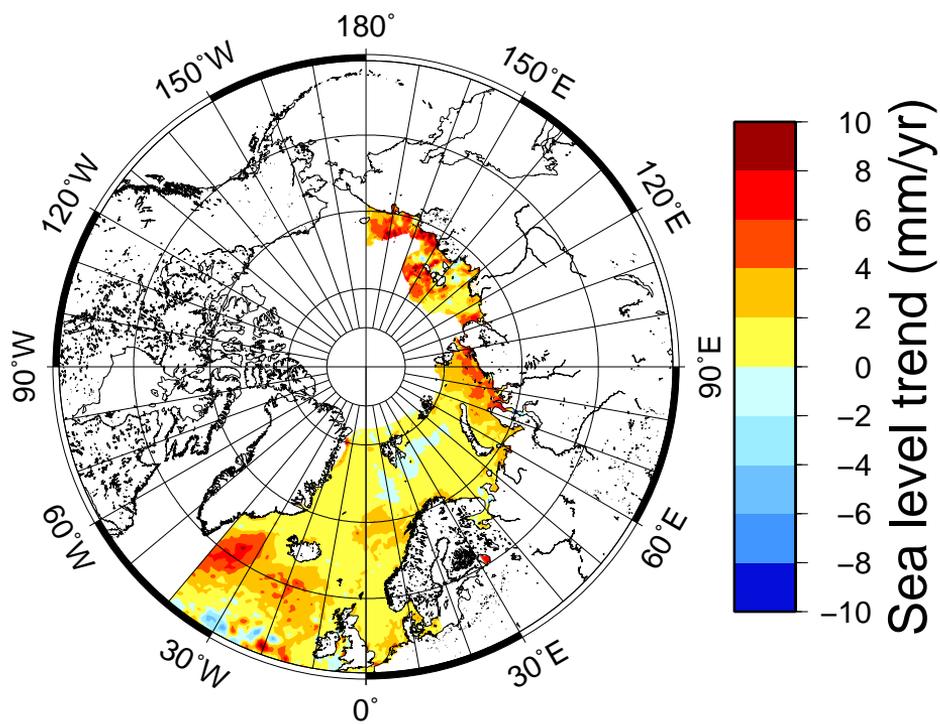
Figure 1.6: Trends in the MONARCH-A reconstruction for the period 1958–
2006.

Data sources

2.1 Tide gauges

The Permanent Service for Mean Sea Level (PSMSL) maintains a database (Holgate et al., 2013; Woodworth and Player, 2003) of tide gauge records from coastlines around the world. It represents a major effort in collecting and validating tide gauge data as far as possible.

PSMSL height records are available as "RLR" (Revised Local Reference) and "Metric" records. The metric records, which PSMSL warns should only be used "with extreme caution", contain "raw" measurements without datum adjustment. The RLR data contains measurements adjusted to have mean sea level at $+7\,\mathrm{m}$, with sudden datum shifts removed in the individual time series. Some gauges are "metric-only" (i.e. unavailable in RLR), due to lack of knowledge of their historical datum.

All PSMSL tide gauges (RLR or metric) around the Arctic Ocean are plotted in Fig. 2.1. The RLR data above 68°N, used to control the reconstruction, is illustrated in Fig. 2.2 (after inverse barometric correction).

An overview of the availability of tide gauge records around the Arctic is given in Plag (2000). Henry et al. (2012) noted that they had sought out alternatives
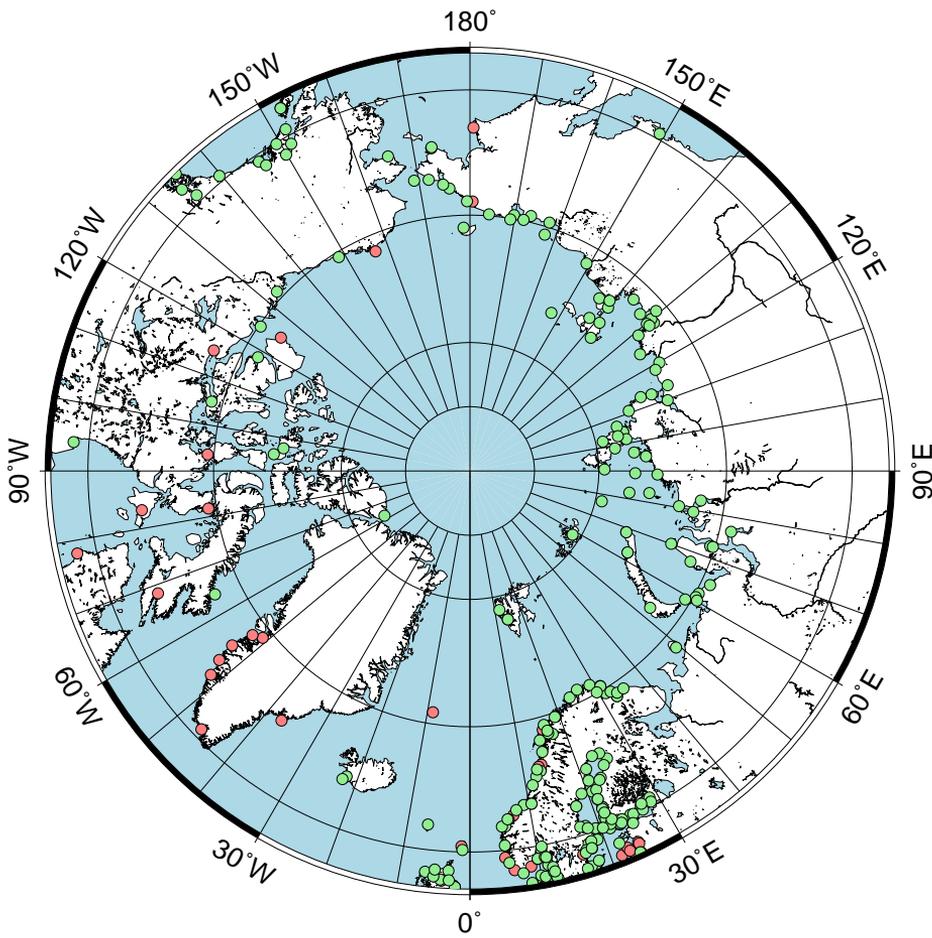
Figure 2.1: PSMSL tide gauges with data in RLR dataset (green) and metric-
only (red).
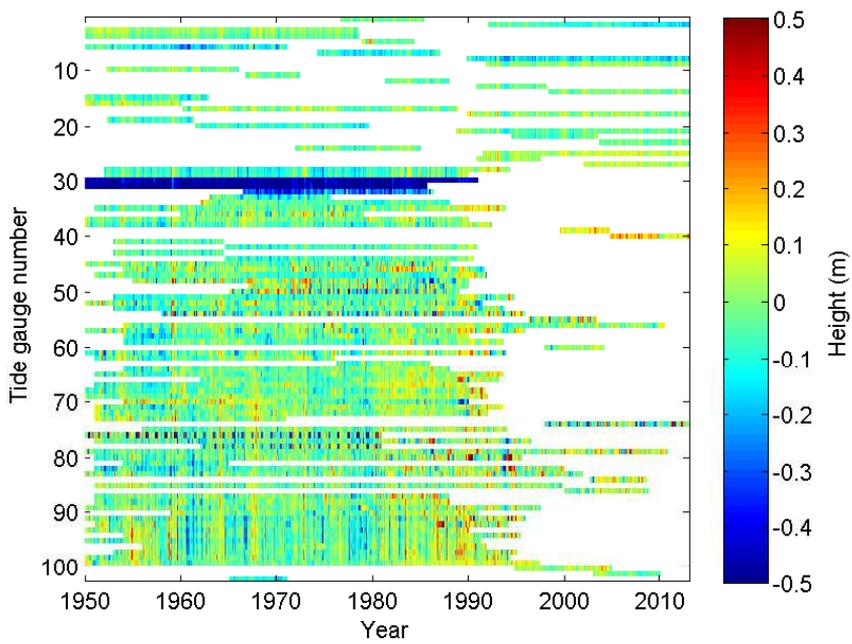
Figure 2.2: Available data from RLR gauges above 68°N, as used in recon-
struction (inverse barometric correction applied).
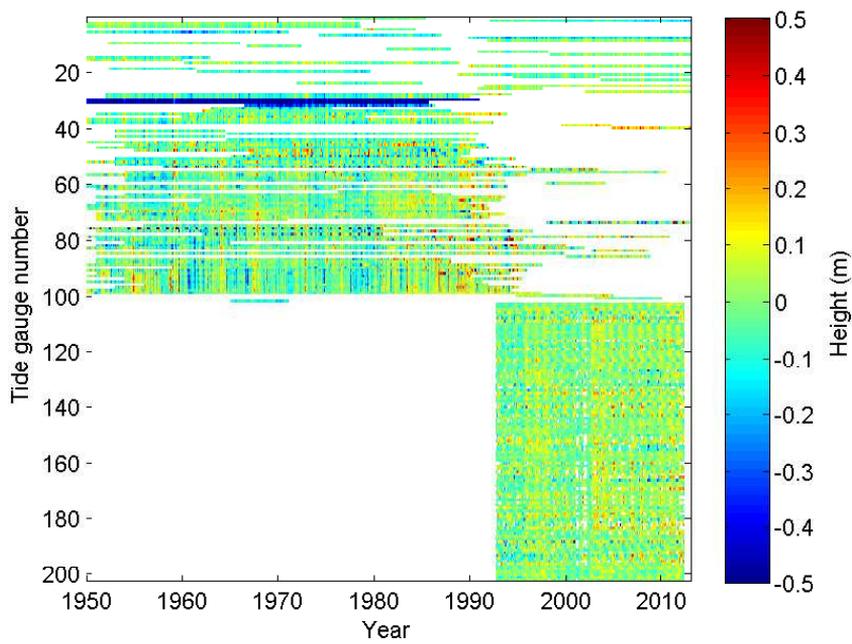
Figure 2.3: The Arctic RLR data as in Fig. 2.2, supplemented with 100 virtual tide gauges.

to the PSMSL data for the Canadian sectors, specifically data from Fisheries and Oceans Canada (DFO), but that they could not find data usable for their study.

2.1.1 Arctic Ocean

The tide gauge records around the Arctic Ocean roughly exhibit three eras: pre-1950, which has little data, 1950–1990 with good coverage of the Russian sector, and post-1990 where, following the collapse of the Soviet Union, many Russian records are discontinued. Only the Norwegian coast is quite consistently covered over the last approx. 60 years; the coastlines of Arctic gauges with data are plotted in Fig. 2.4. It is clear that between 1950 and 1990, the dataset is dominated by Russian gauges, while very little data is available at any time from outside Norway and Russia. Unfortunately, the demise of Russian records occurs just before the beginning of the altimetry era, precluding some opportunities for calibration.

In their tide gauge-based study of Arctic sea level, Henry et al. (2012) identified 62 usable tide gauges around the Arctic Ocean for the period 1950–2009. With the exception of one gauge in Iceland, one in the Faroe Islands, and one in the Shetland Islands, all of these gauges are located in the Norwegian and Russian sectors. That is, there are *zero* gauges in the Canadian sector and Greenland in the study, which unfortunately reflects the amount and/or quality of data available.

In addition to the common removal of best-fit whole- and half-year cycle, Henry et al. (2012) also apply a 12-month running mean smoothing to the tide gauge records, as the seasonal variation is not necessarily sinusoidal.

Determination of Russian-sector pre-altimetry sea level rise was examined in detail in Proshutinsky et al. (2004). For the period 1954–1989, which offers many uninterrupted tide gauge records there, they obtained a trend of 1.23 mm/yr, or 1.85 mm/yr after GIA correction, which is consistent with the global average trend, though larger than the 1.37 mm/yr from simulations made in the same study. They note a substantial difference between the ICE-4G(VM2) and ICE-5G(VM2) GIA models, as the former has been shown to have a poor estimate of glaciation history east of Novaya Zemlya.

In a study comparing 14 different GIA models for the Arctic area, Huang et al. (2013) obtained an overall GIA contribution for the tide gauges ranging from -0.26 to $0.81 \, \text{mm/yr}$.

A substantial problem with many of the Arctic gauges is their location in rivers, rather than facing the open ocean. Among the rivers contributing freshwater to the Arctic Ocean, 8 of the 9 largest are located in the Russian sector (Aagaard and Carmack, 1989). Particularly large runoffs result from the three great Siberian rivers — Yenisei, Ob, and Lena (603, 530 and 520 km^3/yr, respectively), and from the Canadian-sector Mackenzie River (340 km^3/yr).
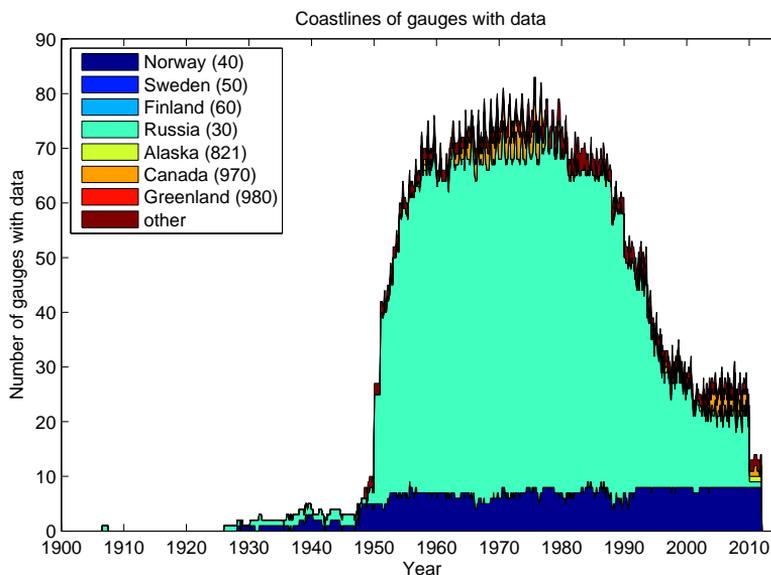
Figure 2.4: Coastlines of (metric) PSMSL gauges above 68°N that have data available, as a function of time. Numbers in parentheses are the PSMSL coastline number.

2.1.2 "Virtual tide gauges"

Due to the significant drop in number of available tide gauges after 1990, this project has investigated the effects of supplementing the tide gauge dataset with a number of altimetry time series, herein referred to as "virtual tide gauges", to stabilize the reconstruction.

These virtual tide gauges inherently cover the altimetry era. To retain coherence with the actual tide gauge data, the number of virtual tide gauge data has been chosen at an order of magnitude similar to the number of true tide gauges; experiments with 50, 100 and 200 virtual gauges have been made. The data

available including 100 virtual gauges is illustrated in Fig. 2.3.

The virtual tide gauge records are simply the altimetry time series at random locations within the reconstructed area (between 68°N and 82°N, within the ocean mask). While it may have theoretical interest to place the virtual gauges at the locations of the discontinued "true" gauges, it should be noted that much of the variability of the Arctic Ocean is concentrated in areas far from the coasts, and sea level within e.g. the Beaufort Gyre should thus be better captured.

2.2   Satellite altimetry

Since the early 1990s, radar altimetry from satellites has provided continual, detailed views of sea level around most of the world's oceans. TOPEX/Poseidon, launched in 1992, was the first satellite mission to provide detailed ocean topography measurements. Jason-1 (launched 2001) and Jason-2 (launched 2008) have yielded continuation of these measurements, being positioned in similar orbits. A further follow-on, Jason-3, is scheduled for launch in 2015.

The orbits of TOPEX/Poseidon and Jason-1/-2 have been carefully chosen for oceanographic measurements. The orbital inclination is $66°$, and with a nadir-pointing altimeter, this provides data coverage between $66°$ N and $66°$ S. The repeat cycle is 10 days, meaning that the satellite passes over a given point on the Earth once every 10 days. This period was chosen so that signals from different tidal constituents will alias to distinct frequencies, allowing near-global maps of tidal variation.

An overview of oceanographic altimetry missions is shown in Table 2.1.

Name	Launch	Retired
TOPEX/Poseidon	1992	2006
Jason-1	2001	2013
OSTM/Jason-2	2008	–

Table 2.1: Oceanographic altimetry missions.

Name	Launch	Retired
ERS-1	1991	2000
ERS-2	1995	2011
Envisat	2002	2012
CryoSat-2	2010	–
HY-2	2011	–
Saral	2013	–

Table 2.2: High-latitude altimetry missions.

2.2.1   High-latitude data

While TOPEX/Poseidon and the Jason missions do not cover latitudes higher than $66°$, the European Remote Sensing satellites (ERS-1 and -2) and Envisat missions had orbital inclinations of $98.5°$.

CryoSat-2, launched in 2010, has an orbit inclination of 92°, giving coverage up to 88° latitude. (The first CryoSat satellite was lost in a launch failure in 2005, and CryoSat-2 quickly built as an identical replacement.)

An overview of high-latitude altimetry missions to date is shown in Table 2.2. For the present project (where altimetry, and not ocean model data, is used) a compound dataset of ERS-1, -2 and Envisat data is used, see Cheng et al. (2015). This compound dataset has been resampled to monthly temporal samples.

The dataset has trends in good agreement with Giles et al. (2012); see Fig. 2.5 for a map of the trends for 1995–2010.
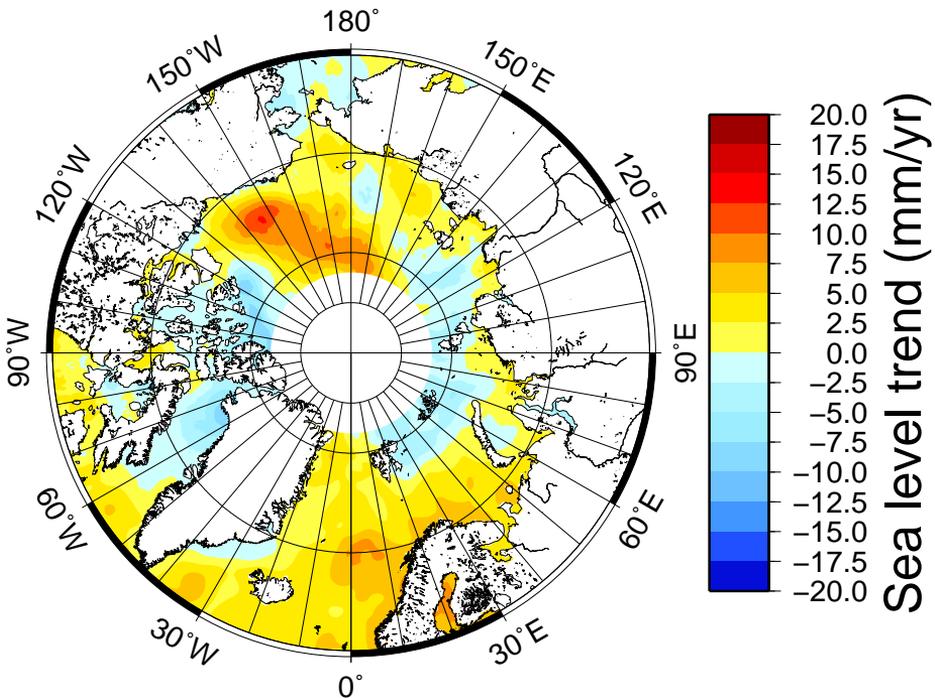
Figure 2.5: Trends in altimetry data for the period 1995–2010.

2.2.2 Data processing levels

To date, satellite altimetry measurements are made with a nadir-pointing radar. This provides point observations along the ground tracks traced out by the satellite's orbit.

For sea-level reconstruction and many other geophysical purposes, it is often more convenient to work with regular grids of observations rather than along-track points. This resampling, along with various other processing of data products, is systematically categorized into "levels", as listed in Table 2.3.

Data level	Description
Level 0	Reconstructed, unprocessed instrument and payload data at full resolution, with any and all communications artifacts (e.g., synchronization frames, communications headers, duplicate data) removed. (In most cases, the EOS Data and Operations System (EDOS) provides these data to the data centers as production data sets for processing by the Science Data Processing Segment (SDPS) or by a SIPS to produce higher-level products.)
Level 1A	Reconstructed, unprocessed instrument data at full resolution, time-referenced, and annotated with ancillary information, including radiometric and geometric calibration coefficients and georeferencing parameters (e.g., platform ephemeris) computed and appended but not applied to Level 0 data.
Level 1B	Level 1A data that have been processed to sensor units (not all instruments have Level 1B source data).
Level 2	Derived geophysical variables at the same resolution and location as Level 1 source data.
Level 3	Variables mapped on uniform space-time grid scales, usually with some completeness and consistency.
Level 4	Model output or results from analyses of lower-level data (e.g., variables derived from multiple measurements).

Table 2.3: Satellite data processing levels. From NASA's Earth Science Division,
`http://science.nasa.gov/earth-science/earth-science-data/`
`data-processing-levels-for-eosdis-data-products/`

2.3 Floats

The Argo project has deployed more than 3,000 automated floats across the world's oceans, regularly measuring temperature and salinity down to a depth of 2 kilometres, automatically diving down once every 10 days. The project seems promising in terms of constraining the steric contributions to sea level, though the timespan covered (since approximately 2007) is deemed too short for this project.

2.4 Ocean models

While ocean models do not constitute true observations, they can be useful in experimental reconstructions or in assessing the plausibility of results. On the other hand, such models attempt to obtain a coherent and physically plausible picture of the state of the ocean.

2.4.1 SODA

The SODA ("Simple Ocean Data Assimilation") model (Carton et al., 2000, 2005; Carton and Giese, 2008) incorporates, as its name indicates, as many oceanic observations as possible. It is provided as monthly $0.5° \times 0.5°$ grids, spanning 1871 to today.

For early experiments in this project, the SODA ocean model (v. 2.2.4) has studied. There appears to be negligible overall trend in this model, however (see Fig. 2.6); it seems to be focused on variability, capturing changes in various modes. The largest trend in the Arctic area occurs around the Beaufort Gyre and in the East Siberian Sea, these being the only areas of more than $2\,\mathrm{mm/yr}$ rise. This is below the global mean trend, and seems implausibly low for the Arctic.
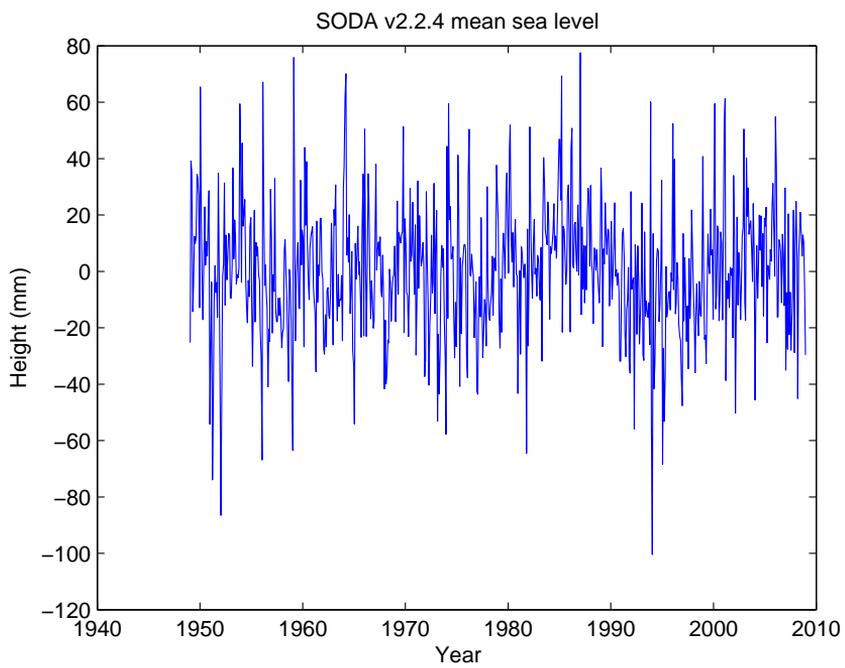
Figure 2.6: Mean sea level from the SODA ocean model (above 68°N).
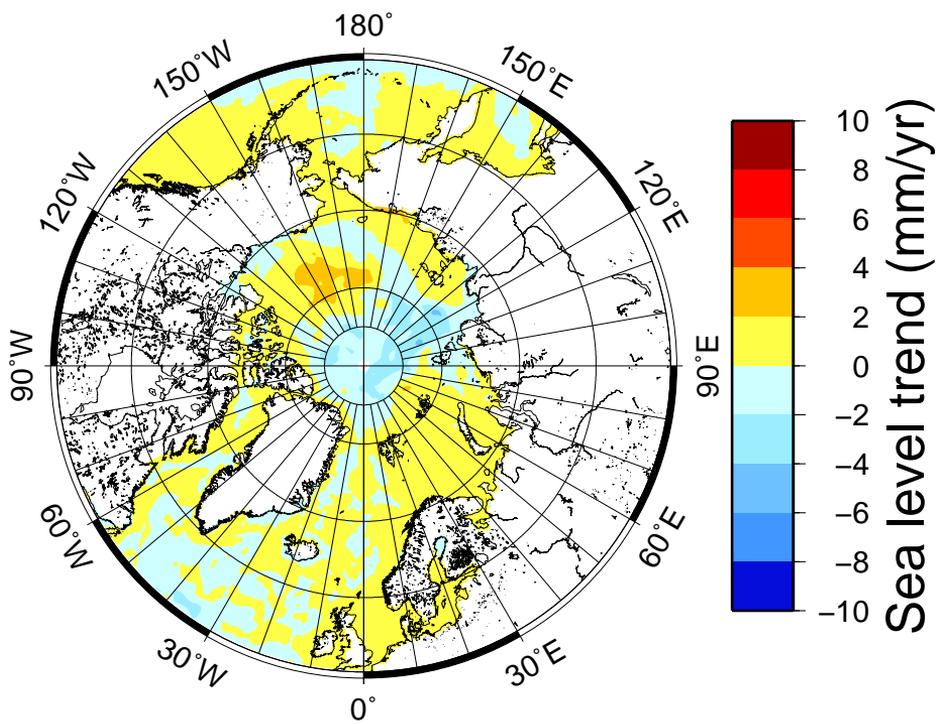
Figure 2.7: Trends in the SODA ocean model for the period 1949–2008.

2.4.2 Drakkar

The Drakkar project (Barnier et al., 2006) provides the ORCA025 and ORCA12 global ocean simulations.

The Drakkar data exhibit a very high sea-level trend, more than 6 mm/yr since 1950 (see Table 2.4 for details). This is considerably higher than the results from e.g. Henry et al. (2012), and also inconsistent with our reconstruction, even when using the Drakkar fields for calibration. A map of the local trends for 1995–2010 is shown in Fig. 2.8. It is readily seen that these trends are much higher than for altimetry observations (see Fig. 2.5 or Giles et al. (2012)).

Period	Trend (mm/yr)
1958–2006 (entire period)	6.57 ± 0.18
1958–1980	6.68 ± 0.49
1980–2006	7.77 ± 0.46
1993–2006	12.16 ± 1.15

Table 2.4: Trends for various time periods of the deseasonalized Drakkar dataset above 68°N.

The Drakkar model was the data source of choice for calibration (EOFs/MAFs) until fairly late in this project. The very high trends in the Drakkar data caused great difficulty in validating the reconstruction, as the trends do not agree well with neither tide gauge nor altimetry studies. The high trend in Drakkar may be due to E-P imbalance related to a change in forcing (Bernard Barnier, personal communication).
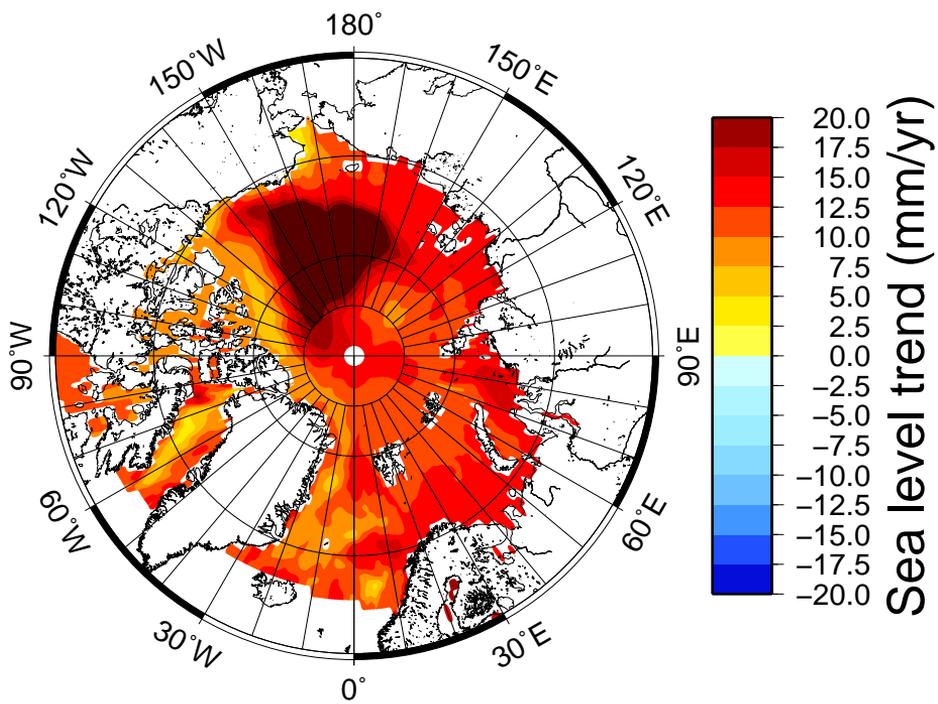
Figure 2.8: Trends in Drakkar for the period 1995–2010.

Geophysical signals

3.1 Seasonal variation

As the seasons change during the year, the Sun will provide different amounts of heat at any given location. This causes a variable thermal expansion of the water (see also the "Thermosteric contribution" section), which is usually modelled as a 1-year harmonic oscillation. The Sun passes over the equator twice a year (at the equinoxes), justifying also the inclusion of a half-year oscillation.

While the one-year and half-year harmonic oscillations are likely sufficient for global sea-level reconstructions as in Church et al. (2004), some Arctic gauges exhibit strongly non-sinusoidal seasonal signals due to large amounts of melt-water in spring (see also section 4.4.1).

3.2 Tidal signals

Both the Earth's oceans and, to a lesser extent, land areas, are affected by tides. Tidal effects occur at a large variety of frequencies, though the most significant tidal constituents have frequencies of a few hours to slightly more

than a day. While tidal signals may locally have amplitudes of several meters, the long-period constituents (longer than approximately one day) generally have amplitudes smaller than 10 cm (Wahr, 2013).

The primary long-period tidal constituents as described in Wahr (2013) are given in Table 3.1.

Constituent	Period (years/days)	Approximate amplitude (cm)
(lunar nodal tide)	18.613 yr	2.79
S_a	365.26 d	0.49
S_{sa}	182.621 d	3.10
M_m	27.555 d	3.52
M_f	13.661 d	6.66

Table 3.1: Long-period tidal constituents, from Wahr (2013).

For the present project, which relies on monthly or annual data, tidal signals will generally be ignored as noise.

3.3   Steric effects

Steric effects refer to the effects of varying density of sea water. The density of sea water is affected by its temperature, salinity and pressure, most significantly by temperature.

As outlined in (e.g.) IPCC AR4 (section 5.5.3), studies indicate an accelerating rise in global steric sea level since the 1950s. Such estimates generally consider only the upper 700 m of the oceans due to uncertainties of abyssal heat content. For the period 1955–2003, the mean rate of change was estimated at approximately 0.3 mm/yr (Antonov et al., 2005; Ishii et al., 2006), while for the period 1993–2003, estimates range between 1.2 mm/yr and 1.8 mm/yr (Antonov et al., 2005; Ishii et al., 2006; Willis et al., 2004; Cazenave et al., 2006).

3.3.1   Thermosteric contribution

The density of sea water decreases with increasing temperature. For fresh water, the maximum density is obtained at approximately 4 °C, with colder water being slightly less dense, though this peak is lowered beyond the freezing point by the salt content of sea water. In other words, the water expands as the temperature increases. This is known as the thermosteric contribution to the sea level.

The thermosteric contribution is dependent upon the entire temperature profile of a water column. However, such measurements must usually be performed in situ, and only the temperature of the highest fraction of a millimetre can be measured from infrared-sensing satellites, which may not be representative of the surface (defined as the upper few metres), much less the entire water column.

3.3.2   Halosteric contribution

As salt water is denser than fresh water, freshening of seawater will correspond to expansion and hence sea level rise. Only about 10% of the recent global steric contribution is estimated as halosteric expansion (Ishii et al., 2006), though it is effectively nearly compensated by the salinization (and, therefore, contraction) of any added freshwater to the oceans (see e.g. Antonov et al. (2002)). However, salinity changes can be highly regionally important, sometimes nearly compensating the thermosteric contribution as in the subpolar gyre in the North Atlantic (IPCC AR4, section 5.5.4.1).

3.3.3   Barometric effects

The inverse barometer (IB) correction for sea level simply follows from the relation between height and pressure change in a water column.

The barometer contribution (i.e., what should be subtracted from observations to obtain the IB-corrected data) becomes

$$-\frac{P - P_{ref}}{\rho g}$$

where ρ is the sea-water density, g is gravitational acceleration and $(P - P_{ref})$ is the atmospheric sea-level pressure anomaly. The reference pressure P_{ref} should be chosen with respect to each particular location (Dorandeu and Le Traon, 1999). A pressure change of 1 mbar (100 Pa) corresponds to approximately 1 cm.

For this project, barometric data are obtained from the Hadley Centre Sea Level Pressure (HadSLP2r) (Allan and Ansell, 2006). The pressure dataset is, like the sea-level reconstruction in this project, a reconstruction based on reduced-space optimal interpolation, and may therefore differ from actual observations. It is given in the form of monthly, global $5° \times 5°$ grids and has in this case been obtained through NOAA's Earth System Research Laboratory.[1]

---

[1]http://www.esrl.noaa.gov/psd/gcos_wgsp/Gridded/data.hadslp2.html
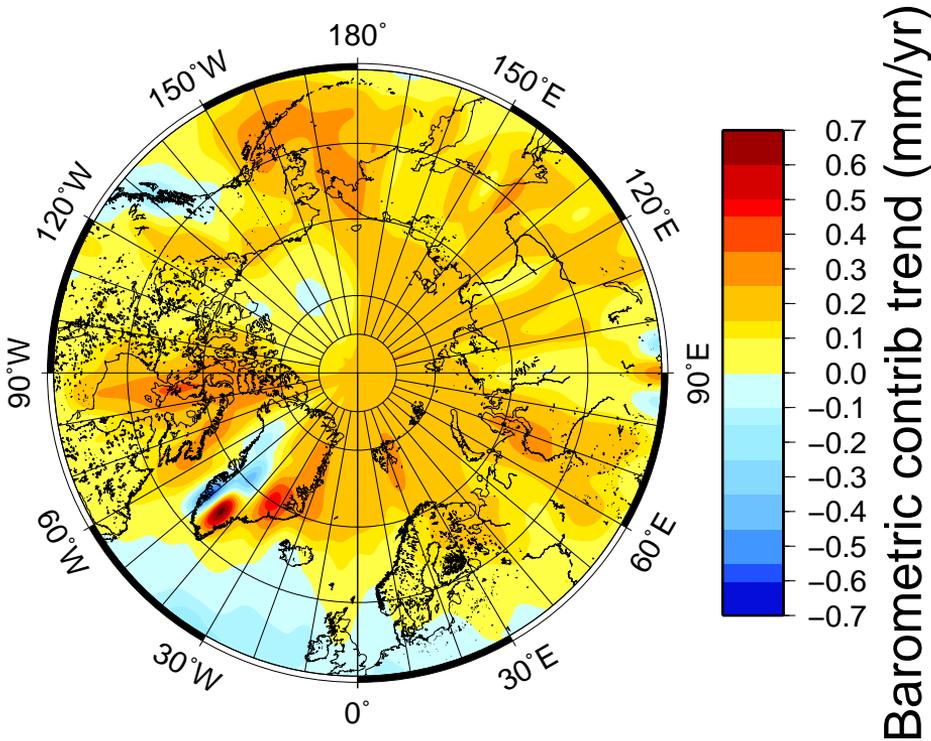
Figure 3.1: Sea level trend (1950–today) contribution from barometric effects, as obtained from HadSLP2r.

The contribution to Arctic sea level trend due to barometric effects, as obtained from HadSLP2r, is shown in Fig. 3.1. It is seen that barometric effects generally contribute around 0.0 to $+0.4\,\mathrm{mm/yr}$ in the Arctic Ocean for this period.

3.4 Climate indices

The global climate system is often described using a variety of empirical, regional indices, defined using temperature or pressure. Most prominent of these indices is the El Niño–Southern Oscillation (ENSO), describing the variations of the Pacific Ocean between El Niño and La Niña phases.

The exact relation between these climate indices and sea level depend of course on how the particular index is defined. Higher temperatures will generally cor-

relate positively with sea level, while higher pressure will correlate negatively with sea level.

For the Arctic Ocean, the most relevant indices are the Arctic Oscillation (AO, also known as the "Northern Annular Mode", NAM) and the related North Atlantic Oscillation (NAO). Also relevant for the Pacific side of the Arctic are the Pacific Decadal Oscillation (PDO), and the North Pacific Index (NPI). Additionally, an "Arctic dipole anomaly" has been proposed as a replacement for the AO/NAO.

For the AO, the positive phase represents a relatively low pressure in the polar region, which causes weather to be wetter in Northern Europe and drier in Southern Europe, as storms are driven northward. The AO indices for the last six decades are illustrated in Fig. 3.2.

The AO and NAO are strongly correlated; Deser (2000) found a temporal correlation of 0.95 for the period 1947–1997 using monthly SLP data.
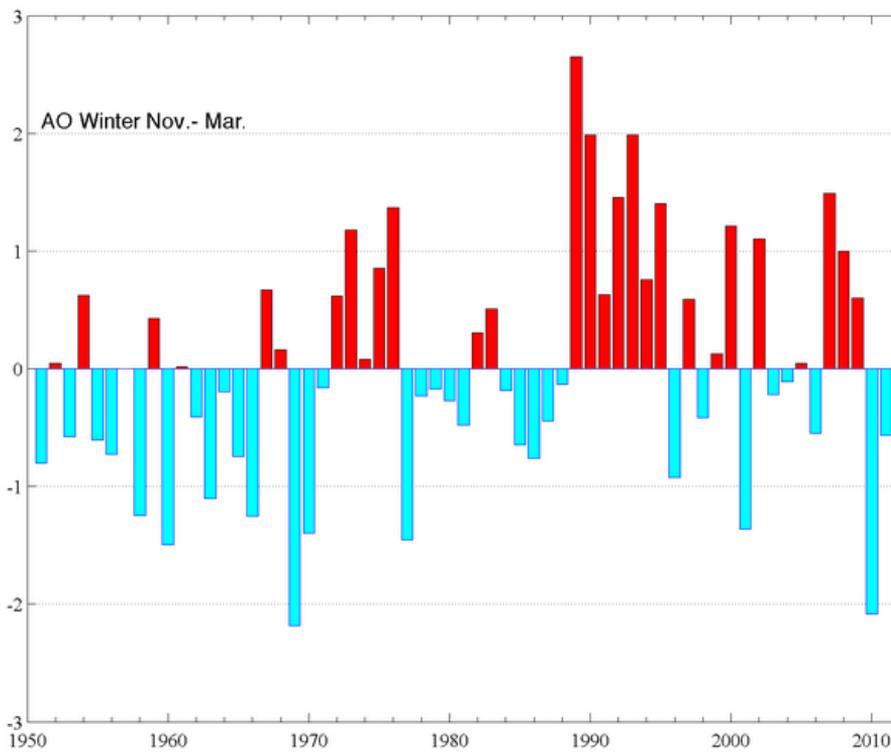
Figure 3.2: Arctic Oscillation (AO) indices for November–March since 1950.
Image credit: NCEP/NOAA (`http://www.arctic.noaa.gov/`
`detect/climate-ao.shtml`).

3.5   Glacial isostatic adjustment (GIA)

Glacial isostatic adjustment (GIA), also known (in a slightly narrower sense) as post-glacial rebound (PGR), refers to the effects of ground movement due to the historical presence of a glacier upon it (in this context, the Last Glacial Maximum). This commonly manifests itself as an upward "rebound" movement of the ground where the glacier used to be, in some places up to 1–2 cm per year. Areas further away may have slight downward movement, and slight horizontal movement may also be present in the adjustment towards isostatic equilibrium.

The vertical movement represents a major uncertainty in estimating trends for tide gauge time series. Much of the rebound occurs in poorly surveyed areas near the poles, and existing GIA models have substantial uncertainties here. Despite the uncertainties, the GIA contribution can be reasonably modelled as linear in time for a 50-year reconstruction, as changes in the movement rates mostly occur on scales of several thousand years. However, it should be noted that accelerating uplift rates can be observed on the margins of thinning ice sheets, see e.g. Jiang et al. (2010).

It is important to distinguish two different effects of GIA when discussing sea level:

1. it causes eustatic changes in sea level by slightly altering the shape of the ocean basin (which will appear in altimetry data), and

2. it causes isostatic changes, affecting relative sea level (as observed by tide gauges, for example), appearing as a downward sea level trend (nearly) corresponding to the upward land rebound.

For convenience, PSMSL provides estimates, for each tide gauge location, of the estimated relative sea level (RSL) rate due to GIA, from the Peltier model using the ICE-5G deglaciation history (Peltier and Tushingham, 1989; Peltier, 2004, 2005).

As noted by Jevrejeva et al. (2014), the choice of GIA model is extremely important when using Arctic gauges; they found a 17 cm difference in accumulated sea level rise in the Arctic since 1925 simply by comparing results using the ICE-4G and ICE-5G models, respectively (the former giving the highest increase in sea level).

3.6   Cryospheric contributions

About 75% of the world's freshwater is stored within the ice sheets of Greenland and Antarctica (IPCC AR4, section 4.1). A complete melting of the Greenland Ice Sheet would result in $7\,m$ of sea level rise, while the Antarctic Ice Sheet holds water equivalent to $57\,m$ of global sea level rise.

While such scenarios are not realistic for the foreseeable future, both the Greenland and Antarctic ice sheets have experienced accelerating mass loss since the early 1990s (Shepherd et al., 2012).

Sea level changes due to glacial contributions were estimated in Dyurgerov and Meier (2005) as 0.51 mm/yr for the period 1961–2003, accelerating to 0.93 mm/yr for the period 1994–2003.

While large amounts of sea ice have melted from the Arctic Ocean over the last few decades, it does not significantly affect sea level. Shepherd et al. (2010) found a global loss of sea ice of $746 \pm 127\,km^3$ for the period 1994–2004, with an estimated associated rise of sea level of only $49 \pm 8\,\mu m$. Interestingly, however, some formerly ice-covered areas may now allow sea-level measurements which were not possible to obtain before.

3.6.1   Sea-level fingerprints

Interestingly, mass loss in ice sheets leads to a local fall in sea level, while the resulting sea level rise is spread around the rest of the globe. This is due to the reduced gravitational force from the (now smaller) ice sheet on the near-field ocean. Detailed estimates for the "fingerprints" of each ice sheet have been made in Mitrovica et al. (2011).

Analysis and reconstruction techniques

4.1 Data representation conventions

Preisendorfer (1988) defines six data matrix representation conventions for decomposition purposes: O-, P-, Q-, R-, S- and T-mode, as elaborated in Table 4.1. These six modes represent the possible permutations of the interpretations of station, time and field. The most relevant modes in this context are S- and T-mode, which use a fixed field (a constant selection of grid points in the ocean). Particular discussion of S-mode versus T-mode, such as the effect on eigenvalues, is made in Compagnucci and Richman (2008). For this project, S-mode analysis is assumed, yielding an $n \times n$ similarity matrix, where n is the number of pixels in the calibration dataset.

Mode	"Variable"	"Individual"	Fixed entity
O-mode	time	field	station
P-mode	field	time	station
Q-mode	station	field	time
R-mode	field	station	time
S-mode	station	time	field
T-mode	time	station	field

Table 4.1: Modes of principal components analysis, from Preisendorfer (1988).

4.2 Covariance estimation

4.2.1 Dealing with missing data

While a covariance matrix will always, theoretically, be positive semi-definite, this will not always be the case when estimating using partially missing data. The effects of partially missing data on covariance matrices is discussed in Rummel (1970).

The amount of missing data that can be allowed is quite dependent on the pattern in which it occurs. Rummel (1970, p. 261) notes that no methodological work seems to be published.

In recent years, the problem of computing SVDs from partially missing data has received extensive attention in recommender systems, including the so-called "Netflix Prize" (2009) to predict user ratings of films, for which nearly all the top entries used some variation on the SVD. SVD-based techniques adapted to handle missing data include iterative SVD (Roweis, 1998), regularized SVD (Paterek, 2007) and SVD with implicit feedback (SVD++, Koren (2008)); see also Hastie et al. (1999).

However, for this project, we will rely on either temporally complete datasets (possibly using interpolation) or estimates of the entire covariance matrix as given by MATLAB's `nancov` function with a `'pairwise'` argument or similar, though adapted to properly handle area weighting. This estimates the covariance between variables according to the number of observation pairs for them. This approach may yield a plausible-looking "covariance" matrix, but it will not generally be positive semi-definite as is the case with no missing data.

4.3   Pattern detection

4.3.1   Empirical orthogonal functions (EOF)

Empirical orthogonal functions (EOF) are, in geophysics, more or less synonymous with principal components. Principal component analysis (PCA) attempts to express a multivariate dataset in a new linear basis, with mutually orthogonal components sorted by decreasing variance, and hopefully thereby allowing us to express most of the variation using only a few dimensions. Finding the PCs is done by solving the eigenvalue problem for the covariance matrix of the data matrix. Often, this covariance matrix may be prohibitively large for practical analysis, and therefore a singular value decomposition (SVD) of the data matrix is used as a computational shortcut to obtain the eigenvalues and eigenvectors.

Computation of EOFs

Terminology in literature regarding empirical orthogonal functions (EOFs) is highly variable, and sometimes contradictory. For the sake of clarity and avoidance of doubt, this section describes the computation of EOFs and their relationship with the singular value decomposition (SVD).

Principal components

Principal component analysis (PCA) and EOF analysis are by some authors considered synonymous in geoscience, e.g. von Storch and Zwiers (1999).

For a column vector $\boldsymbol{x}$ of p random variables (in this project: pixels in an ocean grid),

$$\boldsymbol{x} = \begin{pmatrix} x_1 \\ x_2 \\ \vdots \\ x_p \end{pmatrix}$$

we have the $(p \times p)$ covariance matrix

$$\mathbf{C} = E[(\boldsymbol{x} - \bar{\boldsymbol{x}})(\boldsymbol{x} - \bar{\boldsymbol{x}})^\mathsf{T}]$$

If realizations of $\boldsymbol{x}$ are collected in a data matrix $\mathbf{X}$, with the empirical mean of each variable removed, the empirical covariance matrix can be obtained as

$$\hat{\mathbf{C}} = \mathbf{X}\mathbf{X}^\mathsf{T}/p$$

Relationship with the SVD

For a matrix $\mathbf{X}$ with the singular value decomposition

$$\mathbf{X} = \mathbf{USV}^\mathsf{T}$$

the columns of $\mathbf{U}$ are called the *left-singular vectors*, the diagonal elements of the diagonal matrix $\mathbf{S}$ are the *singular values*, and the columns of $\mathbf{V}$ are the *right-singular vectors*. Then,

- the columns of $\mathbf{U}$ (the left-singular vectors of $\mathbf{X}$) are the eigenvectors of $\mathbf{XX}^\mathsf{T}$, and

- the columns of $\mathbf{V}$ (the right-singular vectors of $\mathbf{X}$) are the eigenvectors of $\mathbf{X}^\mathsf{T}\mathbf{X}$.

The diagonal elements of $\mathbf{S}$ provide the *square roots* of the corresponding nonzero eigenvalues of $\mathbf{XX}^\mathsf{T}$ and $\mathbf{X}^\mathsf{T}\mathbf{X}$ (which are the same).

If $\mathbf{X}$ is a data matrix of variables centred in 0, then the matrix $\mathbf{XX}^\mathsf{T}$ (or $\mathbf{X}^\mathsf{T}\mathbf{X}$, depending on the orientation of $\mathbf{X}$) will be proportional to the covariance matrix of $\mathbf{X}$; the eigenvalues λ_i of the covariance matrix are given from the singular values s_i as $\lambda_i = s_i^2/n$. Thus, we can obtain the principal components from the SVD, without actually computing the (possibly very large) covariance matrix.

Avoiding a large covariance matrix can also be done by means of the "transpose trick", i.e. by swapping variables and observations in $\mathbf{X}$ before computing its covariance matrix. However, the SVD is a computationally efficient way of handling the eigenvalue problem in any case, and it has important applications in regularization analysis.

Missing data

Mathematically, the SVD is only defined for complete data matrices. If any missing data cannot be covered by interpolation, the eigenvectors must be obtained in a different way.

For this project, the problem has been addressed by estimating the full covariance matrix, allowing a variable number of observations for each variable. The data matrix $\mathbf{X}$ is supplemented by a similarly-sized matrix $\mathbf{D}$ indicating whether an observation is available, i.e. $\mathbf{D}_{ij}$ is 1 if $\mathbf{X}_{ij}$ is available, 0 if it is not.

The missing elements of $\mathbf{X}$ are replaced by zeros. In an ordinary covariance matrix, all elements are normalized by $(n-1)$; here, the number of available observation pairs $(=n)$ for each element in the covariance matrix are given by $\mathbf{D}\mathbf{D}^\mathsf{T}$. We can then estimate the covariance matrix as $\mathbf{X}\mathbf{X}^\mathsf{T}$, followed by an elementwise normalization by the computed values of $(n-1)$; for consistency with MATLAB's `cov` function, we normalize by n where $n = 1$.

Area weighting

When computing EOFs on nonuniform grids, the spatial weighting of the data needs to be taken into consideration. For example, for data on a simple lat/lon grid, pixels at high latitudes will represent a much smaller area than those near the equator due to converging meridians. If unhandled, this will bias the resulting EOFs towards mostly explaining variance at high latitudes. This is not desirable; the appearance of the EOF modes should be invariant to choice of gridding.

Per North et al. (1982) and Baldwin et al. (2009), the correct way to apply the weighting to the data matrix is by multiplying with the *square root* of the pixel areas. Intuitively, this is because the elements of the covariance matrix result from multiplying together values from two pixels, and hence include the product of any premultiplied weights.

Empirical orthogonal functions are a discrete version of the *Karhunen-Loève transform*, which, like the Fourier transform, decomposes a function into orthogonal, continuous functions. A detailed analysis for climate purposes is made in North et al. (1982). Importantly, the patterns obtained should be invariant to the choice of gridding.

Obtaining an appropriate scheme for spatial weighting of EOFs is discussed in Baldwin et al. (2009), basing their approach on North et al. (1982). As in their example, we consider an anomaly field $\boldsymbol{x}$ (here, the sea level anomalies in the calibration period). The covariance structure is given by the area integral

$$\int_A \boldsymbol{x}^2 da$$

As we assume $\boldsymbol{x}$ to be centred in 0, its unweighted covariance is $\operatorname{cov}\boldsymbol{x} = \boldsymbol{x}\boldsymbol{x}^\mathsf{T}$.

We are looking for a constant diagonal matrix $\mathbf{W}$ of pixel weights, so that $\operatorname{cov}(\mathbf{W}\boldsymbol{x})$ is the properly area-weighted covariance of the field. Then,

$$\operatorname{cov}(\mathbf{W}\boldsymbol{x}) = \mathbf{W}\operatorname{cov}(\boldsymbol{x})\mathbf{W}^\mathsf{T} = \mathbf{W}\boldsymbol{x}\boldsymbol{x}^\mathsf{T}\mathbf{W}^\mathsf{T} = (\mathbf{W}\boldsymbol{x})(\mathbf{W}\boldsymbol{x})^\mathsf{T}$$

Therefore, $\mathbf{W}^2$ must be the equivalent of da, and the diagonal elements of $\mathbf{W}$ therefore the square roots of their corresponding pixel areas.

Applying these results in practice, one will therefore premultiply the weights (square root of pixel area) onto the $\mathbf{X}$ matrix, then perform the SVD decomposition to obtain eigenfunctions $\mathbf{E}$, and apply the inverse weighting to $\mathbf{E}$ (as specified in Baldwin et al. (2009), section 3.c), before fitting the eigenfunctions to the tide gauge data. That is, the elements in $\mathbf{E}$ should be divided by the square roots of the pixel areas before fitting.

An example of the difference in results caused by area weighting is shown in Fig. 4.3 and 4.4; the EOFs are extracted from a CryoSat-2 altimetry dataset covering 68°N to 88°N. The unweighted analysis causes an overemphasis on high-latitude variation, in this case quite visible in EOF2 near the pole. The CryoSat-2 data were used for a different project, not documented here, but are used for illustration of the latitude weighting due to their coverage up to 88°N.

As an alternative to an area-weighted decomposition altogether, one may resample the calibration dataset grids in an equal-area map projection. Many such projections exist, though an obvious choice for Arctic sea level reconstruction would be an azimuthal equal-area projection ("Lambert azimuthal projection") centred in the North Pole.

If, rather than area, preservation of distance from the North Pole is desired, one can use an azimuthal equidistant projection. If conformality (angle preservation) is desired, a polar stereographic projection can be chosen. As long as the domain is relatively close to the pole, the difference between these projections are relatively small; however, for global reconstructions, the distortions cannot be ignored. See Fig. 4.1 and 4.2 for examples of polar map projections.
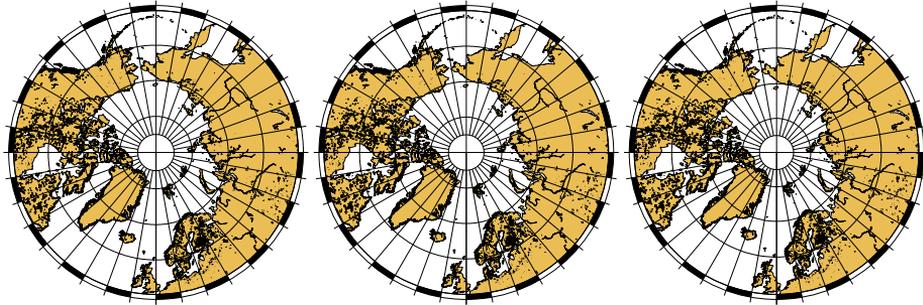
Figure 4.1: Examples of map projections for the Arctic (50°N to 90°N). Left to right: Lambert azimuthal equal-area projection, azimuthal equidistant projection, and stereographic projection (conformal). The differences are subtle for this high-latitude example.
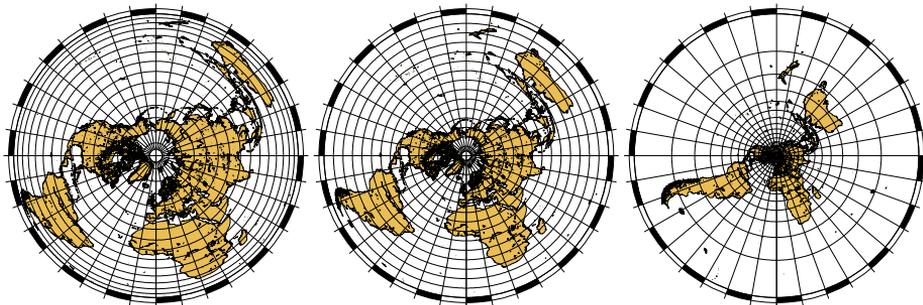
Figure 4.2: Examples of map projections for the Arctic (60°S to 90°N). Left to right: Lambert azimuthal equal-area, azimuthal equidistant, and stereographic projection. Compared to Fig. 4.1, the differences between the projections are much more apparent.
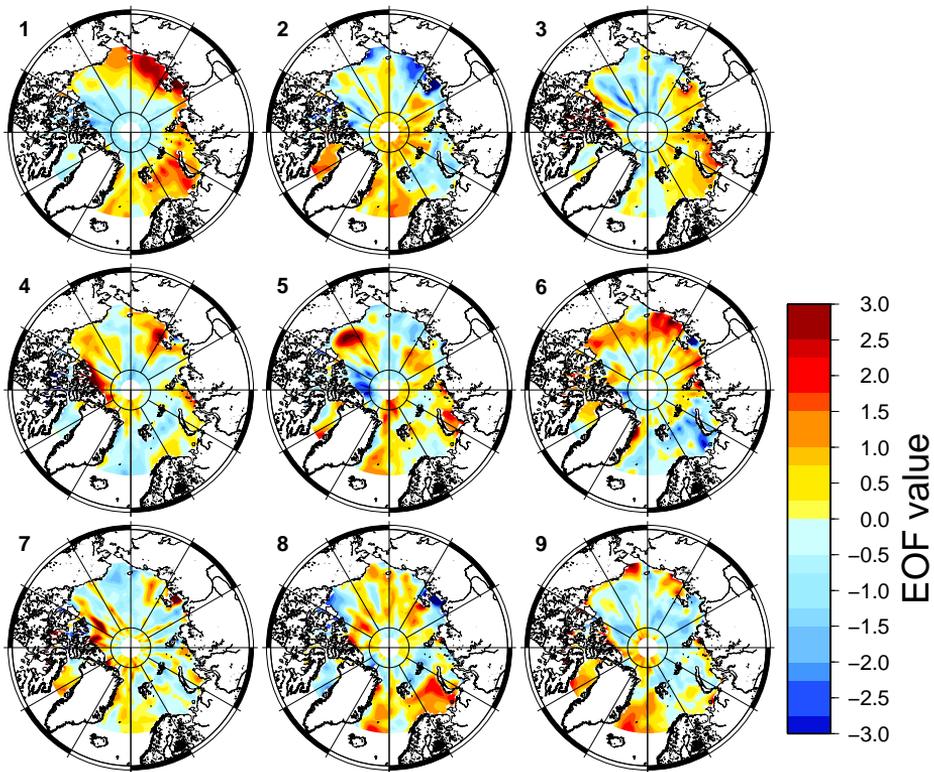
Figure 4.3: Leading EOFs of CryoSat-2 altimetry on a regular lat/lon grid, without area weighting.
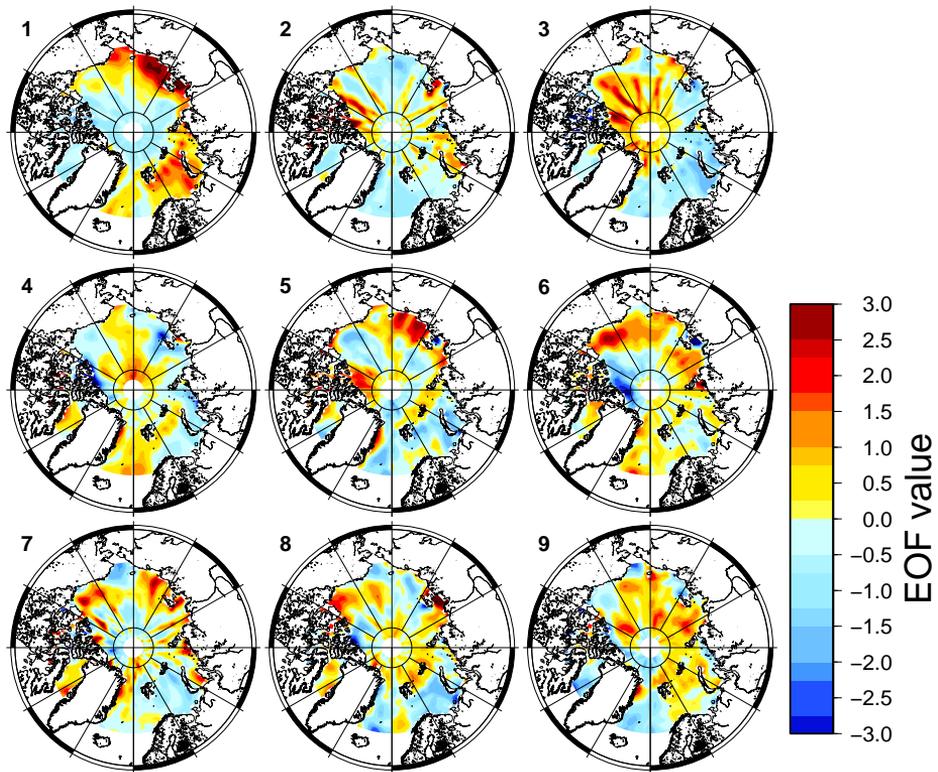
Figure 4.4: Leading EOFs of CryoSat-2 altimetry, with appropriate area weighting.

Cyclostationary EOF (CSEOF)

As opposed to deseasonalizing the calibration dataset before computing the EOFs, an approach introduced in Kim and North (1996) instead involves computing a separate set of EOFs for each calendar month (that is, a set of "January" EOFs, a set of "February" EOFs etc.). This approach is known as cyclostationary EOFs (CSEOF) and has been studied for sea-level reconstruction purposes in Hamlington et al. (2011), who found an improved correlation between reconstructed and actual ENSO indices as compared to ordinary EOFs. They note that the greatest advantage of CSEOFs may lie in the ability to capture changes to the seasonal variability over time.

CSEOFs have not been considered in this project due to time constraints and the relative lack of data in the Arctic. However, it may be interesting as future work since water level at gauges near rivers often exhibit highly non-sinusoidal annual signals (see section 4.4.1).

EOFs of calibration datasets

The leading spatial patterns obtained from Drakkar data above 68°N, as used for initial reconstructions, are shown in Fig. 4.5, while the leading patterns from the altimetry dataset above 68°N are shown in Fig. 4.6. It is seen that a Beaufort Gyre feature is present in EOF1 in both cases, and a strong coastal component is apparent in the East Siberian Sea. It should be noted that the sign of the data is arbitrary.
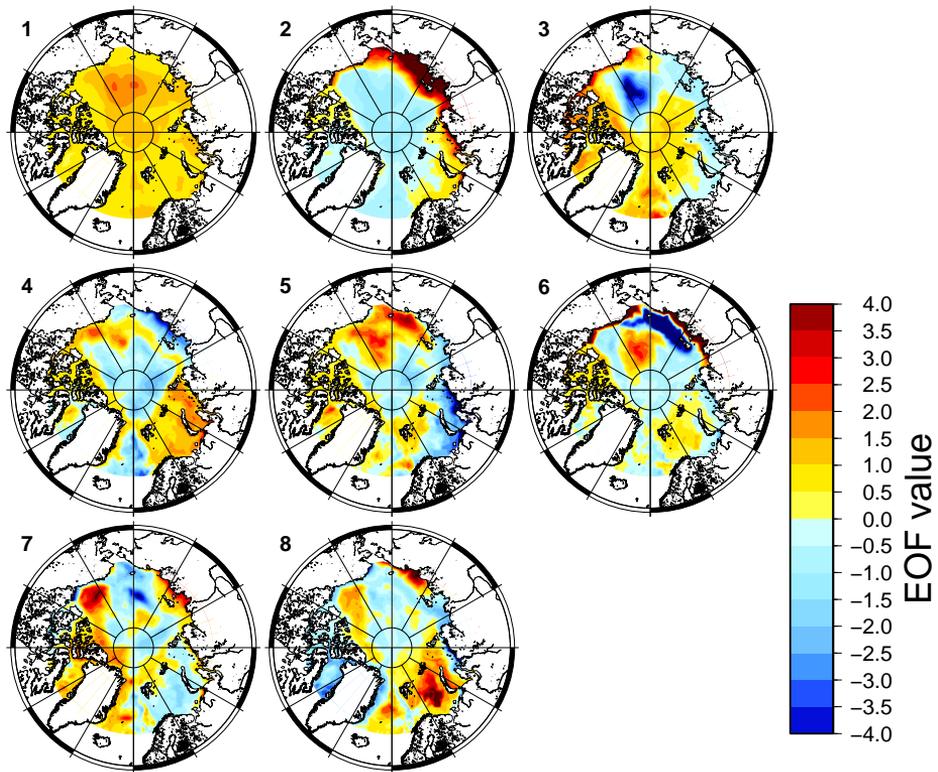
Figure 4.5: Leading EOFs of Drakkar data (1993-2007) above 68°N (arbitrary scaling).
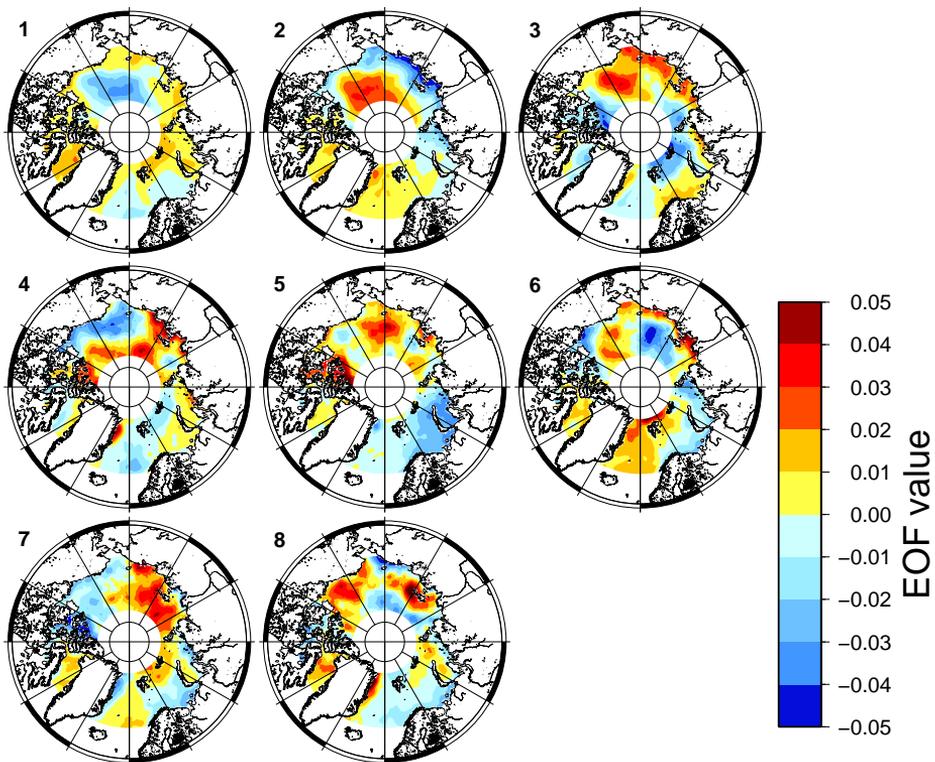
Figure 4.6: Leading EOFs of altimetry data above 68°N (arbitrary scaling).

4.3.2 Effective degrees of freedom

A variety of tactics can be used to decide an appropriate number of EOF modes from the calibration period to retain. In addition to visual inspection ("eye-balling") of the EOFs, some formal approaches are available which attempt to determine the noise level in the data, based on the eigenvalues from the decomposition.

For many common problems, the eigenvalues will decrease sharply among the first few modes and then "level off" to a nearly constant level, corresponding to the noise level in the data.

Explained variance

A simple, intuitive criterion for inclusion of modes is their cumulative explained variance. For example, one may choose only as many modes as necessary to explain 90% or 95% of the variance in the calibration period. Of course, this crude method does not attempt to distinguish mode mixing or noise from physically robust modes, but is trivial to implement.

The explained variance in the Drakkar EOFs, computed from 180 months of data (thus giving 180 EOFs), is shown in Fig. 4.7. It is clear that EOF1 is dominant; 90% explained variance is achieved with the first 3 EOFs, and 95% with 8 EOFs.

The altimetry dataset (considered only north of 68°N) is considerably more noisy than the Drakkar data, see Fig. 4.8. It takes 10 EOFs to get above 50% explained variance; 90% explained variance is obtained only after 78 EOFs, and 95% after 113 EOFs. However, as the spatial patterns appear qualitatively similar to the Drakkar EOFs, it has been chosen to retain 8 EOFs for the altimetry-based analysis as well.

Testing

Assuming eigenvalues ordered non-increasingly, we can define a null hypothesis stating that the last $(k - m)$ eigenvalues are equal (that is, the last $(k - m)$ modes are noise-like):

$$H_0 : \lambda_1 \geq \cdots \geq \lambda_m \geq \lambda_{m+1} = \cdots = \lambda_k$$
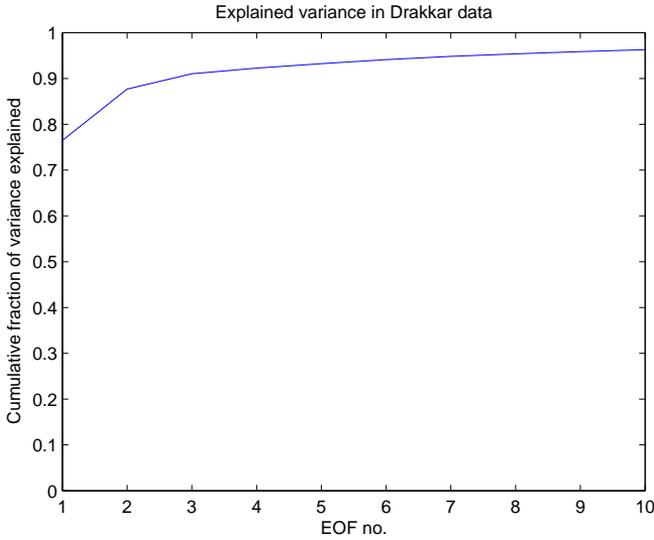
Figure 4.7: Cumulative explained variance for Drakkar EOFs (for data from the period 1993–2007, above 68°N).

and an alternative hypothesis stating that we have strict inequalities $(\lambda_i > \lambda_{i+1})$ between the last $(k-m)$ eigenvalues (the last $(k-m)$ modes are not noise-like):

$$H_1 : \lambda_1 \geq \cdots \geq \lambda_m > \cdots > \lambda_k$$

We then obtain a test statistic (Ersbøll and Conradsen, 2007, p. 265):

$$Z_1 = -n' \ln \frac{\hat{\lambda}_{m+1} \cdots \hat{\lambda}_k}{\hat{\lambda}^{k-m}}$$

where

$$n' = n - m - \frac{1}{6} \left(2(k-m) + 1 + \frac{2}{k-m} \right)$$

and

$$\hat{\lambda} = \frac{\hat{\lambda}_{m+1} + \cdots + \hat{\lambda}_k}{k-m}.$$

Then, Z_1 will be approximately chi-square distributed, and a test at significance level α will be against

$$\chi^2 \left(\frac{(k-m+2)(k-m-1)}{2} \right)_{1-\alpha}.$$
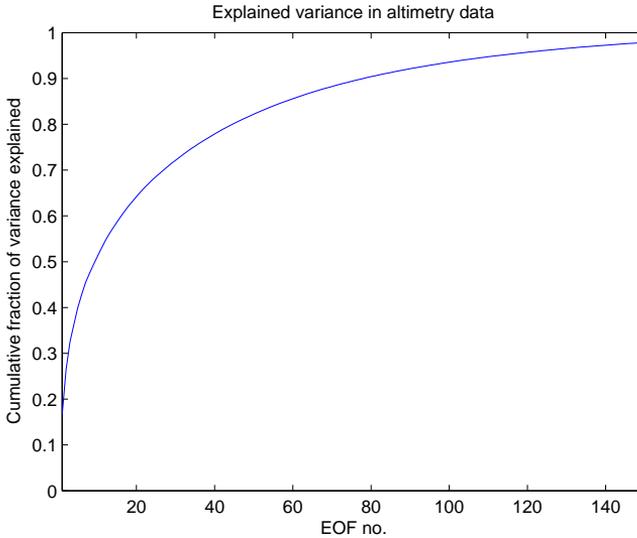
Figure 4.8: Cumulative explained variance for altimetry EOFs (for data from the period 1992–2012, above 68°N).

Eigenvalue uncertainty and North's rule of thumb

Each eigenvalue may be treated as approximately normally distributed with mean λ_i and variance $2\lambda_i^2/N$ (see e.g. Anderson (2003, p. 474)). Thus, the standard deviation for each eigenvalue becomes

$$\sigma_{\lambda_i} \approx \lambda_i \left(\sqrt{\frac{2}{N}} \right).$$

If the error bars of neighbouring eigenvalues overlap (assuming ordered eigenvalues), it suggests that the corresponding modes are not physically robust.

Owing to the discussion in North et al. (1982), application of this error estimate is also known as "North's rule of thumb". According to that paper, if the spacing between neighbouring eigenvalues is comparable to the error on one of these eigenvalues, the sampling error of one EOF will be comparable to the neighbouring EOF.

Applying these considerations to the Drakkar data, we obtain the results shown in Fig. 4.9. Only the first four eigenvalues do not fall within the upper bound (one standard deviation) for the next eigenvalue, while all eigenvalues from λ_2 on fall within the lower bound for the previous eigenvalue.
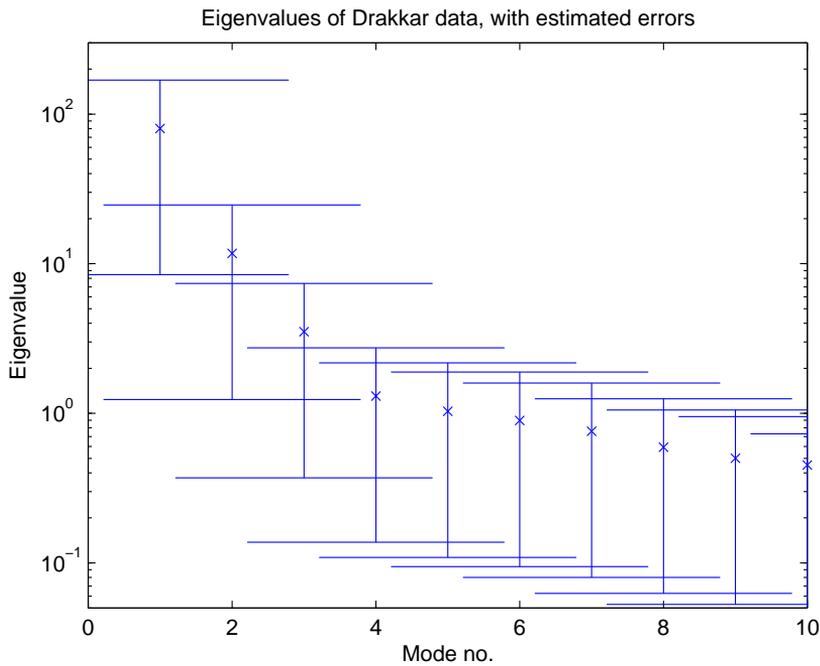
Figure 4.9: Eigenvalues for Drakkar EOFs (for data from the period 1993–
2007, above 68°N) with corresponding error bars (showing one
standard deviation on each side).

Scrambling

An empirical estimate for the noise level can be obtained by randomly permuting the calibration data, then re-estimating the eigenvalues. With many such eigenvalue estimates, the mean and variance for each eigenvalue of the randomized data can be estimated. This approach is known as scrambling (see e.g. Hastie et al. (2009, p. 537)).

Applying the scrambling approach to the calibration fields implies permuting the sea pixels randomly, with a new permutation for each timestep in the data, before computing the EOFs. Unfortunately, the area weighting of pixels is not trivial to apply (resampling the data to an equal-area projection seems to be the simplest solution). Also, the presence of a trend will perturb the results.

Results from scrambling the Drakkar data above 68°N from the altimetry era are shown in Fig. 4.10 (no detrending prior to analysis) and Fig. 4.11 (with detrending). Qualitatively, the results are quite similar with and without detrending; the eigenvalue for EOF1 in both cases falls within the results from scrambling, while EOF2, -3, -4 and -5 are above the noise floor by more than one standard deviation. However, EOF6 and -7 are also (barely) above one standard deviation from the scrambled results when detrending is applied.
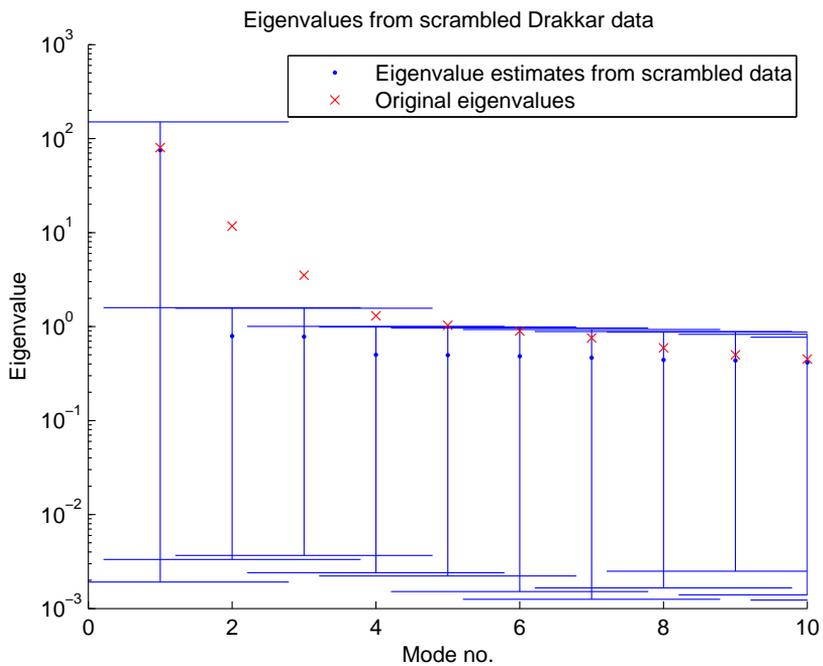
Figure 4.10: Eigenvalues for Drakkar EOFs (for data from the period 1993–
2007, above 68°N) compared with eigenvalues from 100 scram-
blings of the same data (68% confidence intervals for eigenvalues
of scrambled data shown). No detrending applied.
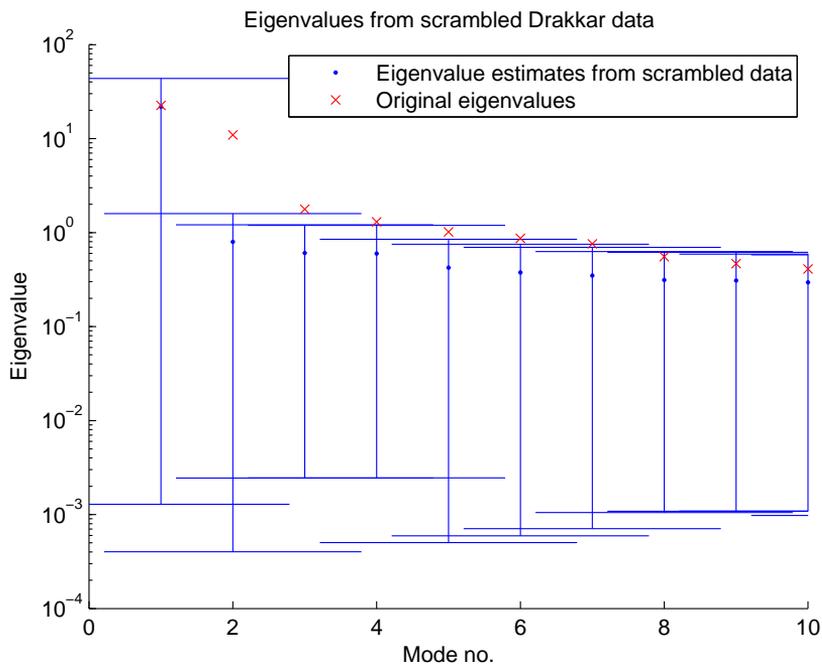
Figure 4.11: Eigenvalues for Drakkar EOFs (for data from the period 1993–2007, above 68°N) compared with eigenvalues from 100 scramblings of the same data (68% confidence intervals for eigenvalues of scrambled data shown). Detrending applied.

4.3.3   Minimum/maximum autocorrelation factors (MAF)

The EOF decomposition traditionally used in sea level reconstruction orders its modes by explained variance. As an alternative, one may instead maximize autocorrelation in the data; thus, we obtain so-called maximum autocorrelation factors (MAF), as described by Switzer and Green (1984). The basic idea is that the data will contain an autocorrelated "signal" (which we will attempt to extract) and uncorrelated (high-frequency) "noise", which the MAF decomposition may separate more neatly than EOFs. For this particular study, we aim to improve explainability of the leading modes, compared to what is provided by EOFs; i.e., the MAFs may yield less mode mixing by forcing a measure of "coherence" in the modes.

Theory

For a data set (an observation vector) $\mathbf{Z}(Z_1, \ldots, Z_p)$, we are interested in obtaining a set of (mutually orthogonal) linear combinations $\mathbf{Y}(Y_1, \ldots, Y_p)$ given by

$$Y_i(x) = \boldsymbol{a}_i' \mathbf{Z}(x), \quad i = 1, \ldots, p$$

Additionally, we define autocorrelations

$$r_i(\Delta) = \text{correlation}(Y_i(x), Y_i(x + \Delta))$$

such that $\boldsymbol{a}$ satisfies

$$r_i(\Delta) = \max_a \text{correlation}(\boldsymbol{a}' Z(x), \boldsymbol{a}' Z(x + \Delta))$$

and

$$\text{correlation}(\boldsymbol{a}' Z(x), \boldsymbol{a}_j' Z(x)) = 0 \text{ for } j < i$$

That is, for each value of i, we choose $\boldsymbol{a}$ so that the correlation between the transformed data and its shifted counterpart is minimized, subject to orthogonality with previous values of $\boldsymbol{a}$. We thus obtain *minimum* autocorrelation factors as the leading modes as in Switzer and Green (1984), which can be turned into *maximum* autocorrelation factors simply by reversing their order.

Considerations for geographical grids

In the form described by Switzer and Green (1984), the differencing is performed as a unit horizontal shift and a unit vertical shift in the data grid, and the

covariances are then pooled together. For geophysical data sets covering large areas, the data grids will necessarily have nonuniform spacing, which intuitively might ruin the method's invariance with respect to choice of gridding.

One way to address this has been experimentally implemented for a global grid; for a regular lat/lon grid, the zonal (east–west) differencing shift is for each latitude chosen as the integer that best approximates the (constant) distance between grid points in the north–south direction.

However, Switzer and Green (1984) actually point out that it "seems prudent to use single step lags for the MAF procedure", as in practice, they argue, only very short lags will help in approximating the spatial structure of the data.

Temporal MAF (T-MAF)

Instead of using spatial differences, one can use temporal differences to obtain the MAFs. Thus, we now decompose our data in a way that maximizes the temporal autocorrelation of the signals. This may be an equally valid approach; many oceanographic signals follow distinct time series (e.g. the Arctic Oscillation, North Atlantic Oscillation and the El Niño Southern Oscillation).

The T-MAF has the advantage of being uncomplicated to apply to irregular grids, since one need not perform geometric shifts. However, irregular sampling may still bias the appearance of the MAF patterns.

Adapting the procedure for sea level reconstruction

Like the EOF reconstruction, the MAF-based reconstruction also includes a "MAF0" (a spatially uniform pattern) to capture mean sea level changes. As for the EOF-based case, the MAF0 has no eigenvalue associated with it (which is necessary for the regularization). As in the EOF case, the MAF0 is assigned the eigenvalue of the first mode.

Results of the decomposition

The MAF analyses in this project have been carried out using the MATLAB functions by Allan Aasbjerg Nielsen (Nielsen et al., 1998), modified to work with incomplete datasets (specifically, land/ocean masks).

To illustrate the behaviour of the MAF procedure in the context of this project, the leading spatial patterns obtained from three variations of the technique:

- differencing spatially to the right and down (Fig. 4.12)

- the same, but with a lag of 2 so that the differences are centered in the proper data pixels (i.e. comparing the pixel 1 step to the left with the one 1 step the right) (Fig. 4.13)

- a T-MAF (temporal differences) (Fig. 4.14)

The procedure has, in all cases, been applied to Drakkar ocean model fields of the satellite era (1993–2007) above 68°N with whole- and half-year oscillations removed.

It is notable that both variations of the spatial MAF struggle with noise in the leading patterns, even though many of the modes resemble patterns from EOFs. Indeed, when using a lag of 2 (Fig. 4.13), the very first mode appears to be rather noise-like, capturing possibly eddies. On the other hand, the T-MAF yields quite smooth patterns (Fig. 4.14), though they have more detail than EOF patterns. Thus, it seems that the general remarks on data point adjacency by Switzer and Green (1984) are very relevant, though in terms of physical explainability, the MAF approach could provide some interesting revelations.

Thus, if spatial MAFs are to be used in a sea level reconstruction, the overall model may need substantial adaptation, as the leading modes may not be "leading" in an oceanographic sense, and the proper way to regularize the fit is still largely an open question. The MAF procedure's lack of robustness when using non-adjacent data causes it to be less appropriate for data with many gaps, such as is the case with altimetry data in the Arctic Ocean.
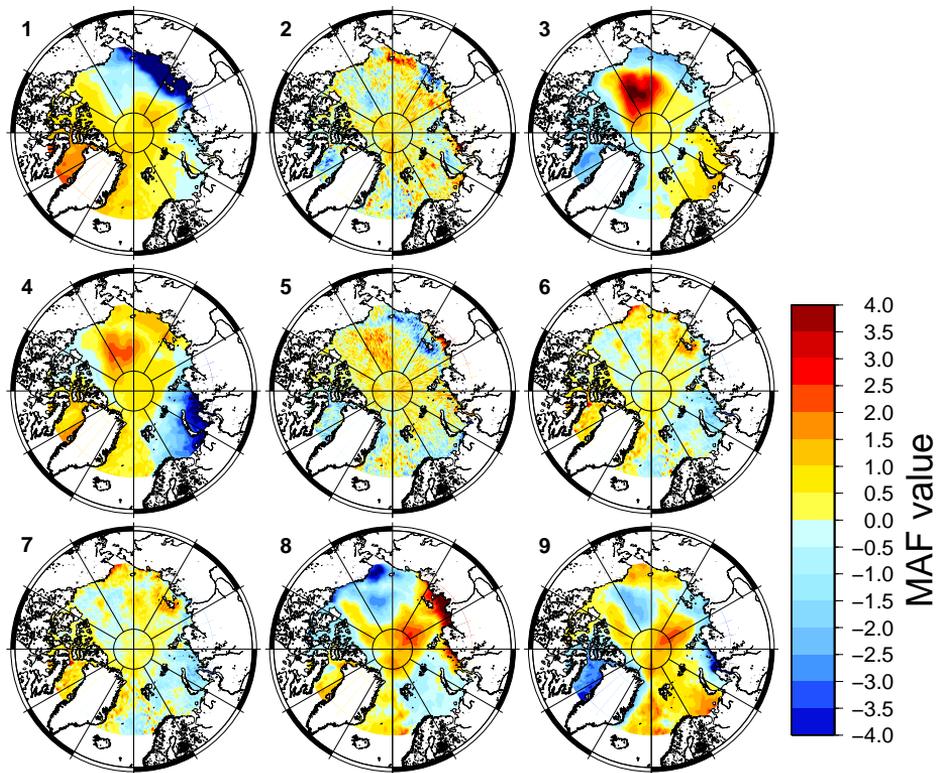
Figure 4.12: Drakkar MAF patterns obtained using spatial differences (lag 1, right and down).
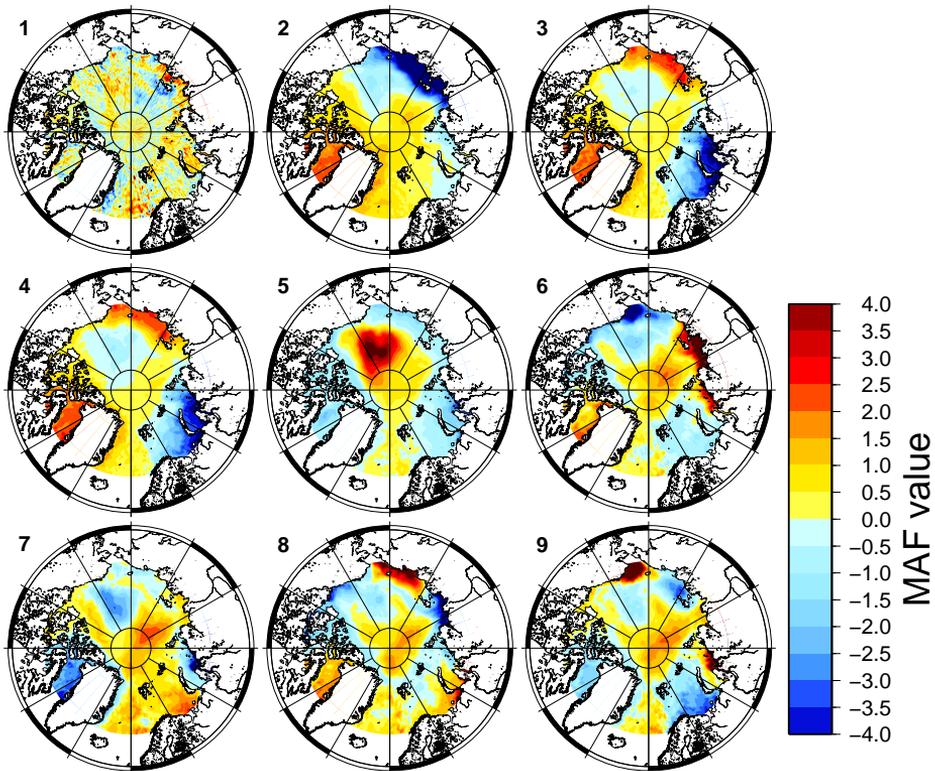
Figure 4.13: Drakkar MAF patterns obtained using spatial differences (lag 2).
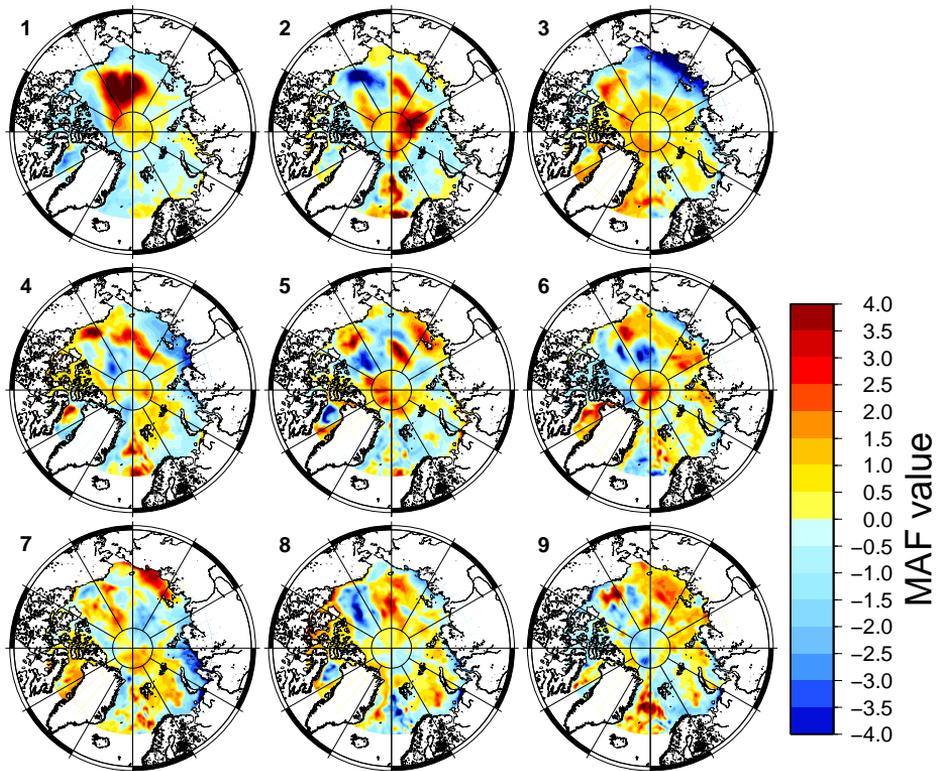
Figure 4.14: Drakkar T-MAF patterns.

4.3.4 Overall remarks on decomposition

There seems to be no simple answer to the question of how many spatial patterns to retain. Throughout this project, a choice of 8 EOFs in addition to a uniform pattern have been used, as this accounts for 95% of the variance in the Drakkar data, and it seems reasonable to retain such a handful of EOFs to avoid overfitting, given the dominant mode of Beaufort Gyre freshwater content and the limited number of gauges.

Getting a spatial MAF decomposition to provide robust (non-noisy) results for an irregular grid proved exceedingly difficult. The temporal MAF seems to more consistently produce coherent, plausible patterns when using Drakkar data, but the Arctic altimetry data is not generally temporally coherent, limiting the method's usefulness for this project. Thus, the more refined results in this project rely on EOFs.

4.4   Tide gauge selection

Church et al. (2004) acknowledged the "inadequate geographical distribution of tide gauges, particularly in the Southern Hemisphere" and unknown geophysical signatures in the tide gauge records as major sources of uncertainty in their (global) sea level reconstruction. These challenges are much exacerbated when considering only the Arctic area.

The tide gauges used in Church et al. (2004) include both RLR and some metric-only gauges. They rejected gauges beyond 66° latitude, and allowed a maximum distance of 250 km between the gauge and its corresponding pixel in the altimetry grids. Record segments shorter than 2 years of data were rejected entirely, though gaps of 1 or 2 months were covered using interpolation. Any month-to-month changes larger than 25 cm were considered likely datum shifts, causing the record to be split in two. Additionally, manual editing was applied to remove gauges deemed unreliable in some way, for example those located in estuaries, or exhibiting very large residual trends (more than $\pm 10\,\mathrm{mm/yr}$). This left some 150–320 gauges with data at any time in the period 1950–2000.

Tide gauge records shorter than 50–60 years will not yield a robust estimate for sea level trend, as interdecadal variation will perturb the results (Douglas, 1991, 1992, 1997; Peltier and Tushingham, 1989). Even with such long records available, only a minority of gauges have sufficiently low vertical crustal motion to provide globally consistent trends on their own, as established in Douglas (1997). In that study, only 24 gauges in the world were deemed to provide usable trend estimates, even after GIA correction using the ICE-3G model. It should be noted, however, that the study placed stringent requirements on the locations of the tide gauges — not being located on collisional plate boundaries and not in areas substantially ice-covered during the last glacial period. Also, the substantial progress in satellite altimetry since that study has allowed trend estimation without relying on the tide gauge records alone.

Cazenave et al. (1999) examined the correspondence between TOPEX/Poseidon altimetry and 6 tide gauges located within 10 km of a DORIS geodetic station, allowing very accurate determination of vertical land motion. These tide gauges were the only ones thus favourably located.

Wenzel and Schröter (2010) studied the possibility, for a global sea-level reconstruction, of using a neural network to deal with the varying availability of tide gauge records.

4.4.1   Examples of tide gauge records

Decade-long gaps

In the Canadian sector of the Arctic, a few tide gauges do have data between
1950 and today, but none cover anything resembling the entire timespan, see
Fig. 4.15. Therefore, a whole-Arctic reconstruction will need to rely on the
EOF basis and gauges from other areas, unless further records or proxy data is
introduced.
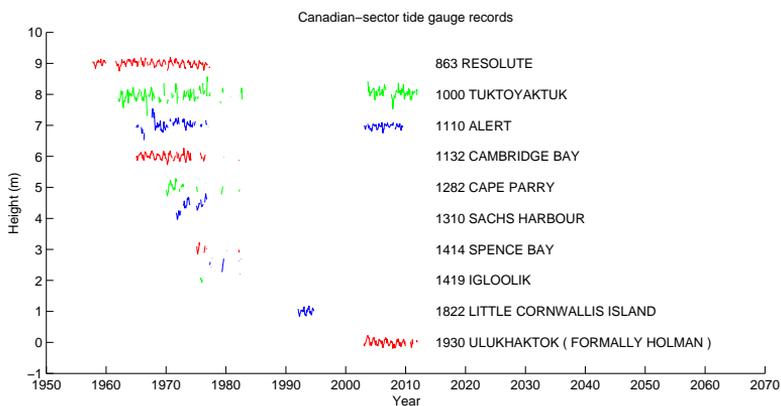
Figure 4.15: All PSMSL (metric) records for Canadian-sector gauges above
68°N, showing decade-long gaps and a complete lack of usable
data between the late 1970s and early 2000s. The vertical offsets
are arbitrary.

Strong seasonal peaks

Many of the river- or estuary-based gauges exhibit strong seasonal signals, often with very prominent peaks in June. These are far from harmonic oscillations, and result from the runoff of meltwater.

To procedurally detect such gauges, the difference between the mean heights for June and mean heights for the rest of the year have been computed. For the 106 gauges above 68°N, these differences have been plotted in Fig. 4.16. From the appearance of this, an empirical threshold could be set at 0.3 m. 11 gauges among these are found to have a June peak prominence larger than 0.3 m; these gauges are listed in Table 4.2. The most extreme of these gauges is Ust Olenek (ID 610), having a mean June prominence of 1.18 m (time series shown in Fig. 4.17).

PSMSL ID	Name	June peak prominence (m)
610	UST OLENEK	1.18
709	UADEI	0.63
741	MALYSHEVA (MALYSHEVA OSTROV)	0.98
767	TADIBE-IAHA	0.30
797	NEMKOVA (NEMKOVA OSTROV)	0.56
917	SOPOCHNAIA KARGA	0.61
1019	SAGYLLAH-ARY	0.98
1128	ANTIPAIUTA	0.79
1200	SE-LAHA	0.34
1399	BYKOV MYS (BYKOV MYS)	0.63
1780	ANABAR	0.61

Table 4.2: RLR gauges above 68°N with June peak prominence larger than 0.3 m.

An example of a tide gauge with prominent June peak (610 Ust Olenek) is shown in Fig. 4.17.
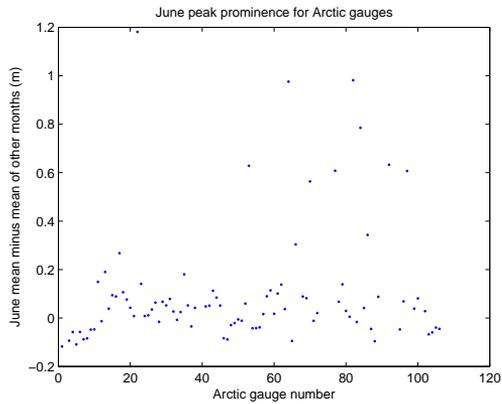
Figure 4.16: Differences between mean heights for June and mean heights for the rest of the year for the 106 PSMSL (RLR) gauges above 68°N, as an indicator for excessive meltwater peaks in the records.
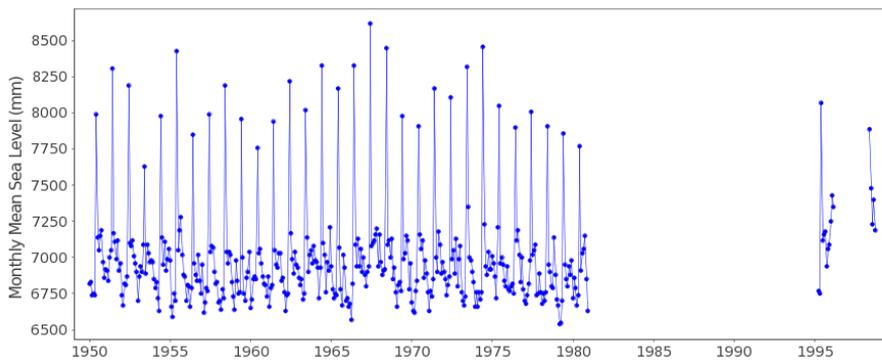
Figure 4.17: PSMSL record for the Ust Olenek tide gauge (ID 610, 73.00°N, 119.87°E), the most extreme case of June peak heights in the Arctic.

Extreme monthly differences

The monthly data contains some Russian-sector gauges affected by a combination of strong seasonal peaks and data availability only for the few months including and following this peak (being under ice for the rest of the year). Three Russian gauges exhibit this behaviour to a very strong degree, such that the mean value of the available month-to-month differences corresponds to a trend beyond $-1\,\mathrm{m/yr}$, a physically extremely implausible value. These three gauges are Uadei, Malysheva and Nemkova (PSMSL ID 709, 741 and 797, respectively), with Malysheva being the most extreme (see Fig. 4.19). Uadei and Malysheva are located at the coast of the Laptev Sea, while Nemkova is at the East Siberian Sea, at the mouth of the Indigirka River. Their locations are shown in Fig. 4.18.

Raw inclusion of such time series will obviously ruin a reconstruction based on monthly differences, and these stations therefore absolutely must be removed or very carefully processed if a good reconstruction is to be obtained.
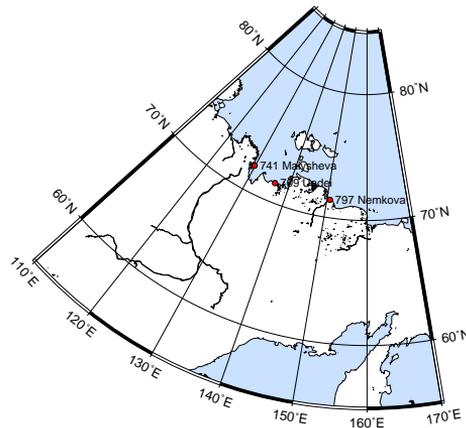
Figure 4.18: Locations of the gauges Uadei, Malysheva and Nemkova, which exhibit extremely high monthly differences.

4.4.2 Leverage

In addition to empirical criteria for selecting tide gauges, it is also possible to use approaches based in statistics. One such criterion could be *leverage*, which quantifies the influence of an observation upon the regression solution. More precisely, it is given as the variance of the response variable estimates.
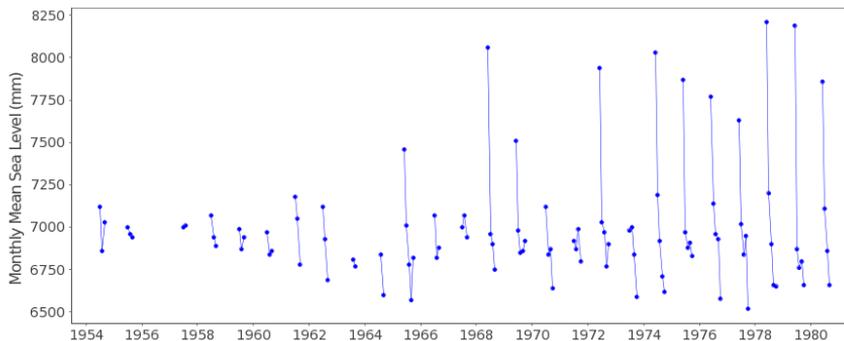
Figure 4.19: PSMSL record for the Malysheva tide gauge (ID 741), which
is covered in ice for most of the year, giving only data in the
summer months following a large meltwater peak. Note how this
gives consistently large negative month-to-month differences.

It is hoped that the computed leverage will help identify outliers among the tide
gauges, in order to obtain a more suitable selection of gauges for the reconstruction.

The leverage is given from the "hat matrix" of the regression, that is, the matrix
that relates the observations to their estimates:

$$\hat{\boldsymbol{y}} = \boldsymbol{X}\hat{\boldsymbol{\theta}}_{OLS} = \boldsymbol{X}(\boldsymbol{X}^{\mathsf{T}}\boldsymbol{X})^{-1}\boldsymbol{X}^{\mathsf{T}}\boldsymbol{y}$$

Then, the diagonal elements of the hat matrix $\boldsymbol{X}(\boldsymbol{X}^{\mathsf{T}}\boldsymbol{X})^{-1}\boldsymbol{X}^{\mathsf{T}}$ give the leverages
of the respective observations.

In this case, since we are using the RSOI model as in Kaplan et al. (1997) rather
than a simple least-squares fit, we estimate the leverage as the diagonal elements
of the matrix

$$\mathbf{HEPE}^{\mathsf{T}}\mathbf{H}^{\mathsf{T}}\mathbf{R}^{-1}$$

In the OLS case, the sum of the leverages will sum up to the number of param-
eters in the model; that is not the case for this regularized approach.

A common rule of thumb for "conspicuousness" of the observations is a leverage
of more than three times the mean leverage, meaning that such observations are
potential outliers.

Results

To illustrate leverage in Arctic sea level reconstruction, we consider a calibration period using Drakkar model data. Considering only data north of 68°N, we also exclude gauges with mean difference values equivalent of more than $\pm 2\,\mathrm{cm/yr}$ or less than 5 years of data in the reconstruction period. The gauges removed due to the trend criterion are listed in Table 4.3 (values are estimated after removal of seasonal harmonics, barometric contribution and GIA).

For convenience, the leverages of the individual gauges have been normalized so that the mean normalized leverage across all gauges is 1. The gauges with the highest and lowest mean leverages are listed in Table 4.4 and 4.5, respectively. The ranked, normalized leverages are also visualized in Fig. 4.20, and the time series for the gauges with the 5 highest leverages are shown in Fig. 4.21. Based on visual inspection of this, and bearing in mind the rule of thumb of three times the mean leverage, the reconstruction has been performed again with the two highest-leverage gauges (608 Vrangelia and 641 Kotelnyi) removed. It is notable that these two gauges have fairly good temporal coverage and no apparent datum shifts, possibly suggesting a local discrepancy in the GIA model.

Removing the two gauges from the reconstruction very slightly increases the root mean squared error for the fits across the Arctic gauges (from 0.128 m to 0.129 m), but lowers it the RMSE for a majority of gauges (63 gauges); see Fig. 4.22. While that result may seem interesting, it should be noted that simply omitting some gauges will make a better fit possible for the rest.

PSMSL ID	Name	Est. trend (m/yr)
524	VARDO	-0.0389
599	AMDERMA	-0.0219
604	AMBARCHIK	0.0303
605	RAU-CHUA	0.0220
606	PEVEK	-0.0233
609	MALYE KARMAKULY	-0.0312
653	POPOVA (BELYI OSTROV)	0.3390
654	LESKINA (LESKINA MYS)	-0.1505
709	UADEI	-1.3225
710	RUSSKAIA GAVAN II	0.0260
741	MALYSHEVA (MALYSHEVA OSTROV)	-2.4378
758	HAMMERFEST	-0.0426
784	RISOYHAMN	0.2539
797	NEMKOVA (NEMKOVA OSTROV)	-1.5140
863	RESOLUTE	-0.0259
890	CAPE SCHMIDT	-0.0370
901	CAPE ZHELANIJA	0.0554
909	POINT BARROW	-0.1243
1000	TUKTOYAKTUK	-0.1098
1132	CAMBRIDGE BAY	-0.0551
1282	CAPE PARRY	0.1146
1310	SACHS HARBOUR	0.1657
1399	BYKOV MYS (BYKOV MYS)	-0.0772
1414	SPENCE BAY	-0.0582
1419	IGLOOLIK	-0.1160
1421	NY-ALESUND	-0.0222
1497	NAIBA	0.0395
1820	ILULISSAT	0.0439
1822	LITTLE CORNWALLIS ISLAND	-0.0387
1857	PRUDHOE BAY, ALASKA	-0.0371
2025	BUGRINO	0.0466

Table 4.3: Arctic gauges removed due to trend criterion ($\pm 2 \, \mathrm{cm/yr}$). Trend computed as mean of available month-to-month differences.

Rank	PSMSL ID	Arctic gauge no.	Name	Mean leverage (normalized)
1	608	20	VRANGELIA	3.54
2	641	30	KOTELNYI	3.03
3	730	58	AION	2.74
4	541	9	BARENTSBURG	2.66
5	569	11	TIKSI	2.29
6	602	15	SANNIKOVA	2.28
7	642	31	KIGILIAH	2.09
8	917	77	SOPOCHNAIA KARGA	2.02
9	616	26	MYS SHMIDTA	1.93
10	650	36	CHETYREHSTOLBOVOI	1.90

Table 4.4: Tide gauges having the highest leverage (strong-trend gauges having been rejected in preprocessing).

Rank	PSMSL ID	Arctic gauge no.	Name	Mean leverage (normalized)
60	1019	82	SAGYLLAH-ARY	0.36
61	2028	106	TERIBERKA	0.35
62	687	49	MURMANSK II	0.35
63	601	14	FEDOROVA	0.34
64	1200	86	SE-LAHA	0.33
65	1382	91	JAN MAYEN	0.32
66	531	8	EVENSKJAER	0.28
67	655	41	RUSSKII	0.25
68	2026	104	MYS PIKSHUEVA	0.24
69	667	45	MARII PRONCHISHEVOI	0.20

Table 4.5: Tide gauges having the lowest leverage (strong-trend gauges having been rejected in preprocessing).
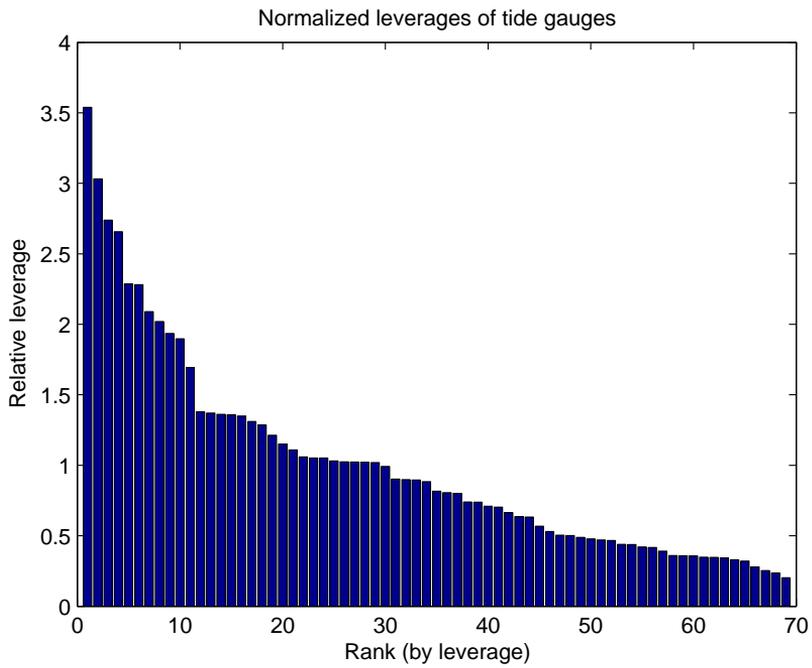
Figure 4.20: Leverages of the 69 gauges that fulfil the empirical criteria, sorted by descending leverage.
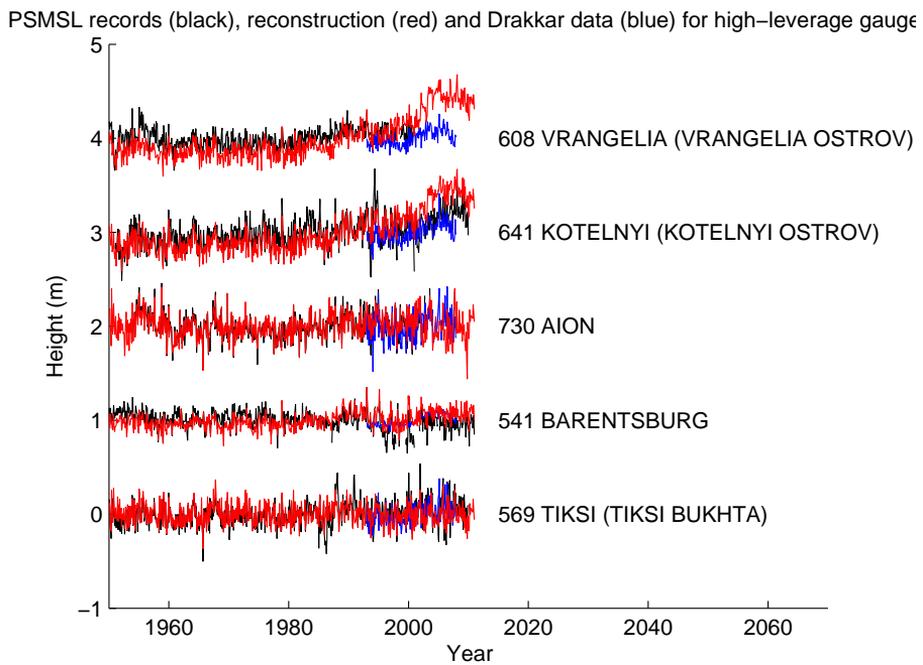
Figure 4.21: Measured (black) and reconstructed (red) time series for the highest-leverage gauges, along with corresponding Drakkar data (blue).
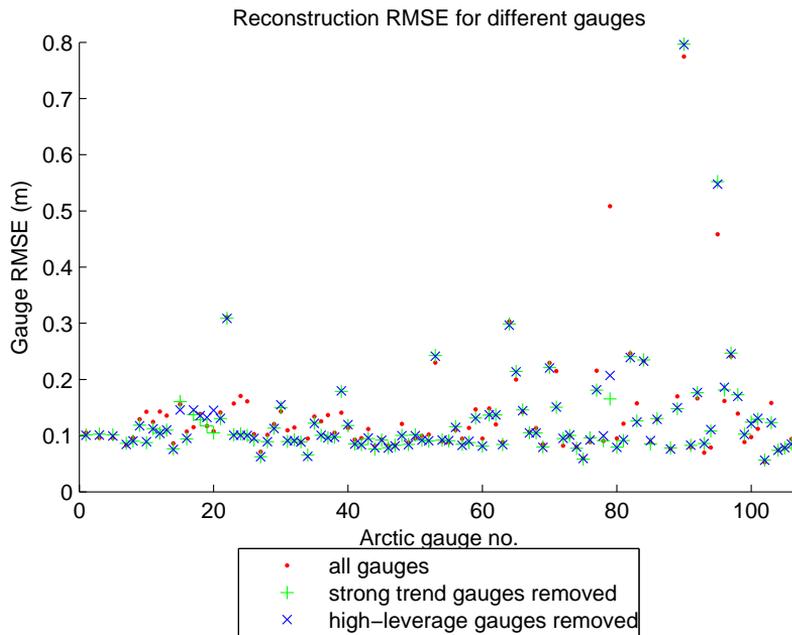
Figure 4.22: RMSE for reconstruction vs. tide gauge records for reconstructions based on different selections of tide gauges.

4.5 Reconstruction techniques

4.5.1 Regression

Assuming two datasets to be related by a linear equation, one may obtain the parameters for that linear equation through regression.

Defining a multivariate response variable $\mathbf{y}$, a predictor $\mathbf{X}$ and model parameters θ

$$\mathbf{y} = \mathbf{X}\theta + \mathbf{e}$$

where $\mathbf{e}$ is the residuals, we want to obtain the "best" estimate for θ. In an *ordinary least squares* (OLS) regression, this is obtained by the θ estimate $\hat{\theta}_{OLS}$ that minimizes the sum of squares of $\mathbf{e}$. It is defined by

$$\hat{\theta}_{OLS} = (\mathbf{X}^\mathsf{T}\mathbf{X})^{-1}\mathbf{X}^\mathsf{T}\mathbf{y}$$

For an OLS model, the covariance matrix (dispersion) of the model parameter estimates in $\hat{\theta}_{OLS}$ is given by

$$\mathrm{cov}(\hat{\theta}_{OLS}) = \sigma^2(\mathbf{X}^\mathsf{T}\mathbf{X})^{-1}$$

where σ is the root mean squared error (RMSE). The variance of the individual parameters θ_i is given by the diagonal elements of this matrix, so the standard error of these parameters, σ_{θ_i}, is given as the square roots of the diagonal elements.

There may be other concerns to take into account other than simply minimizing the residuals. In some cases, particularly with noisy data, solutions for θ may produce implausibly extreme values to accomodate the noise. This can be addressed using regularization, meaning that some measure of "extremeness" of the solution is punished. A common form of regularization is Tikhonov regularization, also known as "ridge regression". Instead of minimizing only the norm of the residuals, one minimizes a weighted combination of the norm of the residuals and norm of the solution. This gives us the following estimate for θ:

$$\hat{\theta}_{tikh} = (\mathbf{X}^\mathsf{T}\mathbf{X} + \lambda\mathbf{I})^{-1}\mathbf{X}^\mathsf{T}\mathbf{y}$$

where $\mathbf{I}$ is the identity matrix and λ is an adjustable scalar parameter.

Our reconstruction will use a slightly more elaborate form of ridge regression, see section 4.5.2.

4.5.2   Kaplan et al.'s optimal interpolation

The canonical technique for satellite- and tide gauge-based sea level reconstruction is established in Church et al. (2004). The technique comprises an EOF decomposition of a calibration period of satellite altimetry, which yields spatial patterns that are fitted to tide gauge records. The fit is made using an optimal interpolation (OI) technique described in Kaplan et al. (1997, 1998, 2000), which respectively reconstruct sea-surface temperature, temperature and pressure.

Here, we will follow the notation of Christiansen et al. (2010), as that paper is very specific and elaborate regarding nomenclature and description of variables. As the technique is based on two parts, a calibration from altimetry, and a reconstruction based on tide gauges, we will need two primary datasets. For clarity, these are elaborated in Table 4.6.

Dataset	Name/size	Description
Calibration data (altimetry)	$\mathbf{X}(n \times m)$	Data matrix of heights at n grid points, sampled at m points in time.
Tide gauges	$\mathbf{G}(N \times M)$	Data matrix of heights at N tide gauges, sampled at M points in time.

Table 4.6: The primary datasets used in the reconstruction.

The timespan of our reconstruction will correspond to the M temporal points of the tide gauge dataset, while spatially covering the n pixels of the calibration dataset.

The covariance of the calibration data $\mathbf{X}$ is the matrix $\mathbf{C}(n \times n)$. We will select the l leading eigenfunctions (spatial patterns) of the calibration data. These will form the columns of a matrix $\mathbf{E}(n \times l)$, which will be the basis of our reconstruction.

The calibration covariance matrix and the eigenfunctions are related by

$$\mathbf{C} = \mathbf{E}\mathbf{\Lambda}\mathbf{E}^{\mathsf{T}} + \mathbf{E}'\mathbf{\Lambda}'\mathbf{E}'^{\mathsf{T}}$$

where $\mathbf{E}$ and $\mathbf{\Lambda}$ are the l retained eigenfunctions and eigenvalues of $\mathbf{C}$ ($\mathbf{\Lambda}$ is a diagonal matrix). Correspondingly, $\mathbf{E}'$ and $\mathbf{\Lambda}'$ contain the $(n - l)$ discarded eigenfunctions and eigenvalues. In practice, $\mathbf{E}$ and $\mathbf{\Lambda}$ will be obtained from a singular value decomposition (SVD) of $\mathbf{X}$ if possible, as it is much less memory-intensive for $n \gg m$.

Having obtained $\mathbf{E}$, we shall solve for coefficients $\alpha(l \times M)$, that is, a scalar coefficient for each eigenfunction per timestep.

To connect the two datasets in an appropriate way, an indicator matrix $\mathbf{H}(N \times n)$ is introduced. The matrix will be zero everywhere, except at $\mathbf{H}_{j,k} = 1$ where j is the tide gauge index, and k is the index of its closest pixel in the calibration grid. For this reconstruction, we use the great-circle distance, allowing up to 500 km distance between gauge and pixel, and otherwise discarding the tide gauge.

A simple, traditional least-squares solution for α can be obtained by defining a cost function

$$(\mathbf{HE}\alpha - \mathbf{G})^{\mathsf{T}}(\mathbf{HE}\alpha - \mathbf{G})$$

In effect, we punish mismatch between the reconstructed time series at the tide gauges ($\mathbf{HE}\alpha$) and the actual tide gauge records ($\mathbf{G}$). The cost function is minimized by the traditional ordinary least squares solution:

$$\alpha = ((\mathbf{HE})^{\mathsf{T}}\mathbf{HE})^{-1}(\mathbf{HE})^{\mathsf{T}}\mathbf{G}$$

However, as in Kaplan et al. (1997), we introduce a regularization term to dampen higher-order EOFs, so that the cost function becomes (still in the notation of the Christiansen et al. (2010)):

$$(\mathbf{HE}\alpha - \mathbf{G})^{\mathsf{T}}\mathbf{R}^{-1}(\mathbf{HE}\alpha - \mathbf{G}) + \alpha^{\mathsf{T}}\mathbf{\Lambda}^{-1}\alpha$$

The matrix $\mathbf{R}(N \times N)$ is the error covariance matrix, that is, the sum of the observation error covariance and the truncation error. In this case, for simplicity, $\mathbf{R}$ is set to a diagonal matrix with its nonzero elements set at 3 cm; in Christiansen et al. (2010), only the truncation error contribution is considered. Kaplan et al. (1997) note that non-independence in the observational error would increase the effective observation error, but that they had no information substantially suggesting anything but independence.

Minimizing the cost function, one obtains the solution for α:

$$\boldsymbol{\alpha} = \mathbf{PE}^{\mathsf{T}}\mathbf{H}^{\mathsf{T}}\mathbf{R}^{-1}\mathbf{G}$$

where

$$\mathbf{P} = (\mathbf{E}^{\mathsf{T}}\mathbf{H}^{\mathsf{T}}\mathbf{R}^{-1}\mathbf{HE} + \mathbf{\Lambda}^{-1})^{-1}$$

To capture changes in mean sea level, the basis $\mathbf{E}$ is augmented with a uniform pattern, i.e. a column of ones, called "EOF0". This leaves the issue of which corresponding "eigenvalue" to use; we have used the same value as for EOF1 like

Church et al. (2004) (N. White, personal communication). Christiansen et al. (2010) set the corresponding eigenvalue to infinity, eliminating damping for the mean sea level fit.

In order to clearly distinguish mean sea level changes from water redistribution, Church et al. (2004) subtract the (area-weighted) mean from each eigenfunction, except of course EOF0. That is, since all other patterns have spatial mean 0, the coefficients of EOF0 will capture all changes in mean sea level.

4.5.3 Sea-level-specific adaptations

The PSMSL tide gauges, while a uniquely valuable resource of sea level records, generally suffer from a lack of robust, absolute vertical reference; the tide gauge records are provided in individual, generally unknown vertical datums. Church et al. (2004) remedy this by using the differences between neighboring timesteps of the tide gauge records and fitting to those, then temporally integrating the α coefficients to obtain the reconstruction.

A different approach is discussed in Ray and Douglas (2011), where no differencing is used, and instead one uses the original tide gauge records and solves for the vertical datum of each individual tide gauge as part of the solution. This is done to address the integration error that can accumulate as one moves back in time, as nothing forces the reconstruction back to reality when errors appear in α. However, datum shifts in the time series may then need more careful handling — possibly by splitting the tide gauge record into several records — whereas suspected datum shifts can simply be skipped when using the differenced time series method.

For the purposes of tide gauge-/altimetry-based reconstruction, we need further datasets in addition to the altimetry and tide gauges, as they describe slightly different physical properties. Satellite altimetry provides sea-level heights with respect to a global reference frame, whereas tide gauges provide *relative sea level* (i.e. sea level with respect to the local continental crust) (Cazenave et al., 1999). To make the two datasets comparable, in the sense of describing the same physical quantity, we apply inverse barometric (IB) and glacial isostatic adjustment (GIA) corrections to the tide gauge dataset.

The barometric data is taken from the HadSLP2 dataset (Allan and Ansell, 2006), in this case obtained from NOAA's Earth System Research Laboratory[1]. The dataset is a sea-level pressure anomaly reconstruction on a $5° \times 5°$ grid,

---

[1] http://www.esrl.noaa.gov/psd/gcos_wgsp/Gridded/data.hadslp2.html

interpolated to the tide gauge locations.

GIA corrections were made using the Peltier dataset available from the PSMSL website[2], specifically the current-day predicted rate-of-change contribution to relative sea level at each tide gauge location. The dataset is based on ice model ICE-5G v1.3 with the VM2 earth model (Peltier, 1998, 2004, 2005).

A significant adaptation of the technique from Church et al. (2004) is necessary when reconstructing Arctic sea level, as the tide gauge records are too short and scattered for the reconstruction to demand continuous time series throughout the period 1950 to today. To extract as much information as possible from the tide gauge dataset, we solve for the α coefficents once per timestep (rather than all at once), with a time-variable $\mathbf{H}$ matrix that selects the available tide gauges at that point in time.

4.5.4 Regularization

The regularization is based upon the eigenvalues of the calibration covariance, and thus is closely related to the explained variance of the EOF modes.

4.5.5 Estimating uncertainties

There are several ways to estimate uncertainties in the reconstruction; one example could be cross-validation, e.g. a leave-one-out scheme, performing the reconstruction once for each tide gauge with that gauge omitted.

4.5.6 Rationale for choice of technique

In Christiansen et al. (2010), a comparison is made between five different approaches: simple regression (the "projection method") with and without EOF0, Kaplan et al.'s regularized approach with and without EOF0, and a simple mean of the tide gauges. They concluded that the inclusion of EOF0 causes a much improved reconstruction of the trend and lower sensitivity to the calibration period length.

However, Calafat et al. (2014) point out that while including EOF0 much improves the reconstruction of the trend, it significantly affects the reconstruction

---

[2]http://www.psmsl.org/train_and_info/geo_signals/gia/peltier/
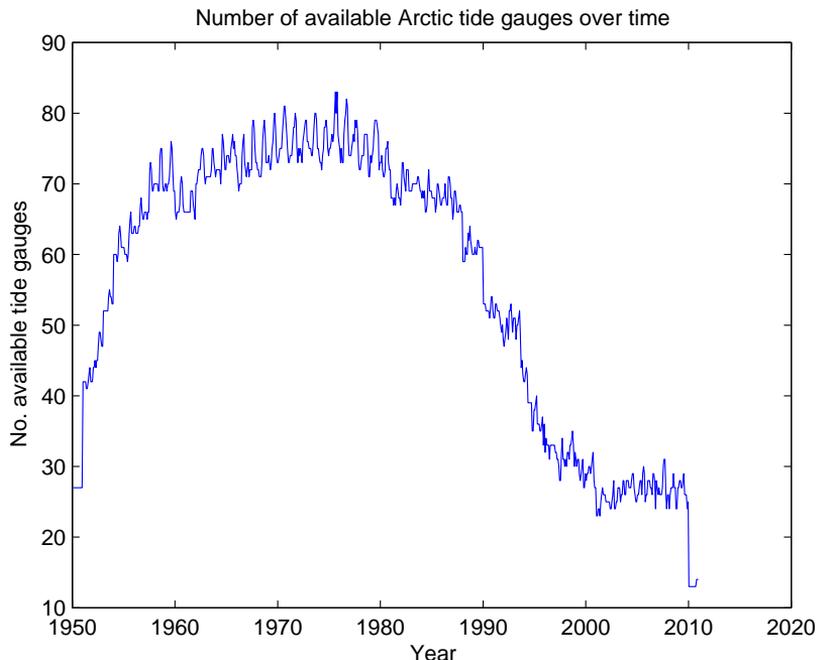
Figure 4.23: Number of gauges above 68°N with data available, as a function of time.

of the internal variability of the climate system; the reconstructed mean sea level, when including EOF0, is essentially a simple mean of the tide gauge records, while an improved reconstruction of the interannual variability (specifically, in their case, ENSO) can be achieved by omitting the EOF0.

A simple mean of the tide gauges above 68°N is shown in Fig. 4.24; compare with the number of available tide gauges at a given time (Fig. 4.23).

4.5.7   Adaptations for Arctic sea level

For the Arctic Ocean, Pavlov (2001) found increasing regional variability since the 1980s using tide gauges from the Russian sector, and altimetry-era data indicate an increase in sea level largely concentrated in the Beaufort Gyre (Giles et al., 2012). Thus, we expect a sea level reconstruction for the Arctic area to exhibit mostly stationary behaviour until the 1980s, with sea level rise from approx. 1995 (or earlier) in the Beaufort Gyre area; these two constraints may
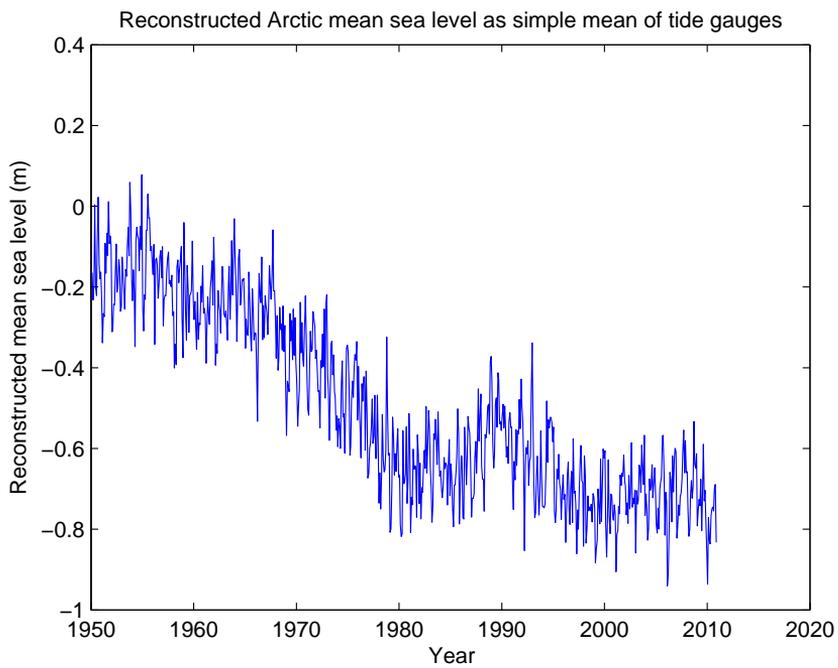
Figure 4.24: Reconstructed mean sea level above 68°N using simple means of available tide gauge records, corrected for GIA and barometric contribution.

be difficult to satisfy using only EOFs and tide gauges, as the latter does not particularly affect coastal areas.

To address this, one may introduce virtual tide gauges, with records extracted from altimetry, so that the reconstruction is driven also by some mid-ocean data. This way, the reconstruction becomes more of a data assimilation.

CHAPTER 5

Results and discussion

A variety of reconstructions have been made over the course of this project as methods were refined. For most of the project, EOFs (and MAFs) from Drakkar ocean model data has been used for calibration, whereas altimetry data were introduced fairly late in the project. For this reason, some of the analyses are discussed here only for Drakkar data and have not been remade with altimetry data due to time constraints.

It was discovered during the project that the Drakkar data contains fairly extreme trends in the Arctic (see section 2.4.2). Also, much time was spent trying to stabilize the model, with focus eventually shifting from EOF/MAF comparison to criteria for tide gauge inclusion (including leverage), and finally towards the use of the datum-fit method of Ray and Douglas (2011) and inclusion of virtual tide gauges.

Thus, sections 5.1 and 5.2 discuss results obtained with the cumulated differences approach and not the datum-fit approach, as well as using Drakkar model data for calibration, rather than altimetry; section 5.3 uses both Drakkar and altimetry data. A more refined, systematic method comparison using altimetry EOFs is given in section 5.4.

5.1   MAF-based reconstruction

Due to concerns of the effects of gaps in the data, particularly when using the MAF decomposition, the Arctic sea level reconstruction has been performed using Drakkar ocean model fields (Barnier et al., 2006), using only data from the altimetry era (1993–2007).

The reconstruction includes the 8 leading modes, in addition to the "MAF0"; this choice is for similarity with the EOF-based analysis. Both the Drakkar and tide gauge data have a cutoff latitude at 68°N, and gauges with a mean timestep difference value of more than 2 cm/yr have been removed.

Only a T-MAF-based reconstruction has been performed here, the spatial MAF caused some computational issues (non-real results).

5.1.1   Mean sea level

As reconstructed mean sea level is generally dominated by the spatially uniform pattern ("EOF0"/"MAF0") (Christiansen et al., 2010; Calafat et al., 2014), using MAFs instead of EOFs in the reconstruction should not in itself affect the overall character of the results too much. However, regularization is an important consideration, and as the MAF0 has been assigned the same "eigenvalue" as MAF1, it is also affected by the results from the decomposition.

From Fig. 5.1, it may seem that the reconstructed mean sea level from the T-MAF analysis is usable, even if it gives a somewhat larger trend (4.3 mm/yr over the 60 years compared to 2.3 for the EOF-based reconstruction). However, as Fig. 5.2 shows, the reconstruction includes highly physically implausible features, such as a 3-meter increase in sea level over the 60-year period.

5.1.2   Regularization

The reconstruction is in general highly sensitive to the choice of regularization. An EOF-based reconstruction will yield a broadly similar MSL if similar eigenvalues are forced upon it.

If an unregularized least-squares fit is used, the reconstruction will break down entirely, both with EOF and MAF basis.
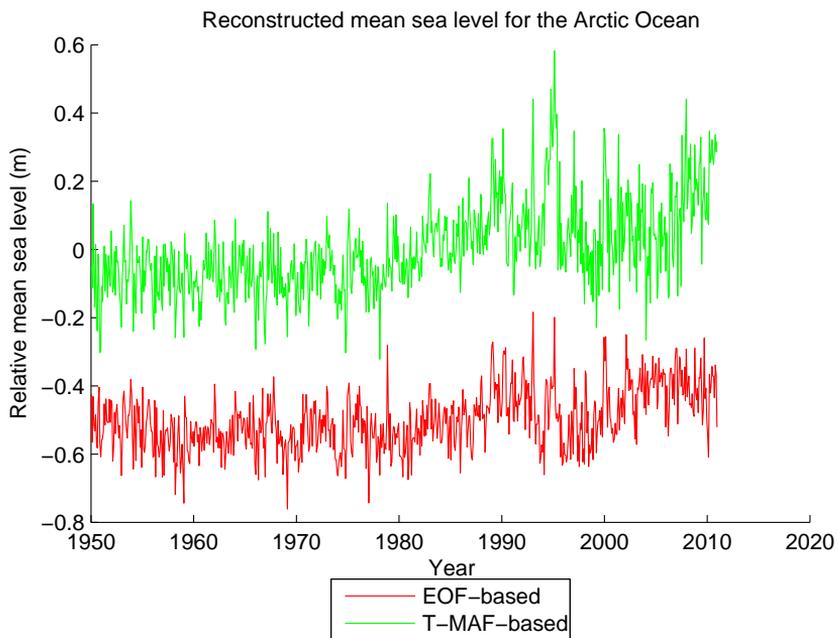
Figure 5.1: Reconstructed mean sea level above 68°N using the 8 leading modes from Drakkar fields, using a traditional EOF-based analysis, and T-MAFs for the basis, respectively.
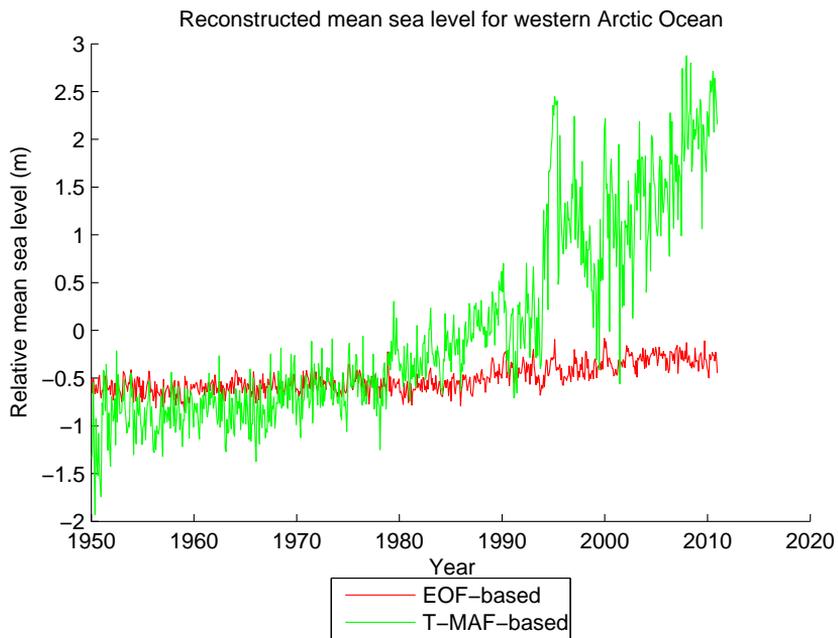
Figure 5.2: Reconstructed mean sea level for the western Arctic Ocean. Note the highly implausible sea level rise of about 3 meters in 60 years.
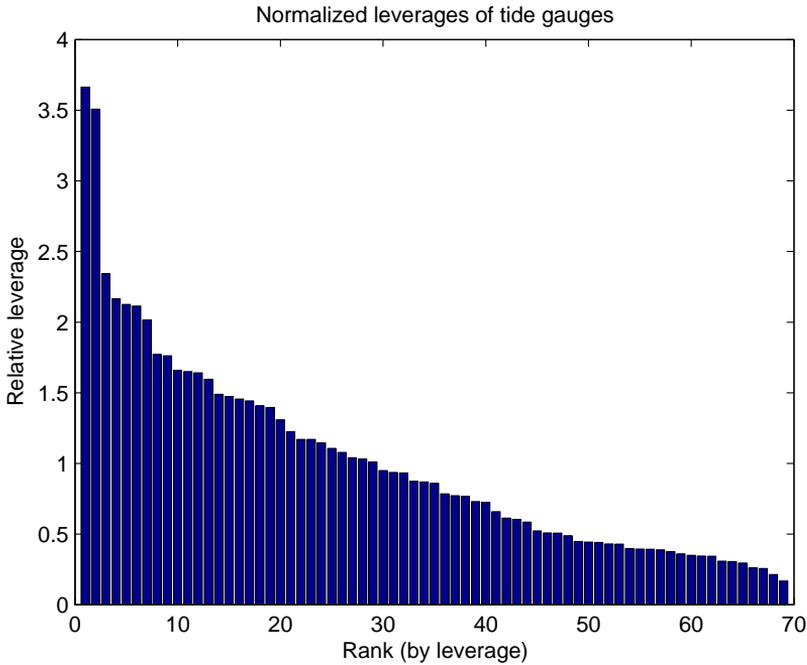
Figure 5.3: Leverages of the Arctic gauges when used in a T-MAF-based reconstruction.

5.1.3 Tide gauge correspondence and influence

Ranked, normalized leverages for the Arctic gauges in the T-MAF-based reconstruction are shown in Fig. 5.3. Clearly, two gauges stand out as being influential, having more than three times the main leverage. These two gauges are 608 Vrangelia (on Wrangel Island, north of East Siberia) and 541 Barentsburg (on Svalbard). While this is quite consistent with results from an EOF-based reconstruction, in this case careful consideration of the regularization would be much more important in stabilizing the reconstruction.

The root mean squared errors (RMSE) for each gauge in the T-MAF reconstruction are shown in Fig. 5.4. Whereas a traditional EOF-based reconstruction gives a mean RMSE of 12.8 cm across the gauges, the T-MAF yields 16.9 cm. While this increase seems rather moderate, some gauges show much more strongly increased RMSE (cf. Fig. 5.4).

Similarly, a traditional reconstruction gives a mean correlation coefficient of
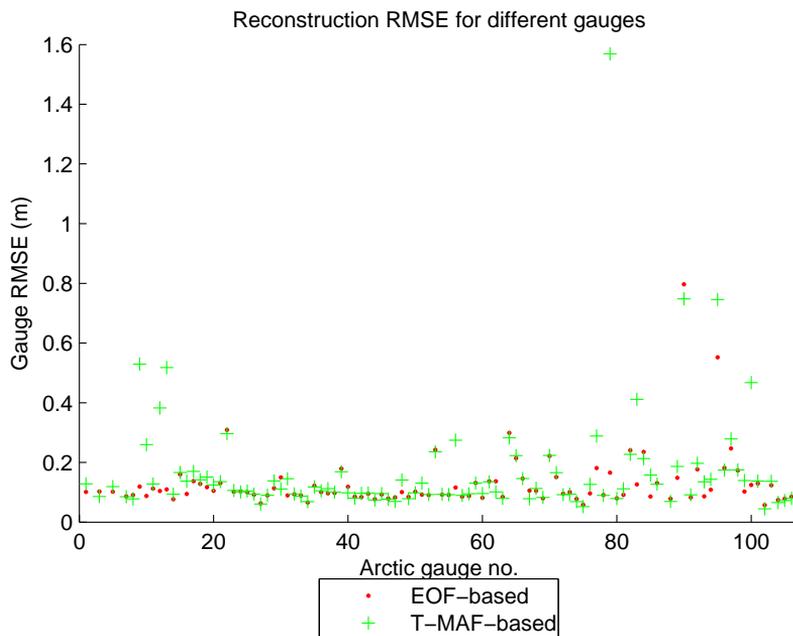
Figure 5.4: RMSE for all included gauges when using EOF and T-MAF patterns in the basis, respectively.

0.592 across the gauges, using T-MAF yields a poorer correspondence, with a mean correlation coefficient of 0.547, and with some gauges being considerably worse, see Fig. 5.5.

In summary, the difficulty in achieving non-noisy spatial patterns with

Reconstruction correlation for different gauges
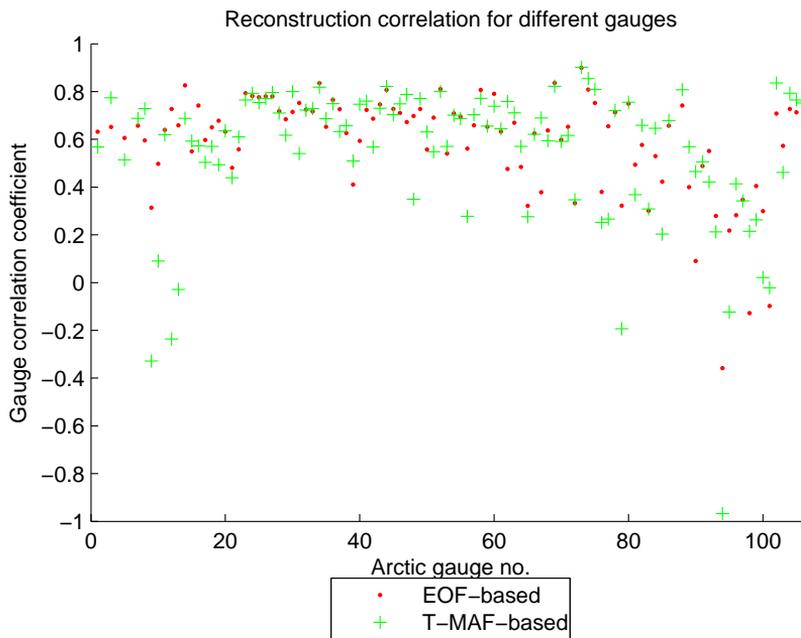
Figure 5.5: Correlation coefficients for all included gauges when using EOF and T-MAF patterns in the basis, respectively.

5.2 Sensitivity to gauge inclusion criteria

Very few published studies to date have addressed reconstructed sea level for the whole Arctic prior to the altimetry era. Generally, most are restricted to particular sectors (typically Russian and/or Norwegian) and do not discuss sea level in poorly studied sectors or the areas covered by ice. Thus, when assessing reconstructed mean sea level in the Arctic, it seems most appropriate to compare with a combination of regional data (where available) and general knowledge of the physics of the Arctic Ocean.

Due to the extreme characteristics of many Arctic tide gauges, which make them unrepresentative for the open ocean, the selection criteria for these are paramount in obtaining a good reconstruction. Fig. 5.6 shows the resulting reconstructed developments in Arctic mean sea level with three different threshold values for the mean month-to-month differences in the gauge time series. It is apparent that the reconstruction is destabilized when this threshold is set higher than approx. $\pm 2 \, \text{cm/yr}$. Therefore, we will choose $\pm 2 \, \text{cm/yr}$ as our threshold to include as much data as possible.

The reconstructed mean sea level using altimetry-era Drakkar fields for calibration is illustrated in Fig. 5.7. It is clear that we obtain a more or less stable sea level until about 1980, while the Drakkar data yield an increasing trend all the way back to 1950. Trends for different various timespans of our reconstruction are listed in Table 5.1.

Period	Trend (mm/yr)
1958–2006 (entire period)	2.25 ± 0.33
1958–1980	-0.53 ± 0.81
1980–2006	4.04 ± 0.96
1993–2006	7.59 ± 2.22

Table 5.1: Trends for various time periods of our reconstruction (above $68°$N, calibration with altimetry-era Drakkar fields).

The large uncertainty on GIA estimates for the Arctic Ocean is another major consideration in terms of validity of the results; this was studied in detail in Huang et al. (2013). While the GIA trend contribution for tide gauge records is large and uncertain ($-1.88 \pm 1.02 \, \text{mm/yr}$), it is less relevant for altimetry fields ($0.15 \pm 0.11 \, \text{mm/yr}$. In the present context, GIA correction is considered a preprocessing step for the tide gauge data, and thus some gauges may appear as outliers due to poor GIA estimates.

Reconstructed Arctic Ocean MSL for different trend thresholds
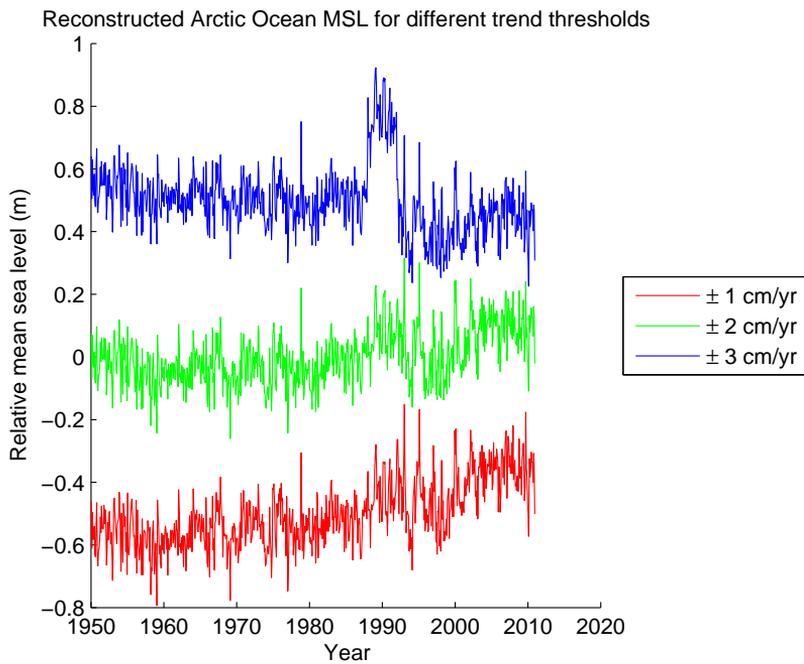
Figure 5.6: Reconstructed mean sea level above 68°N, with Drakkar fields (1993–2007) for calibration, with various trend-threshold criteria for inclusion of tide gauges.
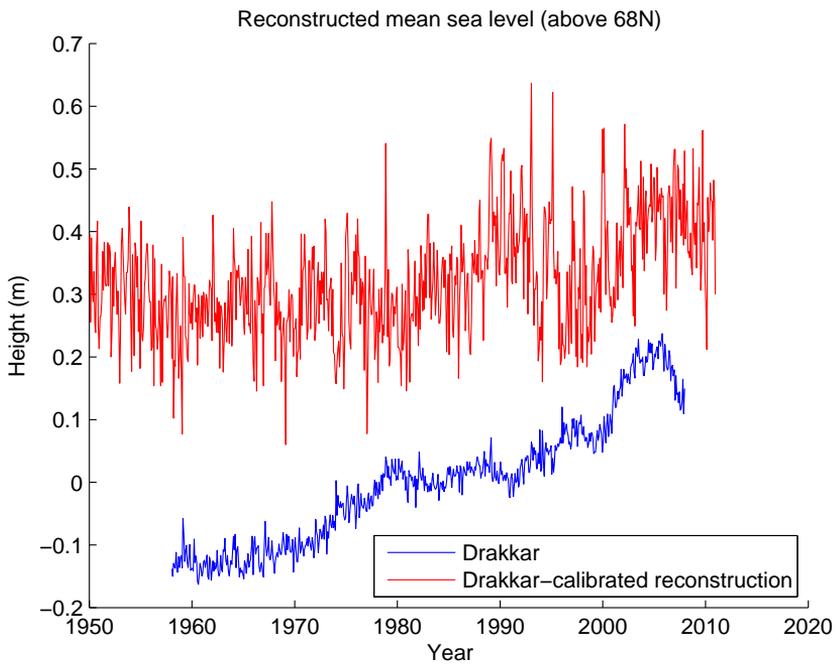
Figure 5.7: Mean sea level of tide-gauge-based, Drakkar-calibrated reconstruction vs. the mean sea level of the entire Drakkar dataset. Arbitrary vertical offset.

5.3 Reconstructed decadal means (Drakkar- and altimetry-based)

For comparison with the decadal sea level anomalies estimated in Pavlov (2001), maps of decadal means for the present reconstruction have been made, both with Drakkar as calibration (Fig. 5.8) and with altimetry calibration (Fig. 5.9). The most striking feature of both is a dramatic increase in sea level in the Beaufort Gyre area, as would be expected from the increased freshwater content there. The sea level in the reconstruction for that area increases by nearly 1 m from the 1980s to the 2000s, or nearly $+5\,\mathrm{cm/yr}$, a rather high value.

For the Drakkar-based reconstruction, a slight rise between the 1970s and 1980s is obtained for the East Siberian Sea, coinciding with a sea level fall around the Beaufort Gyre. This is consistent with the modelling results in Pavlov (2001).

Decadal means for an altimetry-calibrated reconstruction (using 8 EOFs) are shown in Fig. 5.9. It also exhibits about 1 m of sea level rise in the Beaufort Gyre from the 1980s to the 2000s.

A reconstruction calibrated with altimetry fields (Fig. 5.10) and including 50 virtual tide gauges shows an increasing trend around Greenland, while a strong downward trend results in the Russian and Canadian sector; there is little upward trend in the Beaufort Gyre. Even though this would be expected to drive the reconstruction closer to reality, this reconstruction seems less plausible than without virtual tide gauges.

Finally, to test the effect of longer records in the virtual tide gauges, the reconstruction has been performed using altimetry EOFs and virtual tide gauges using Drakkar data, replaced with altimetry where available. This results (Fig. 5.11) in a moderate increase in sea level in the Beaufort Gyre, accompanied by a considerable rise in the East Siberian Sea, and a very strong fall (about 50 cm in 50 years) in the Canadian Arctic Archipelago. It should be noted that this approach cannot be recommended due to the large discrepancy between Drakkar and altimetry data.
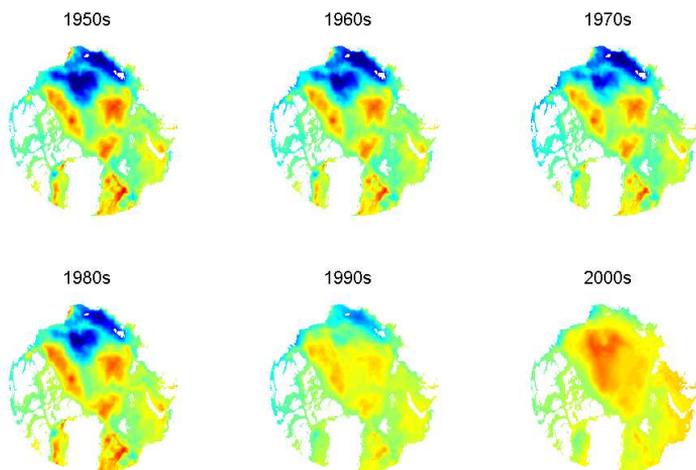
Figure 5.8: Decadal sea level means for a reconstruction based on Drakkar
fields (1993–2007). The colour scale ranges from −0.5 m (dark
blue) to 0.5 m (dark red); the fields are relative to an arbitrary
MDT.
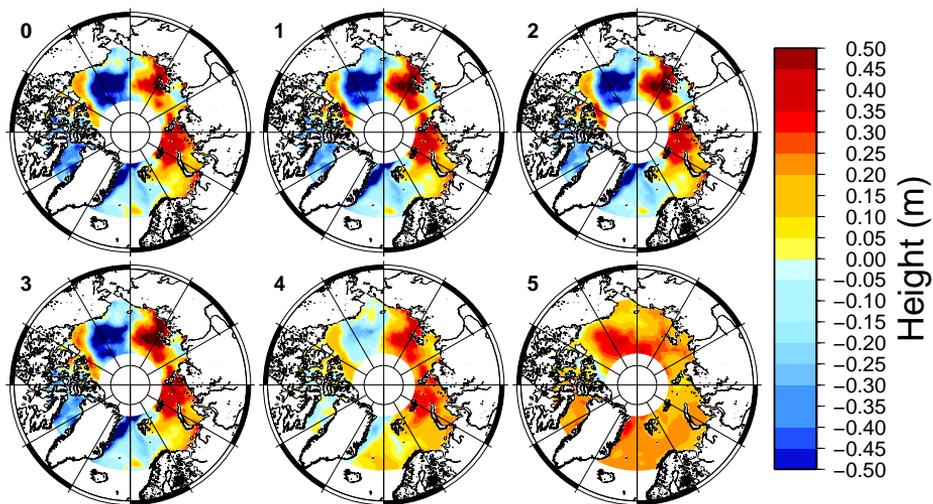
Figure 5.9: Decadal sea level means (1950s through 2000s) for a reconstruction
based on altimetry fields. The heights are relative to an arbitrary
MDT.
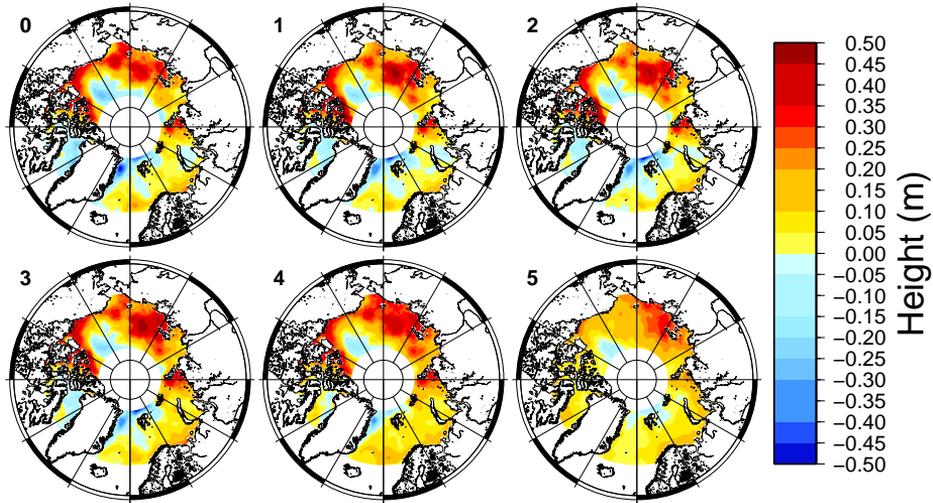
Figure 5.10: Decadal sea level means (1950s through 2000s) for a reconstruction based on altimetry fields. 50 randomly placed virtual tide gauges were included. The heights are relative to an arbitrary MDT.
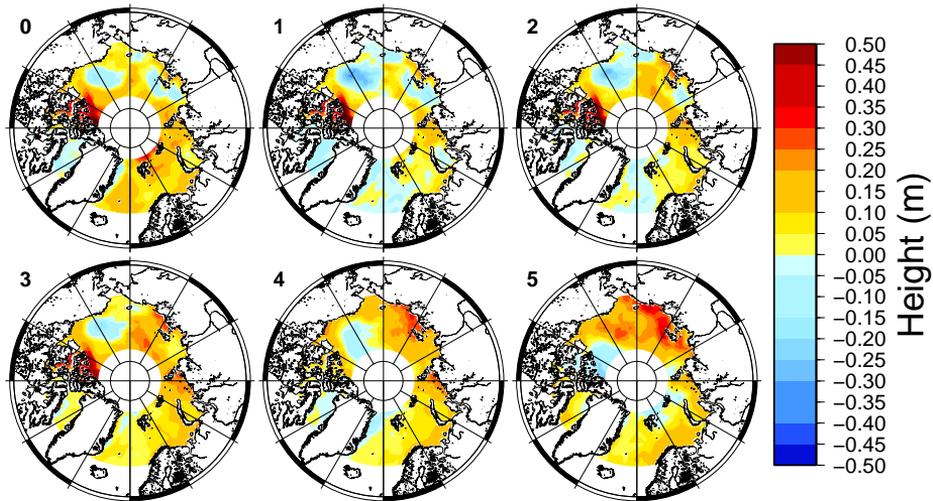
Figure 5.11: Decadal sea level means (1950s through 2000s) for a reconstruction based on altimetry EOFs. 50 randomly placed virtual tide gauges were included, with records extended back in time using Drakkar data. The heights are relative to an arbitrary MDT.

5.4   Reconstruction method comparison (altimetry-based)

To compare results from a reconstruction using cumulated differences (as Church et al. (2004)) and a reconstruction using the full time series, solving for the tide gauge datums, as in Ray and Douglas (2011), a reconstruction suite of 18 different approaches has been set up. We consider only data north of 68°N, and tide gauges with a trend within $\pm 2\,\mathrm{cm/yr}$. The two overall methods have each been implemented using EOF0 and EOF1–8 from altimetry, as well as using only the EOF0. All use the regularized (OI) method, except where noted.

The resulting MSL trends for all the reconstructions tried is given in Table 5.2. It includes MSL trends for the pre-altimetry period, the altimetry period and for the entire reconstruction period. As the reconstructions appear less stable prior to about 1958–1960 (where many tide gauge records begin), trends for the period 1960–2010 are also given.

The different approaches in Table 5.2 show the effects on MSL of using annual tide gauge data rather than monthly, of not using regularization of the EOFs (the "projection method" in Christiansen et al. (2010)), of splitting the tide gauge records at suspected datum shifts, and of introducing virtual tide gauges from altimetry.

It is immediately apparent from Figs. 5.12 and 5.13 that the datum-fit reconstructions are much more mutually consistent than those using cumulated differences. An interesting observation from Table 5.2 is an apparent consistent slight fall in sea level before 1980 (as also described in Henry et al. (2012)), and a quite consistent rise of 3 to 6 mm/yr between 1980 and 1993.

It seems that using an unregularized fit does not make much difference compared to the OI fit, and the use of annual rather than monthly data also does not affect the reconstructed MSL much.

| Method	1950–1980	1960–1980	1980–1993	1993–2012	1995–2010	1950–2010	1960–2010
Cum. diffs, EOF0 only	-1.2 ± 0.6	-1.8 ± 1.1	4.3 ± 2.1	-1.5 ± 1.1	0.9 ± 1.4	0.3 ± 0.2	0.4 ± 0.3
Cum. diffs, EOF0–8	0.1 ± 0.6	-1.3 ± 1.1	3.1 ± 1.9	3.2 ± 2.1	5.0 ± 2.6	3.4 ± 0.3	4.3 ± 0.4
Cum. diffs, EOF0–8, no regularization	1.0 ± 0.6	-0.4 ± 1.1	2.2 ± 2.0	6.0 ± 3.4	6.8 ± 4.5	4.5 ± 0.4	5.5 ± 0.6
Cum. diffs, EOF0–8, annual t.g. data	-1.4 ± 0.4	-1.8 ± 0.7	4.1 ± 1.5	-1.8 ± 0.9	-1.2 ± 1.2	-0.1 ± 0.2	-0.0 ± 0.2
Cum. diffs, EOF0–8, 50 virtual gauges	0.1 ± 0.6	-1.3 ± 1.0	3.1 ± 1.9	11.6 ± 0.9	10.9 ± 1.2	4.1 ± 0.3	5.3 ± 0.4
Cum. diffs, EOF0–8, 100 virtual gauges	0.1 ± 0.6	-1.3 ± 1.0	3.2 ± 1.9	23.6 ± 0.8	24.4 ± 1.1	5.9 ± 0.4	7.8 ± 0.5
Cum. diffs, EOF0–8, 200 virtual gauges	0.1 ± 0.6	-1.3 ± 1.0	3.2 ± 1.9	15.1 ± 0.8	15.7 ± 1.1	3.9 ± 0.3	5.0 ± 0.4
Cum. diffs, EOF0–8, split at gaps	0.1 ± 0.6	-1.3 ± 1.0	3.1 ± 1.9	3.2 ± 2.1	5.0 ± 2.6	3.4 ± 0.3	4.3 ± 0.4
Cum. diffs, EOF0–8, split at jumps	-7.0 ± 0.9	-12.0 ± 1.7	-5.2 ± 2.7	-9.4 ± 1.7	-7.2 ± 2.0	-4.8 ± 0.3	-5.1 ± 0.4
Datum fit, EOF0 only	-0.5 ± 0.6	-0.5 ± 1.2	5.5 ± 2.1	1.7 ± 1.1	3.7 ± 1.4	1.6 ± 0.2	2.0 ± 0.3
Datum fit, EOF0–8	-0.4 ± 0.6	-0.6 ± 1.0	6.1 ± 2.0	-0.5 ± 1.7	2.0 ± 2.4	1.2 ± 0.2	1.5 ± 0.3
Datum fit, EOF0–8, no regularization	-0.6 ± 0.6	-0.6 ± 1.1	6.0 ± 2.0	-0.2 ± 1.9	2.4 ± 2.7	1.2 ± 0.3	1.5 ± 0.3
Datum fit, EOF0–8, annual t.g. data	-0.5 ± 0.4	-1.1 ± 0.7	5.8 ± 1.6	-2.1 ± 1.6	-2.0 ± 2.4	0.8 ± 0.2	0.9 ± 0.3
Datum fit, EOF0–8, 50 virtual gauges	-0.5 ± 0.6	-0.6 ± 1.0	5.5 ± 2.0	1.9 ± 0.7	2.0 ± 1.0	1.2 ± 0.2	1.5 ± 0.2
Datum fit, EOF0–8, 100 virtual gauges	-0.6 ± 0.6	-0.6 ± 1.1	5.6 ± 2.0	1.8 ± 0.8	1.8 ± 1.1	1.2 ± 0.2	1.5 ± 0.3
Datum fit, EOF0–8, 200 virtual gauges	-0.6 ± 0.6	-0.6 ± 1.1	5.7 ± 2.0	1.9 ± 0.9	1.8 ± 1.2	1.2 ± 0.2	1.5 ± 0.3
Datum fit, EOF0–8, split at gaps	-0.1 ± 0.6	-0.5 ± 1.1	9.0 ± 2.0	5.3 ± 1.8	2.2 ± 2.3	2.0 ± 0.2	2.4 ± 0.3
Datum fit, EOF0–8, split at jumps	0.4 ± 0.6	0.4 ± 0.9	4.5 ± 2.1	-5.6 ± 1.7	-5.0 ± 2.3	-0.8 ± 0.3	-1.5 ± 0.4

Table 5.2: Reconstructed MSL trends (mm/yr) for areas between 68°N and 82°N, using altimetry for calibration.
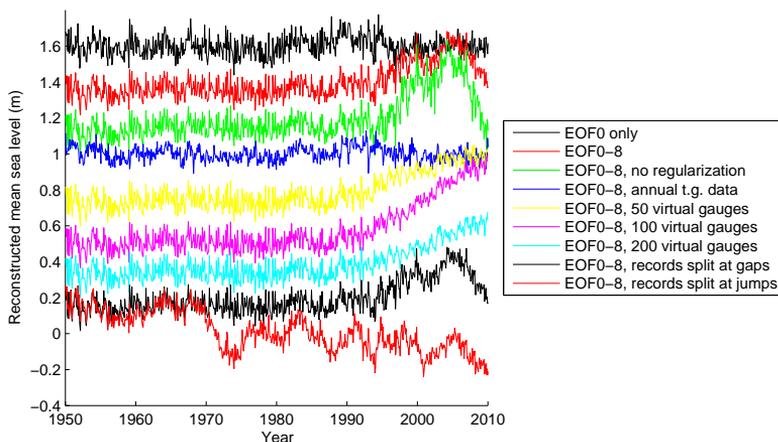
Figure 5.12: Reconstructed mean sea levels between 68°N and 82°N for a variety of approaches using cumulated timestep differences. (Arbitrary vertical offsets)
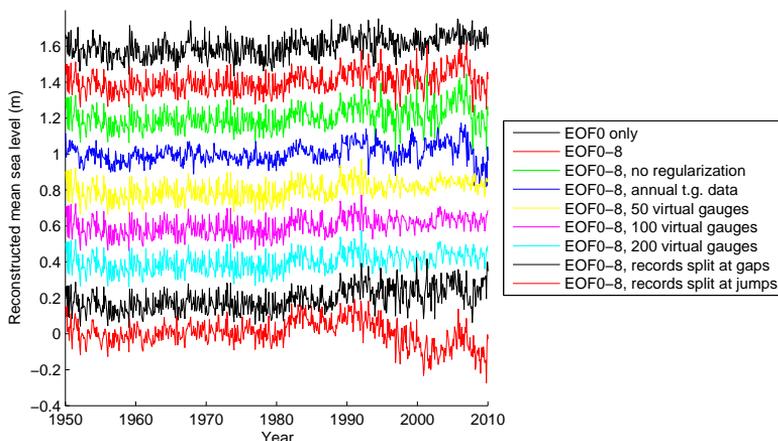
Figure 5.13: Reconstructed mean sea levels between 68°N and 82°N for a variety of approaches using the datum-fit method. Note the relative similarity between the curves compared to Fig. 5.12. (Arbitrary vertical offsets)

5.4.1   Inclusion of virtual tide gauges

To investigate the effect of including a number of altimetry time series as if they were tide gauge records, reconstructions have been made using 50, 100 and 200 virtual tide gauges at random locations in the altimetry dataset. While the inclusion of the virtual gauges makes a significant difference compared to not including them, the reconstruction does not appear very sensitive to the number of virtual gauges used. For an easier overview, a relevant subset of the reconstructed trends is given in Table 5.3.

Including virtual tide gauge records extracted from altimetry causes an extremely high increasing trend in the Beaufort Gyre area when using the cumulated differences approach. This may be due to the seasonal availability of the altimetry data, causing unavailability of data in months of falling sea level. Possible remedies include interpolating gaps in the data, using the datum-fit approach from Ray and Douglas (2011), or restricting oneself to annual data.

The trends for 1960–2010 and for the altimetry era (1993–2012), using the datum-fit method with different numbers of virtual gauges in the altimetry era, are given in Table 5.3. It is readily seen that using the cumulated differences approach in combination with virtual gauges yields extreme trends in MSL.

On the other hand, the results are remarkably robust when using the datum-fit approach. The altimetry-era trends are consistent with Cheng et al. (2015), which found an MSL trend of $2.1 \pm 1.3\,\mathrm{mm/yr}$ (66°N to 82°N). While the reconstruction with no virtual gauges provides MSL trend estimates consistent with those including virtual gauges, the trend uncertainty becomes much lower (approximately $\pm 1.1\,\mathrm{mm/yr}$ rather than $\pm 2.4\,\mathrm{mm/yr}$). It is also interesting to note the insensitivity to the number of virtual gauges used; all trend estimates, when using the datum-fit method, are mutually consistent. The higher uncertainty when using no virtual gauges is likely due to the peak in MSL around 2006, which is in any case likely caused by a lack of data (so that e.g. trends in the Beaufort Gyre are not sufficiently determined from the few remaining tide gauges).

The precise number of virtual gauges to use, if desired, thus appears to be a matter of choice. The choices of 50, 100, and 200 here were made to be of the same order of magnitude as the number of actual gauges, so that its effect may be more readily apparent.

Method	Trend (1960–2010, mm/yr)	Trend (1993–2012, mm/yr)
Cum. diffs, no virtual gauges	4.3 ± 0.4	3.2 ± 2.1
Cum. diffs, 50 virtual gauges	5.3 ± 0.4	11.6 ± 0.9
Cum. diffs, 100 virtual gauges	7.8 ± 0.5	23.6 ± 0.8
Cum. diffs, 200 virtual gauges	5.0 ± 0.4	15.1 ± 0.8
Datum fit, no virtual gauges	1.5 ± 0.3	2.0 ± 2.4
Datum fit, 50 virtual gauges	1.5 ± 0.2	2.0 ± 1.0
Datum fit, 100 virtual gauges	1.5 ± 0.3	1.8 ± 1.1
Datum fit, 200 virtual gauges	1.5 ± 0.3	1.8 ± 1.2

Table 5.3: MSL trends in different reconstructions above 68°N, for different numbers of virtual tide gauges.

5.4.2 Splitting at suspected datum shifts

To remedy datum shifts in tide gauge records, the effect of splitting tide gauge records at suspected datum shifts has been examined. Splitting at all gaps in the time series does not appear to have much effect. On the other hand, splitting at any vertical jumps larger than ± 25 cm much disrupts the reconstructed MSL curve, both when using cumulated timestep differences and the datum-fit method. This behaviour may be due to the new time series having sharp changes at their end points, which must be accommodated, or lack of record coherence (increased fragmentation of the tide gauge data, leaving the reconstruction more free to drift off vertically).

5.4.3 Comparison with previous results

Proshutinsky et al. (2009) found that freshwater content in the Beaufort Gyre region had little interdecadal variation in the period 1950–1980. It therefore makes sense to compare reconstructed sea level for later periods with this time interval, though the number of gauges available in the Russian sector increases considerably during the 1950s, potentially destabilizing the reconstruction during the early part of that decade, which is also why the 1960–1980 trend is given separately here.

The largely stationary pre-1980 conditions found by Pavlov (2001) provide a basic reference (near-zero trend) against which to compare the trends in the reconstruction. For later-era results, Giles et al. (2012) describe sea level trends, derived from altimetry, for the period 1995–2010, in particular obtaining a +2 cm/yr trend in the Beaufort Gyre area and near-zero trends elsewhere.

5.4.4   Maps of reconstructed trends

Maps of some of the reconstructed trends are shown in Figs. 5.14, 5.15 and 5.16. It is evident that the cumulated differences approach produces much stronger regional variations in the trend.
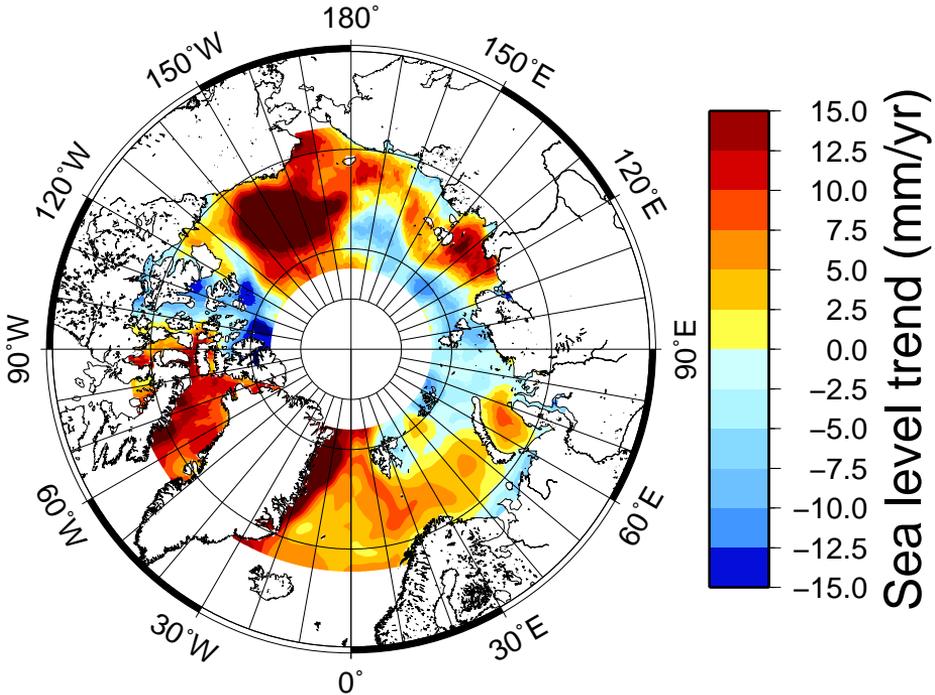
Figure 5.14: Sea level trend in reconstruction (1960–2010) using a reconstruction based on cumulated differences and EOF0 through EOF8.
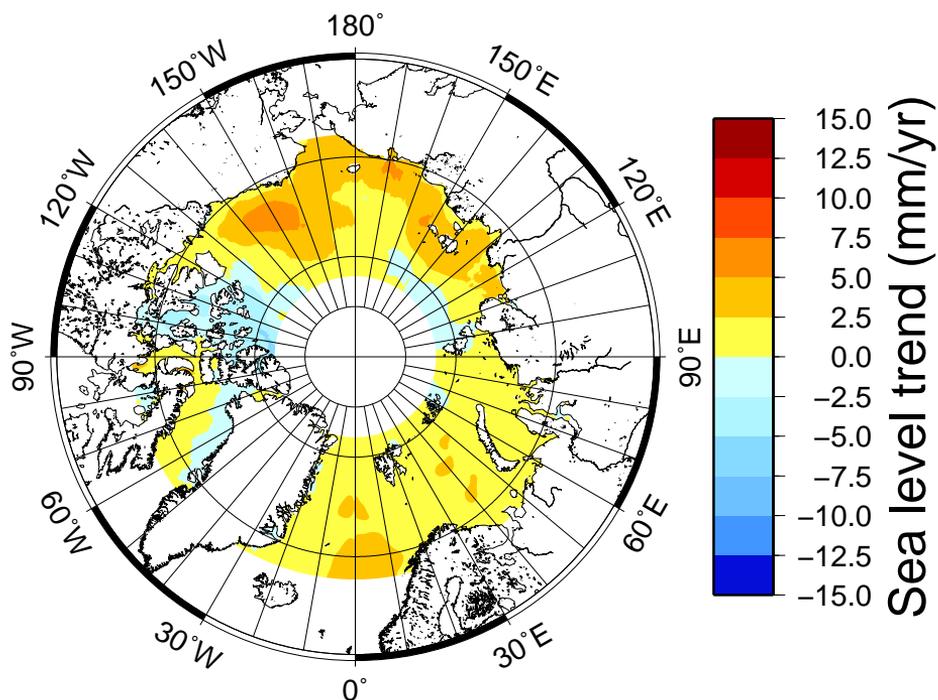
Figure 5.15: Sea level trend in reconstruction (1960–2010) using a datum-fit reconstruction and EOF0 through EOF8.
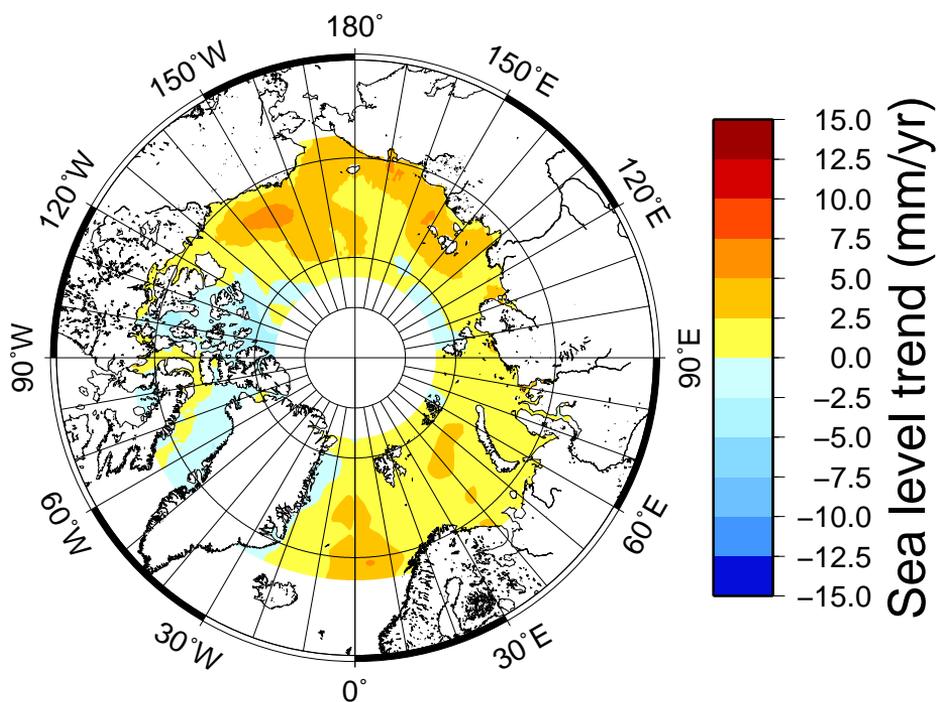
Figure 5.16: Sea level trend in reconstruction (1960–2010) using a datum-fit reconstruction and EOF0 through EOF8, with 100 virtual tide gauges.

To further illustrate the behaviour of the reconstructions, decadal means for a
cumulated-differences reconstruction and a datum-fit reconstruction have been
plotted in Figs. 5.17 and 5.18, respectively. It is clear that the rise is mostly
concentrated within the Beaufort Gyre area and largely begins after 1990.
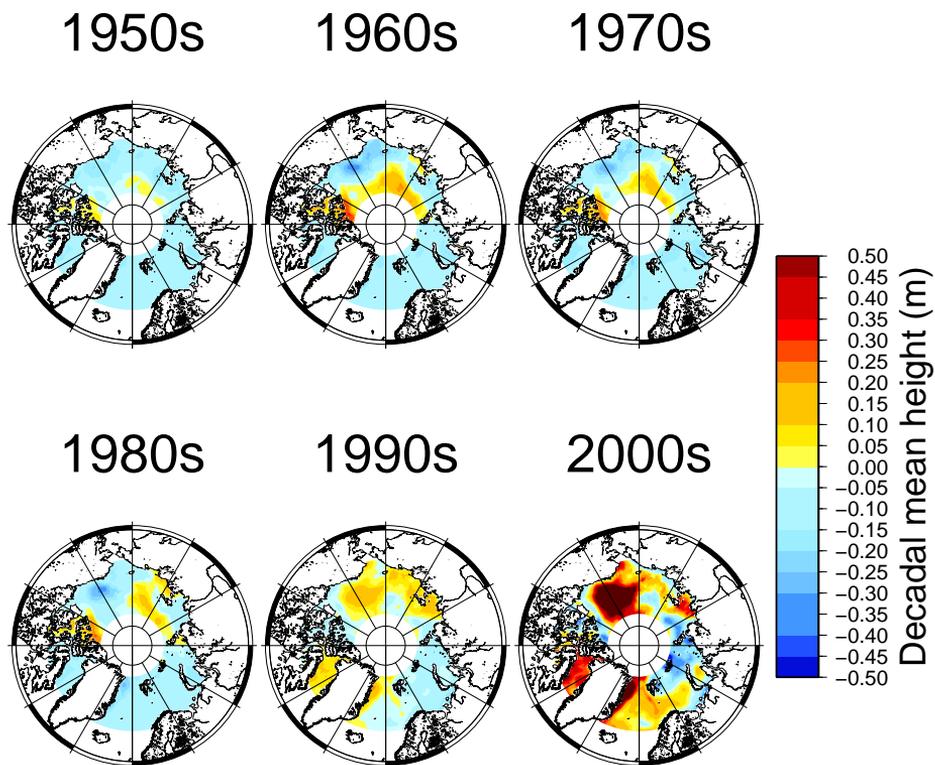
Figure 5.17: Decadal sea level means (1950s through 2000s) using a recon-
struction based on cumulated differences and EOF0 through
EOF8.
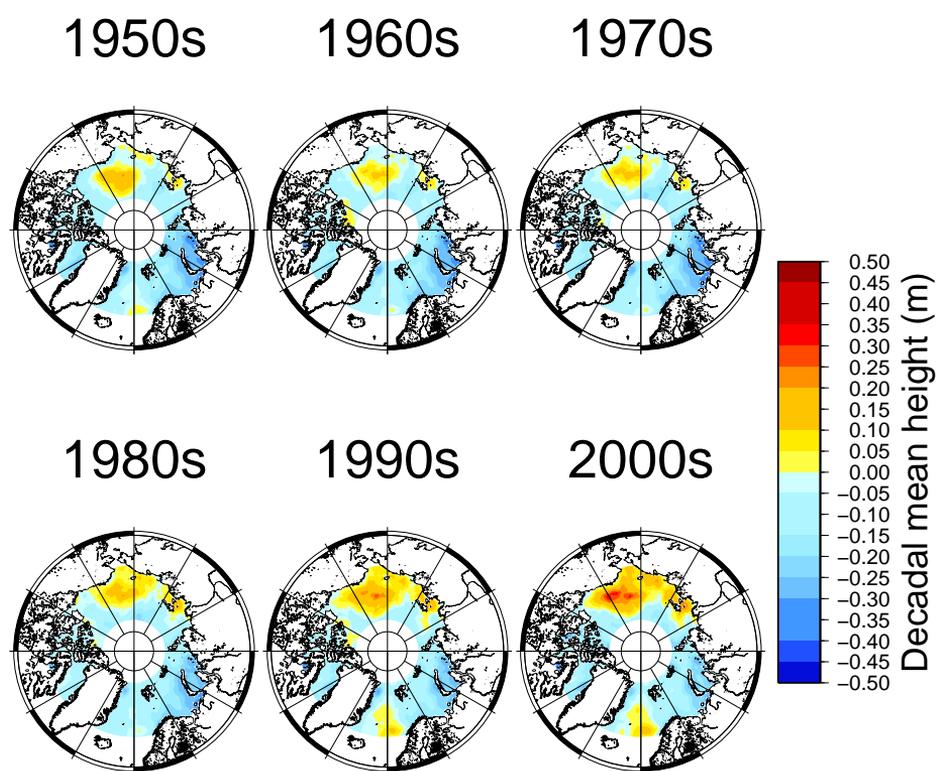
Figure 5.18: Decadal sea level means (1950s through 2000s) using a datum-fit reconstruction and EOF0 through EOF8.

CHAPTER 6

Conclusions

Reconstructing historical Arctic sea level is a considerable challenge, due to the relatively small amount of usable data. Previous reconstructions and analyses going back to the 1950s have generally dealt only with areas close to the Norwegian and/or Russian coasts. This project represents an attempt to extend the area coverable in such reconstructions, such that the western Arctic and the deeper areas of the Arctic Ocean can be handled with plausible results.

The spatial distribution of usable Arctic tide gauges is concentrated along the Norwegian and Russian coasts, and tide-gauge-based reconstructions will therefore rely on a representative expression of variability in these. A number of the Russian gauges are located in rivers and contain strong seasonal peaks due to meltwater, in some cases around 1 m; these gauges have not received special treatment for the reconstructions studied here, but may be an interesting future use case for cyclostationary EOFs (CSEOFs).

The Drakkar dataset used for calibration until the Arctic altimetry data were available were discovered to have very high trend, about two to three times higher than expected given the results from Henry et al. (2012) and Giles et al. (2012). This caused much difficulty in getting tide-gauge-based reconstructions to simultaneously agree with tide gauges and the Drakkar fields used for calibration.

The MAF decomposition works under the assumption of an autocorrelated signal and non-autocorrelated noise. This makes it generally useful for denoising, but when applied to the Arctic sea-level data, it appears to struggle with the many spatial and temporal gaps, and robustly obtaining physically plausible leading patterns using MAF was not achieved in this project. Thus, it appears sensible to recommend the continued use of EOF as the decomposition of choice for reconstructions.

The precise number of EOFs to retain in the reconstruction may be a matter of choice; the Beaufort Gyre water content will generally be expressed in EOF1, and it seems a handful of EOFs is appropriate for Arctic reconstructions. For this project, 8 spatial patterns have been retained, which should contain most of the significant signals.

In attempting to classify the Arctic tide gauges as suitable or not suitable for use in the reconstruction, it has been found that empirical trend-based criteria (around $\pm 2\,\text{cm/yr}$) can provide a reasonable stability in terms of reconstructed regionally averaged sea level. As described in Svendsen et al. (2015), computed leverage may be useful for further refinement and seems to identify areas which may have errors in the GIA model. It should be noted that this inclusion criteria study was made only for the approach of cumulated month-to-month differences, not for the datum-fit method.

GIA uncertainties are generally a major issue for the Arctic area, and uncertainty interval for the GIA contribution to Arctic tide gauge trends may be on the order of $1\,\text{mm/yr}$ (Huang et al., 2013). Therefore, the choice of GIA model merits further attention.

The reconstruction period described here is 1950 to 2010. Many of the relevant tide gauge time series begin during the 1950s, and the reconstructions generally seem less stable through this decade. Therefore, trends may be more reliable from 1958–1960 onwards. It should be noted that there is some delay in registering tide gauge observations in the PSMSL database, and the latest months to years at any time should be treated with more caution as these will have few records available.

The early reconstruction attempts in this project relied on the approach of cumulated month-to-month differences to handle the unknown vertical datums of the tide gauges. While this approach can produce a reasonably stable reconstruction when using only EOF0, it is prone to exaggerating the sea level trends in areas far from the tide gauges, in particular in the Beaufort Gyre and around Greenland, when using more EOFs. Also, it does not gracefully deal with the inclusion of virtual tide gauges, likely due to the seasonal availability of the altimetry on which these are based.

The datum-fit method produces an Arctic ($> 68°$N) MSL trend for 1995–2010 of 2.0 ± 2.4 mm/yr, but includes a spike of about $+100$ mm around 2006. Introducing virtual tide gauges from altimetry results in a trend (1.8 ± 1.1 mm/yr) consistent with this value, though without the aforementioned spike. This suggests that the spike is caused by lack of robustness of the reconstruction due to lack of data, as the number of Russian-sector gauges is significantly lower since around 1990. More specifically, the regional differences in trend are not adequately handled without virtual gauges, as the reconstructed MSL appears relatively stable when using only EOF0.

Based on the overall results from the reconstructions in section 5.4, it seems the most likely Arctic MSL trend is around 1.5 ± 0.3 mm/yr for the period 1960 to 2010, between $68°$N and $82°$N. This value is also in good agreement with the global mean trend of 1.8 ± 0.3 mm/yr for 1950–2000, as found by Church et al. (2004).

To remedy the effects of datum shifts in the tide gauges, one may use different empirical criteria for detecting these, and split the record into two "tide gauge" records at these suspected datum shifts. Splitting at gaps in the time series seems to have little effect, while splitting at jumps of more than ± 25 cm considerably destabilizes the reconstruction. Thus, it appears the splitting of tide gauges should be reserved for known or very strongly suspected datum shifts.

For future studies of Arctic sea level reconstruction, it appears reasonable to recommend the datum-fit approach in combination with altimetry EOFs. The effects of inclusion of virtual tide gauges would also be an interesting matter to study in greater detail, as it seems to provide considerable extra stability for the post-1990 period.

Bibliography

Aagaard, K. and Carmack, E. C. (1989). The role of sea ice and other fresh water in the arctic circulation. *Journal of Geophysical Research*, 94(C10):14485–14498.

Allan, R. and Ansell, T. (2006). A new globally complete monthly historical gridded mean sea level pressure dataset (hadslp2): 1850-2004.

Andersen, O. B. and Knudsen, P. (2009). Dnsc08 mean sea surface and mean dynamic topography models. *Journal of Geophysical Research - Part C - Oceans*, 114(C11):–.

Anderson, T. W. (2003). *An Introduction to Multivariate Statistical Analysis.* Wiley, third edition.

Antonov, J. I., Levitus, S., and Boyer, T. P. (2002). Steric sea level variations during 1957-1994: importance of salinity. *Journal of Geophysical Research*, 107(C12):–.

Antonov, J. I., Levitus, S., and Boyer, T. P. (2005). Thermosteric sea level rise, 1955-2003. *Geophysical Research Letters*, 32(12):1–4.

Baldwin, Stephenson, and Jolliffe (2009). Spatial weighting and iterative projection methods for eofs. *J. Clim. (USA)*, 22(2):234–243.

Barnier, B., Madec, G., Penduff, T., Molines, J.-M., Treguier, A.-M., Le Sommer, J., Beckmann, A., Biastoch, A., Boening, C., Dengg, J., Derval, C., Durand, E., Gulev, S., Remy, E., Talandier, C., Theetten, S., Maltrud, M., McClean, J., and De Cuevas, B. (2006). Impact of partial steps and momentum advection schemes in a global ocean circulation model at eddy-permitting resolution.

Berge-Nguyen, M., Cazenave, A., Lombard, A., Llovel, W., Viarre, J., and Cretaux, J. F. (2008). Reconstruction of past decades sea level using thermosteric sea level, tide gauge, satellite altimetry and ocean reanalysis data. *Global and Planetary Change*, 62(1-2):1–13.

Calafat, F. M., Chambers, D. P., and Tsimplis, M. N. (2014). On the ability of global sea level reconstructions to determine trends and variability.

Carton, J., Chepurin, G., Cao, X., and Giese, B. (2000). A simple ocean data assimilation analysis of the global upper ocean 1950-95. part i: Methodology. *Journal of Physical Oceanography*, 30(2):294–309.

Carton, J. A. and Giese, B. S. (2008). A reanalysis of ocean climate using simple ocean data assimilation (soda). *Monthly Weather Review*, 136(8):2999–3017.

Carton, J. A., Giese, B. S., and Grodsky, S. A. (2005). Sea level rise and the warming of the oceans in the simple ocean data assimilation (soda) ocean reanalysis. *Journal of Geophsical Research-Part C-Oceans*, 110(C9):–.

Cazenave, A., Dominh, K., Ponchaut, F., Soudarin, L., Cretaux, J., and Le Provost, C. (1999). Sea level changes from topex-poseidon altimetry and tide gauges, and vertical crustal motions from doris. *Geophysical Research Letters*, 26(14):2077–2080.

Cazenave, A., Ramillien, G., Lombard, A., and Garcia, D. (2006). Steric sea level variations inferred from combined topex/poseidon altimetry and grace gravimetry. *European Space Agency, (Special Publication) ESA SP*, (614):–.

Chambers, D. P., Mehlhaff, C. A., Urban, T. J., Fujii, D., and Nerem, R. S. (2002). Low-frequency variations in global mean sea level: 1950-2000. *Journal of Geophysical Research*, 107(C4):–.

Chambers, D. P., Merrifield, M. A., and Nerem, R. S. (2012). Is there a 60-year oscillation in global mean sea level? *Geophysical Research Letters*, 39(17):–.

Cheng, Y., Andersen, O., and Knudsen, P. (2015). An improved 20-year arctic ocean altimetric sea level data record. *Marine Geodesy*, 38(2):146–162.

Christiansen, B., Schmith, T., and Thejll, P. (2010). A surrogate ensemble study of sea level reconstructions. *J. Clim. (USA)*, 23(16):4306–4326.

Church, White, Coleman, Lambeck, and Mitrovica (2004). Estimates of the regional distribution of sea level rise over the 1950-2000 period. *J. Clim. (USA)*, 17(13):2609–2625.

Church, J., Clark, P., Cazenave, A., Gregory, J., Jevrejeva, S., Levermann, A., Merrifield, M., Milne, G., Nerem, R., Nunn, P., Payne, A., Pfeffer, W., Stammer, D., and Unnikrishnan, A. (2013). *Sea Level Change. In: Climate*

Change 2013: The Physical Science Basis. Contribution of Working Group I to the Fifth Assessment Report of the Intergovernmental Panel on Climate Change. Cambridge University Press.

Church, J. A. and White, N. J. (2011). Sea-level rise from the late 19th to the early 21st century. *Surv. Geophys.*, 32(4-5):585–602.

Compagnucci, R. H. and Richman, M. B. (2008). Can principal component analysis provide atmospheric circulation or teleconnecion patterns? *International Journal of Climatology*, 28(6):703–726.

Deser, C. (2000). On the teleconnectivity of the "arctic oscillation". *Geophysical Research Letters*, 27(6):779–782.

Dorandeu, J. and Le Traon, P. (1999). Effects of global mean atmospheric pressure variations on mean sea level changes from topex/poseidon. *Journal of Atmospheric and Oceanic Technology*, 16(9):1279–1283.

Douglas, B. C. (1991). Global seal level rise. *Journal of Geophysical Research*, 96(C4):6981–6992.

Douglas, B. C. (1992). Global sea level acceleration. *Journal of Geophysical Research*, 97(C8):12699–12706.

Douglas, B. C. (1997). Global sea rise: A redetermination. *Surveys in Geophysics*, 18(2-3):279–292.

Dyurgerov and Meier (2005). Glaciers and the changing earth system: a 2004 snapshot. (58). Occasional paper.

Ersbøll, B. K. and Conradsen, K. (2007). *An Introduction to Statistics*, volume 2. DTU Informatics, 7th edition.

Giles, K. A., Laxon, S. W., Ridout, A. L., Wingham, D. J., and Bacon, S. (2012). Western arctic ocean freshwater storage increased by wind-driven spin-up of the beaufort gyre. *Nat. Geosci. (UK)*, 5(3):194–197.

Hamlington, B. D., Leben, R. R., Nerem, R. S., Han, W., and Kim, K. Y. (2011). Reconstructing sea level using cyclostationary empirical orthogonal functions. *J. Geophys. Res.-Oceans*, 116:–.

Hastie, T., Tibshirani, R., and Friedman, J. (2009). *The Elements of Statistical Learning.* Springer, second edition.

Hastie, T., Tibshirani, R., Sherlock, G., Eisen, M., Brown, P., and Botstein, D. (1999). Imputing missing data for gene expression arrays. Technical report, Division of Biostatistics, Stanford University.

Henry, O., Prandi, P., Llovel, W., Cazenave, A., Jevrejeva, S., Stammer, D., Meyssignac, B., and Koldunov, N. (2012). Tide gauge-based sea level variations since 1950 along the norwegian and russian coasts of the arctic ocean: Contribution of the steric and mass components. *J. Geophys. Res.-Oceans*, 117:–.

Holgate, S. J., Matthews, A., Woodworth, P. L., Rickards, L. J., Tamisiea, M. E., Bradshaw, E., Foden, P. R., Gordon, K. M., Jevrejeva, S., and Pugh, J. (2013). New data systems and products at the permanent service for mean sea level. *Journal of Coastal Research*, 29(3):493–504.

Huang, Z., Guo, J.-Y., Shum, C. K., Wan, J., Duan, J., Fok, H. S., and Kuo, C.-Y. (2013). On the accuracy of glacial isostatic adjustment models for geodetic observations to estimate arctic ocean sea-level change. *Terrestrial Atmospheric and Oceanic Sciences*, 24(4):471–490.

Ishii, M., Kimoto, M., Sakamoto, K., and Iwasaki, S. (2006). Steric sea level changes estimated from historical ocean subsurface temperature and salinity analyses. *Journal of Oceanography*, 62(2):155–170.

Jevrejeva, S., Moore, J., and Grinsted, A. (2014). Trends and acceleration in global and regional sea levels since 1807. *Global and Planetary Change*, 113:–.

Jiang, Y., Dixon, T. H., and Wdowinski, S. (2010). Accelerating uplift in the north atlantic region as an indicator of ice loss. *Nature Geoscience*, 3(6):404–407.

Kaplan, A., Cane, M., Kushnir, Y., Clement, A., Blumenthal, M., and Rajagopalan, B. (1998). Analyses of global sea surface temperature 1856-1991.

Kaplan, A., Kushnir, Y., Cane, M., and Blumenthal, M. (1997). Reduced space optimal analysis for historical data sets: 136 years of atlantic sea surface temperatures.

Kaplan, A., Kushnir, Y., and Cane, M. A. (2000). Reduced space optimal interpolation of historical marine sea level pressure: 1854-1992. *Journal of Climate*, 13(PART 16):2987–3002.

Kim, K.-Y. and North, G. R. (1996). Eofs of one-dimensional cyclostationary time series:... *Journal of the Atmospheric Sciences*, 53(7):–.

Koren, Y. (2008). Factorization meets the neighborhood: A multifaceted collaborative filtering model. *Proceedings of the Acm Sigkdd International Conference on Knowledge Discovery and Data Mining, Proc. Acm Sigkdd Int. Conf. Knowl. Discov. Data Min*, pages 426–434.

Llovel, W., Cazenave, A., Rogel, P., Lombard, A., and Nguyen, M. B. (2009). Two-dimensional reconstruction of past sea level (1950-2003) from tide gauge data and an ocean general circulation model. *Climate of the Past*, 5(2):217–227.

Meyssignac, B., Becker, M., Llovel, W., and Cazenave, A. (2012). An assessment of two-dimensional past sea level reconstructions over 1950-2009 based on tide-gauge data and different input sea level grids. *Surveys in Geophysics*, 33(5):945–972.

Mitrovica, J. X., Gomez, N., Morrow, E., Hay, C., Latychev, K., and Tamisiea, M. E. (2011). On the robustness of predictions of sea level fingerprints. *Geophysical Journal International*, 187(2):729–742.

Nerem, R. S., Leuliette, r., and Cazenave, A. (2006). Present-day sea-level change: A review. *Comptes Rendus - Geoscience, C. R. Geosci*, 338(14-15):1077–1083.

Nielsen, A. A., Conradsen, K., and Simpson, J. J. (1998). Multivariate alteration detection (mad) and maf postprocessing in multispectral, bitemporal image data: New approaches to change detection studies. *Remote Sensing of Environment*, 64(1):1–19.

North, Bell, Cahalan, and Moeng (1982). Sampling errors in the estimation of empirical orthogonal functions. *Mon. Weather Rev. (USA)*, 110(7):699–706.

Paterek, A. (2007). Improving regularized singular value decomposition for collaborative filtering. In *KDDCup.07*.

Pavlov, V. K. (2001). Seasonal and long-term sea level variability in the marginal seas of the arctic ocean. *Polar Research*, 20(2):153–160.

Peltier, W. (1998). Postglacial variations in the level of the sea: Implications for climate dynamics and solid-earth geophysics.

Peltier, W. (2004). Global glacial isostasy and the surface of the ice-age earth: The ice-5g (vm2) model and grace. *Annual Review of Earth and Planetary Sciences*, 32:111–149.

Peltier, W. (2005). On the hemispheric origins of meltwater pulse 1a.

Peltier, W. R. and Tushingham, A. M. (1989). Global sea level rise and the greenhouse effect: might they be connected? *Science*, 244(4906):806–810.

Plag, H.-P. (2000). Arctic tide gauges: a status report. Technical report, Norwegian Mapping Authority.

Preisendorfer, R. W. (1988). *Principal Component Analysis in Meteorology and Oceanography*, volume 17 of *Developments in Atmospheric Science*. Elsevier.

Proshutinsky, A., Ashik, I., Dvorkin, E., Hakkinen, S., Krishfield, R., and Peltier, W. (2004). Secular sea level change in the russian sector of the arctic ocean. *Journal of Geophysical Research-Oceans*, 109(C3):–.

Proshutinsky, A., Ashik, I., Hakkinen, S., Hunke, E., Krishfield, R., Maltrud, M., Maslowski, W., and Zhang, J. (2007). Sea level variability in the arctic ocean from aomip models. *Journal of Geophysical Research-Part C-Oceans*, 112(C4):1–25.

Proshutinsky, A., Bourke, R. H., and McLaughlin, F. A. (2002). The role of the beaufort gyre in arctic climate variability: seasonal to decadal climate scales. *Geophysical Research Letters*, 29(23):–.

Proshutinsky, A., Krishfield, R., Timmermans, M.-L., Toole, J., Carmack, E., McLaughlin, F., Williams, W. J., Zimmermann, S., Itoh, M., and Shimada, K. (2009). Beaufort gyre freshwater reservoir: State and variability from observations. *Journal of Geophysical Research-Oceans*, 114:–.

Proshutinsky, A., Pavlov, V., and Bourke, R. H. (2001). Sea level rise in the arctic ocean. *Geophys. Res. Lett.*, 28(11):2237–2240.

Ray, R. D. and Douglas, B. C. (2011). Experiments in reconstructing twentieth-century sea levels. *Progress in Oceanography*, 91(4):496–515.

Roweis, S. (1998). Em algorithms for pca and spca. *Advances in Neural Information Processing Systems 10*, 10:626–632.

Rummel, R. J. (1970). *Applied Factor Analysis*. Northwestern University Press.

Shepherd, A., Ivins, E. R., A, G., Barletta, V. R., Bentley, M. J., Bettadpur, S., Briggs, K. H., Bromwich, D. H., Forsberg, R., Galin, N., Horwath, M., Jacobs, S., Joughin, I., King, M. A., Lenaerts, J. T. M., Li, J., Ligtenberg, S. R. M., Luckman, A., Luthcke, S. B., McMillan, M., Meister, R., Milne, G., Mouginot, J., Muir, A., Nicolas, J. P., Paden, J., Payne, A. J., Pritchard, H., Rignot, E., Rott, H., Sørensen, L. S., Scambos, T. A., Scheuchl, B., Schrama, E. J. O., Smith, B., Sundal, A. V., van Angelen, J. H., van de Berg, W. J., van den Broeke, M. R., Vaughan, D. G., Velicogna, I., Wahr, J., Whitehouse, P. L., Wingham, D. J., Yi, D., Young, D., and Zwally, H. J. (2012). A reconciled estimate of ice-sheet mass balance. *Science*, 338(6111):1183–1189.

Shepherd, A., Wingham, D., Wallis, D., Giles, K., Laxon, S., and Sundal, A. V. (2010). Recent loss of floating ice and the consequent sea level contribution. *Geophysical Research Letters*, 37:–.

Simpson, M., Breili, K., Kierulf, H. P., Lysaker, D., Ouassou, M., and Haug, E. (2012). Estimates of future sea-level changes for norway. Technical report, Norwegian Mapping Authority.

Svendsen, P. L., Andersen, O. B., and Nielsen, A. A. (2015). Statistical selection of tide gauges for arctic sea-level reconstruction. *Advances in Space Research*, 55(9):2305–2314.

Switzer, P. and Green, A. A. (1984). Min/max autocorrelation factors for multivariate spatial imagery. Technical report 6, Department of Statistics, Stanford University, Stanford, California.

Tomczak, M. and Godfrey, J. S. (2005). *Regional Oceanography: an Introduction*. Daya Publishing House, pdf (1.1) edition.

Volkov, D. L. (2014). Do the north atlantic winds drive the nonseasonal variability of the arctic ocean sea level? *Geophysical Research Letters*, 41(6):2041–2047.

Volkov, D. L. and Landerer, F. W. (2013). Nonseasonal fluctuations of the arctic ocean mass observed by the grace satellites. *Journal of Geophysical Research-Oceans*, 118(12):6451–6460.

von Storch, H. and Zwiers, F. W. (1999). *Statistical Analysis in Climate Research*. Cambridge University Press.

Wahr, J. (2013). Earth tides. In *Global Earth Physics*, pages 40–46. American Geophysical Union.

Wenzel, M. and Schröter, J. (2010). Reconstruction of regional mean sea level anomalies from tide gauges using neural networks. *Journal of Geophysical Research - Part C - Oceans*, 115(C8):–.

Willis, J., Roemmich, D., and Cornuelle, B. (2004). Interannual variability in upper ocean heat content, temperature, and thermosteric expansion on global scales. *Journal of Geophysical Research-Oceans*, 109(C12):–.

Woodworth, P. and Player, R. (2003). The permanent service for mean sea level: An update to the 21st century. *Journal of Coastal Research*, 19(2):287–295.

APPENDIX A

Published papers

Two peer-reviewed papers have been published as part of this project, "Acceleration of the Greenland ice sheet mass loss as observed by GRACE: Confidence and sensitivity", and "Statistical selection of tide gauges for Arctic sea level reconstruction". This appendix also includes posters and proceedings produced throughout the project.

A.1 Acceleration of the GrIS mass loss as observed by GRACE

Poster presented at EGU General Assembly 2012, Vienna, Austria.

DTU
Technical University
of Denmark

Acceleration of the GrIS mass loss as observed by GRACE

Peter Linkilde Svendsen, Ole Baltazar Andersen and Allan Aasbjerg Nielsen
{plsv, oa, aa}@space.dtu.dk | DTU Space, Technical University of Denmark, Copenhagen, Denmark

Introduction

The Greenland Ice Sheet (GrIS) has been analysed in great detail in recent years, with a number of studies finding an accelerating mass loss. Satellite gravimetry from the GRACE mission is detailed enough to allow regional estimation of the mass loss in Greenland, and we estimate the mass acceleration and its regional distribution in three different GRACE data products. ICESat altimetry data have been used for verification.

Data

Three different GRACE data products have been used – from CNES/-GRGS [1], DEOS [2] and GGFC [3], respectively. All of these consist of global grids of mass change expressed as equivalent water height (EWH), with 10-day intervals for CNES/GRGS, and monthly intervals for DEOS and GGFC. The spatial resolution is 1 by 1 degree for the CNES/GRGS and GGFC grids, and 0.5 by 0.5 degrees for DEOS.

The CNES/GRGS and GGFC solutions cover 2002 through most of 2011, and DEOS 2003–2010. There are some temporal gaps in the data due to instrument failures, though these can be handled well in a least-squares model, and by performing spectral analysis with a slightly modified DFT matrix.

Model

We use an ordinary least squares (OLS) model, incorporating second-order polynomial terms so as to allow direct establishment of an acceleration term, in addition to 1/1-, 1/2- and 1/3-year harmonic oscillations (determined from spectral analysis; the subannual frequencies are due to the somewhat sawtooth-like annual signal). The mass contribution has been weighted by the cosine of the latitude since the rectangular grids overrepresent the polar regions.

References

[1] S. Bruinsma, J.-M. Lemoine, R. Biancale, and N. Valès, CNES/GRGS 10-day gravity field models release 2 and their evaluation, Adv. Space Research, 45, 587–601, doi: 10.1016/j.asr.2009.10.012, 2010.

[2] P. Ditmar, X. Liu, C. Siemes, H. Hashemi Farahani, R. Klees, E. Revtova, and Q. Zhao, DEOS Mass Transport model release 1 (DMT-1). Description document.

[3] I. Chen et al., available from
http://www.csr.utexas.edu/research/ggfc/dataresources.html.

[4] A. S. Gardner, G. Moholdt, B. Wouters, G. J. Wolken, D. O. Burgess, M. J. Sharp, J. G. Cogley, C. Braun, and C. Labine, Sharply increased mass loss from glaciers and ice caps in the Canadian Arctic Archipelago, Nature, 473, 357–359, doi:10.1038/nature10089, 2011.

[5] L. S. Sørensen, S. B. Simonsen, K. Nielsen, P. Lucas-Picher, G. Spada, G. Adalgeirsdottir, R. Forsberg, and C. S. Hvidberg, Mass balance of the Greenland ice sheet (2003–2008) from ICESat data ? the impact of interpolation, sampling and firm density, The Cryosphere, 5, 173/186, doi:10.5194/tc-5-173-2011, 2011.

[6] I. Velicogna, Increasing rates of ice mass loss from the Greenland and Antarctic ice sheets revealed by GRACE, Geophys. Res. Lett., 36, L19503, doi:10.1029/2009GL040222, 2009.

Processed ICESat data kindly provided by Louise Sandberg Sørensen, DTU Space.

Results

All three data products agree on an accelerating mass loss within Greenland, taking into account the uncertainties on the regression coefficients. The OLS model assumes any uncertainty on the data to be present as white noise; since these data products are highly processed and smoothed, the naively computed confidence intervals may actually be an underestimate of the true uncertainty.


Mass development for entire ice sheet

Regression results
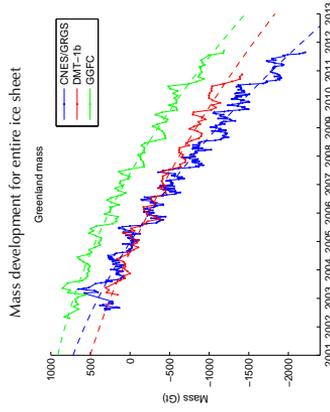
| Product	Timespan	Acc. (Gt/yr²)	RMSE (Gt)	R^2
GRGS	2002–2011	-23.3 ± 2.9	76.6	0.9885
DEOS	2003–2010	-13.5 ± 5.1	55.6	0.9861
GGFC	2002–2011	-19.5 ± 3.4	57.8	0.9893

Confidence intervals for acceleration terms
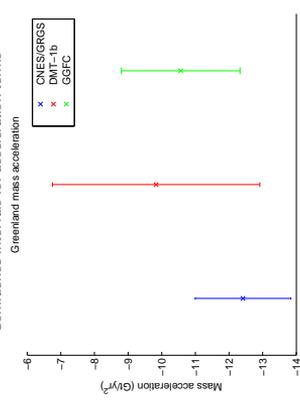
Regional distribution

The three data products analysed agree well on the accelerating mass loss in northwest Greenland, with a particularly strong acceleration focused near Qaanaaq (Thule), though the DEOS solutions yield a strong positive acceleration in southeast Greenland, which cannot be attributed to the different timescale. The region of accelerating mass loss appears to have recently started splitting in two in the CNES/GRGS solutions.

CNES/GRGS:

DEOS:

GGFC:
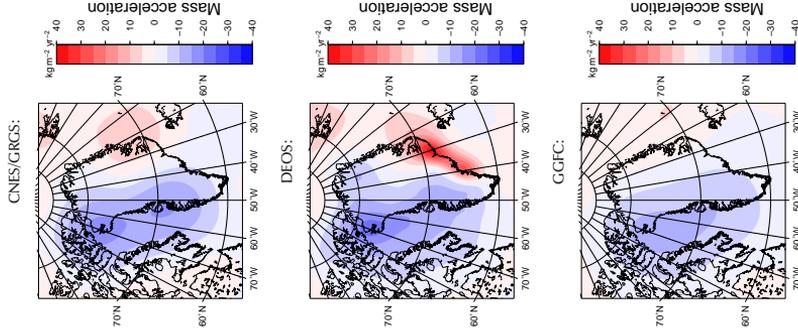
Acceleration term uncertainty

The uncertainty of the acceleration term, as determined from the OLS analysis, decreases with the length of the available time series. GRACE has now provided almost 10 years of data, and we find that at least 5–6 years of observations is required to significantly establish the acceleration found here.

Development of acceleration uncertainty
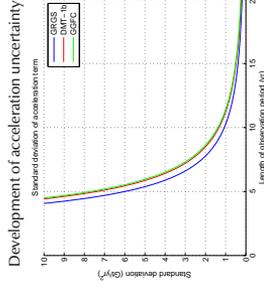
Leakage

The GrIS mass loss observed may be contaminated by leakage from other geophysical signals. The most notable leakage here is from the Canadian Arctic Archipelago (CAA), also studied by Gardner et al. [4]. We have performed a simulation based on these results, finding a CAA leakage to the Greenland mass of approximately -4.7 Gt/yr². Leakage from other geophysical signals have been found to be insignificant [6].

ICESat

The ICESat mission (2003–2009) has provided satellite altimetry for the ice sheet, and knowing the density of pure ice (0.917 kg/m³), we can then use this to provide an upper bound on the acceleration. Using ICESat data processed as in Sorensen et al. [5] and expanding into spherical harmonics of degree and order 50, we get an upper bound of approximately -29.7 Gt/yr².

Conclusions

We find a significantly accelerating mass loss in the ice sheet taking place during the period observed by GRACE, with the acceleration largely confined to northwest Greenland. There appears to be a considerable contribution from the Canadian Arctic Archipelago, and possibly an increase in acceleration around the Disko Bay.

A GRACE follow-on mission would provide longer time series, allowing better confidence in the trend estimation. Even so, the existing GRACE data appears sufficient to establish the presence of an acceleration in the mass loss.

A.2   Sea level reconstruction from satellite altimetry and tide gauge data

Poster presented at EGU General Assembly 2012, Vienna, Austria.

Sea level reconstruction from satellite altimetry and tide gauge data

Peter Limkilde Svendsen, Ole Baltazar Andersen and Allan Aasbjerg Nielsen

{plsv, oa, aa}@space.dtu.dk | DTU Space, Technical University of Denmark, Copenhagen, Denmark

Introduction

Global sea level reconstruction is commonly based on satellite altimetry from the last two decades, combined with data from tide gauge stations at coastlines around the world. Typically, spatial patterns of variations are extracted using empirical orthogonal functions (EOF), which attempt to explain as much variance in the signal as possible; here, we examine the behaviour of a different procedure, *minimum/maximum autocorrelation factors* (MAF), which takes into account the spatial structure of the data.

It is desired to eventually produce a 50–60 year reconstruction, of which MAF is one of the approaches investigated.

Model

Minimum/maximum autocorrelation factors or MAF [1] is a special case of a method known as minimum/maximum noise fractions (MNF). The MAF transform seeks to, depending on ordering, to minimize or maximize the amount of noise, based on the assumption that the signal is correlated with a slightly shifted version of itself, whereas the noise is not. The actual computation of the MAFs is done by solving a generalized eigenvalue problem. In this case, we strive to minimize the noise, i.e. the first MAFs should be the least noisy.

There are various difficulties involved in computing the spatial autocorrelation on a global grid, such as latitude weighting, wrap-around and scale distortion. This has been handled in a preliminary way in the analysis, and the details of implementing such solutions are being investigated.

Data

The MAF procedure has been tested on an existing sea level model, SODA (*Simple Ocean Data Assimilation, v2.2.4*), covering the period 1949–2008 and spatially downsampled for convenience. Thus, we are working on data without "real" noise (eddies may resemble white noise in the downsampled data). Therefore, attempting to minimize the amount of non-autocorrelated noise might not yield a useful separation of the signal.

A compound dataset of actual satellite altimetry from various missions, covering latitudes up to ±66°, has been included for comparison; the dataset has had its seasonal component removed.

Data from tide gauge stations have been obtained from the Permanent Service for Mean Sea Level (PSMSL), going back 200 years and providing data from approximately 2,000 tide gauges.
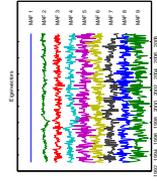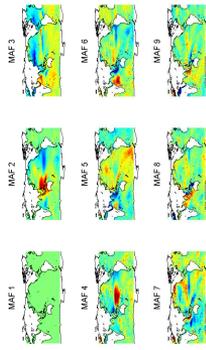
All data are monthly means.

Satellite altimetry era (1992–2008)

SODA 2.2.4, first 9 MAFs:
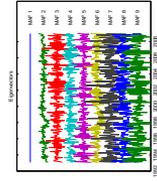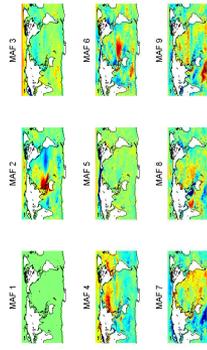
Note how the first MAF captures only noise, while the next one captures an ENSO-like phenomenon well. A pseudo-seasonal signal also seems to be described. Near-polar patterns are very much present, despite the latitude weighting.
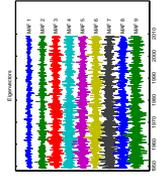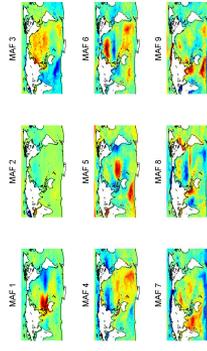

"Raw" satellite altimetry, first 9 MAFs:

The satellite altimetry yields similar results (except for the lack of a seasonal component). Instead, more ENSO-connected details begin to appear, and the MAFs provide increasingly finer detail.

## 60-year period: 1949–2008

SODA 2.2.4, first 9 MAFs:

Interestingly, the noise is not dominant when the procedure is run on the entire 60-year period, though strange "noise" MAFs tend to appear among the first handful.

A spectral analysis of the eigenvectors reveals an annual signal in some of the first few MAFs, as well as a lot of high-frequency noise.

Unlike the MAF analysis for the satellite observation period, the first MAF is not dominated by noise in this case. In all cases, ENSO-like phenomena are captured in one of the first MAFs, suggesting ability to capture significant patterns in the data. Indeed, it seems that only a handful of MAFs can provide a qualitatively good reconstruction, though this has not yet been systematically examined.

Climate indices

Various climate indices will be selected for the reconstruction; shown here is the result of using the Southern Oscillation Index (SOI) as a predictor for satellite altimetry data. Note the similarity to what is captured by the MAFs.

Tide gauge inclusion

The PSMSL database consists of a large number of tide gauge stations, of widely varying quality and coverage. Pre-selection of gauges to include can be done based on correlation with satellite altimetry, temporal coverage, and assessments of geological stability. A very basic test for (temporal) correlation with satellite altimetry within a distance of 500 km is shown below.
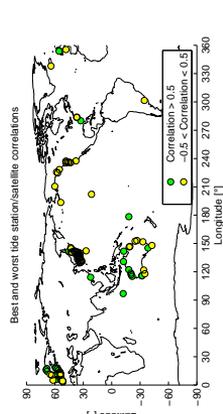
Conclusions

The MAF procedure, when modified to handle global grids, is able to capture some of the most significant features of sea-level variations, and handles physical and reconstructed data very similarly.

The MAF procedure is also able to reconstruct the original signal well; very few MAFs are needed to make a decent re-construction. A systematic comparison to EOF analysis will be performed at a later stage, in addition to various other techniques, such as POP.
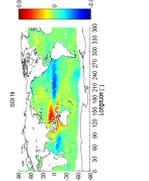
A temporal MAF (T-MAF) also exists, and an interesting possibility could be to combine the spatial and temporal interactions in the data. Otherwise, one could introduce a more physically-based way of separating signal from noise, e.g. by means of discrete Laplacian operators or something similar.

References

[1] P. Switzer and A. A. Green, *Min/max autocorrelation factors for multivariate spatial imagery*, Technical report no. 6, Department of Statistics, Stanford University, 1984.

A.3   Sea level reconstruction: Exploration of methods for combining altimetry with other data to beyond the 20-year altimetric record

Poster presented at 20 Years of Progress in Radar Altimetry, Venice, Italy, 2012, and associated proceedings.

Sea level reconstruction: Exploration of methods for combining altimetry with other data to beyond the 20-year altimetric record

Peter Limkilde Svendsen, Ole Baltazar Andersen and Allan Aasbjerg Nielsen

{plsv, oa, aa}@space.dtu.dk | DTU Space, Technical University of Denmark, Copenhagen, Denmark

DTU Technical University of Denmark

DTU Space
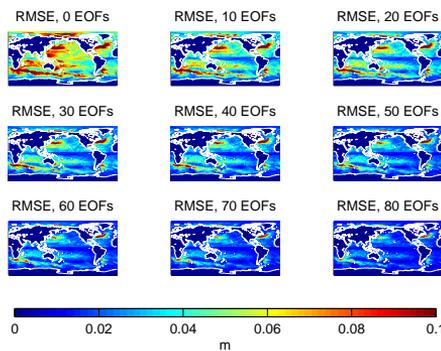National Space Institute

Introduction

For the last two decades, satellite altimetry has provided a near-global view of spatial and temporal patterns in sea surface height (SSH). When combined with records from tide gauges, a historical reconstruction of sea level can be obtained; while tide gauge records span up to 200 years back, their combined quality for reconstruction purposes is limited by the sparsity of their geographical distribution and other factors.

We examine both a traditional EOF analysis of sea surface height, and another method known as minimum/maximum autocorrelation factors (MAF).

The implementation is currently based on data from the Simple Ocean Data Assimilation (SODA) model, an existing reconstruction, where a calibration period can be easily extracted and our model's basic performance can be relatively easily assessed.

Data

For these initial experiments, data from the Simple Ocean Data Assimilation (SODA) model (v. 2.2.4) are used. This is an assimilated model covering the period 1949–2008. This way, we can extract both satellite altimetry and "pseudo-tide gauge" data to test reconstruction from a small spatial subset of the data.

The PSMSL database covers measurements from more than 1000 tide gauges, in some cases going 200 years back. These are spatially and temporally sparse in coverage, and have many issues regarding quality of data. Still, few other options exist when attempting a sea level reconstruction going back beyond the era of satellite altimetry.

Both the SODA and PSMSL data used in this case are monthly data.

EOF analysis

Empirical orthogonal functions (EOFs) try to explain the maximum amount of variance in the data, subject to mutual orthogonality. This of course allows for a minimization of model residuals with as few components as possible, though possibly at the cost of physical explicability.
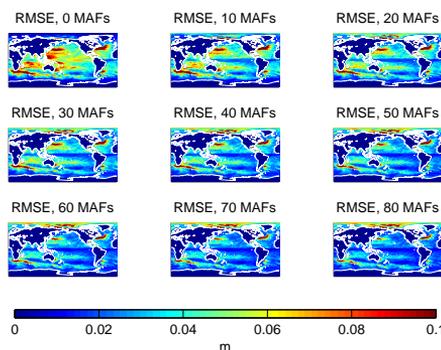

Residuals after removal of different numbers of EOFs. The EOFs have been applied after removal of a constant, a one-year and a half-year signal. Note how the first few EOFs readily describe the ENSO-like phenomena, while eddy signals are among the last to disappear.

MAF analysis

Minimum/maximum autocorrelation factors (MAF) [4] work by instead trying to maximize (or minimize) the autocorrelation in the data. This autocorrelation may be spatial, temporal or a combination. In this case, we consider spatial autocorrelation.
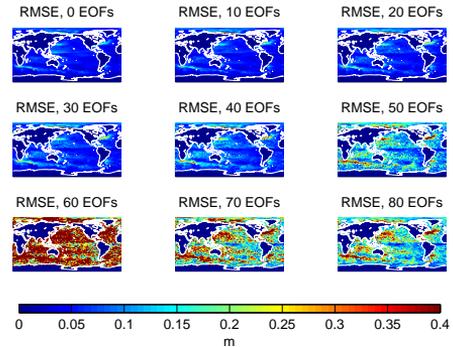
The MAF method, unlike the EOF, is not oblivious to the spatial structure of the data. Therefore, the method has here been adapted to work on a global grid with wraparound and land masks, as opposed to a simple rectangular image.

Residuals after removal of different numbers of MAFs, similar to the EOF plot above. While the method also captures ENSO phenomena relatively quickly, the results do not seem as good as with the EOFs. There seems to be some convergence problems, possibly due to errors in the adaptation to global datasets.
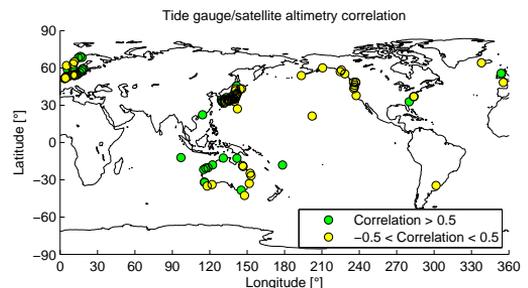
Reconstruction ability

A basic EOF-based reconstruction has been performed using the SODA data. Removing first a best-fit constant and whole- and half-year oscillations (based on patterns from the satellite altimetry era), a set of 59 pseudo-tide-gauge time series are then extracted from the SODA data. Expansion coefficients corresponding to the "tide gauge measurements" at these historical points in time are then determined and applied to the spatial EOF patterns found from the satellite altimetry era.

Standard deviations of reconstruction compared to SODA for the full 1949–2008 period. It is interesting that including higher-order EOFs does not necessarily improve quality when reconstructing historical data. Kaplan et al. (1997) [3] proposed a cost function approach to reconstruction, allowing simultaneous inclusion and regularization. This is also followed by Church et al. [2] and Christiansen et al. [1].

Quality of tide gauges

A simple correlation computation between actual tide gauge time series (from PSMSL) and nearby satellite altimetry gives the result shown below. No detrending has been performed, giving an idea of the similarity of the two datasets.

Correlation of tide gauge data with satellite altimetry for points in time where both are available. The satellite altimetry is sampled within a radius of 500 km from the tide gauges. Only 113 of the 1291 PSMSL stations have enough overlap with satellite altimetry to allow this analysis, and of those, only 52 have a correlation larger than 0.5. Only 3 have a correlation larger than 0.9.

Conclusions

A preliminary EOF-based reconstruction has been established, with an apparently reasonable ability to recreate historical data from the SODA model. Since no regularization is done apart from truncating higher-order EOFs, it is rather sensitive to noise-like signals if the truncation is not chosen wisely. A full model in the style of Kaplan et al. would likely yield better results.

Some climate indices, including the Southern Oscillation Index (SOI) and the North Atlantic Oscillation (NAO) have been investigated as possible predictors for sea level. However, such indices are sometimes based on EOFs and therefore should be used cautiously in an EOF-based analysis.

It is intended to focus the reconstruction particularly on the Arctic area, and with retracked ERS and Envisat data hopefully available in the future, it should be possible to improve on existing models there.

Eventually, it is desired to investigate a variety of dimension reduction techniques, such as a temporal MAF or principal oscillation patterns (POP). Particularly interesting would be an approach for simultaneously identifying spatial and temporal interaction. Further interesting possibilities could include independent component analysis to identify "non-noise-like" signals, as well as tensor decomposition.

References

[1] B. Christiansen, T. Schmith and P. Thejll: A surrogate ensemble study of sea level reconstructions, *Journal of Climate*, Volume 23, Issue 16, pp. 4306–4326, 2004.

[2] J. A. Church, N. J. White, R. Coleman, K. Lambeck, J. X. Mitrovica: Estimates of the regional distribution of sea level rise over the 1950–2000 period, *Journal of Climate*, Volume 17, Issue 13, pp. 2609–2625, 2004.

[3] A. Kaplan, Y. Kushnir, M. A. Cane and M. B. Blumenthal: Reduced space optimal analysis for historical data sets: 136 years of Atlantic sea surface temperatures, *Journal of Geophysical Research*, Volume 102, Issue C13, pp. 27835–27860, 1997.

[4] P. Switzer and A. A. Green: *Min/max autocorrelation factors for multivariate spatial imagery*, Technical report no. 6, Department of Statistics, Stanford University, 1984.

SEA LEVEL RECONSTRUCTION: EXPLORATION OF METHODS FOR COMBINING ALTIMETRY WITH OTHER DATA TO BEYOND THE 20-YEAR ALTIMETRIC RECORD

Peter Limkilde Svendsen, Ole Baltazar Andersen, and Allan Aasbjerg Nielsen

DTU Space, Technical University of Denmark, 2800 Kgs. Lyngby, Denmark, Email: {plsv, oa, aa}@space.dtu.dk

ABSTRACT

Ocean satellite altimetry has provided global sets of sea level data for the last two decades, allowing determination of spatial patterns in global sea level. For reconstructions going back further than this period, tide gauge data can be used as a proxy for the model. We examine different methods of combining satellite altimetry and tide gauge data using optimal weighting of tide gauge data, linear regression and EOFs, including automatic quality checks of the tide gauge time series. We investigate alternative transformations such as maximum autocorrelation factors (MAF), which better take into account the spatio-temporal structure of the variation. The SODA ocean model is used for a preliminary reference. Our focus is a timescale going back approximately 50 years, allowing more detailed analysis and a later high-latitude reconstruction.

Key words: sea level reconstruction; EOF; MAF.

1. INTRODUCTION

For the last two decades, satellite altimetry has provided a near-global view of spatial and temporal patterns in sea surface height (SSH). When combined with records from tide gauges, a historical reconstruction of sea level can be obtained; while tide gauge records span up to 200 years back, their combined quality for reconstruction purposes is limited by the sparsity of their geographical distribution and other factors.

We examine both a traditional EOF analysis of sea surface height, and another method known as minimum/maximum autocorrelation factors (MAF).

The implementation is currently based on data from the Simple Ocean Data Assimilation (SODA) model, an existing reconstruction, where a calibration period can be easily extracted and our model's basic performance can be relatively easily assessed.

2. DATA

For these initial experiments, data from the Simple Ocean Data Assimilation (SODA) model (v. 2.2.4) are used. This is an assimilated model covering the period 1949–2008. This way, we can extract both satellite altimetry and "pseudo-tide gauge" data to test reconstruction from a small spatial subset of the data.

The PSMSL database covers measurements from more than 1000 tide gauges, in some cases going 200 years back. These are spatially and temporally sparse in coverage, and have many issues regarding quality of data. Still, few other options exist when attempting a sea level reconstruction going back beyond the era of satellite altimetry.

Both the SODA and PSMSL data used in this case are monthly data.

3. EOF ANALYSIS

Empirical orthogonal functions (EOFs) try to explain the maximum amount of variance in the data, subject to mutual orthogonality. This of course allows for a minimization of model residuals with as few components as possible, though possibly at the cost of physical explicability.

4. MAF ANALYSIS

Minimum/maximum autocorrelation factors (MAF) [4] work by instead trying to maximize (or minimize) the autocorrelation in the data. This autocorrelation may be spatial, temporal or a combination. In this case, we consider spatial autocorrelation.

The MAF method, unlike the EOF, is not oblivious to the spatial structure of the data. Therefore, the method has here been adapted to work on a global grid with wraparound and land masks, as opposed to a simple rectangular image.
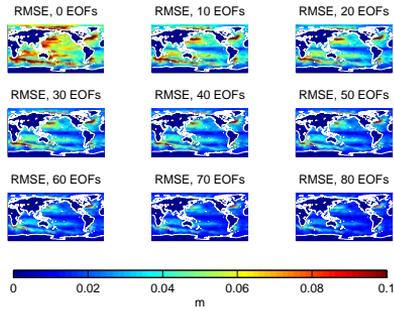
Figure 1. Residuals after removal of different numbers of EOFs. The EOFs have been applied after removal of a constant, a one-year and a half-year signal. Note how the first few EOFs readily describe the ENSO-like phenomena, while eddy signals are among the last to disappear.
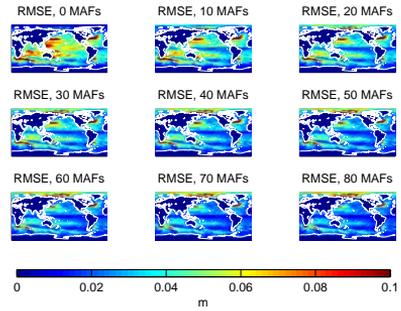
Figure 2. Residuals after removal of different numbers of MAFs, similar to the EOF plot above. While the method also captures ENSO phenomena relatively quickly, the results do not seem as good as with the EOFs. There seems to be some convergence problems, possibly due to errors in the adaptation to global datasets.

As seen in Figure 2, the MAF method also quickly captures ENSO-like phenomena.

5. RECONSTRUCTION ABILITY

A basic EOF-based reconstruction has been performed using the SODA data. Removing first a best-fit constant and whole- and half-year oscillations (based on patterns from the satellite altimetry era), a set of 59 pseudo-tide-gauge time series are then extracted from the SODA data. Expansion coefficients corresponding to the "tide gauge measurements" at these historical points in time are then determined and applied to the spatial EOF patterns found from the satellite altimetry era.

Kaplan et al. (1997) [3] proposed a cost function approach to reconstruction, allowing simultaneous inclusion of and regularization. This is also followed by Church et al. [2] and Christiansen et al. [1].

6. QUALITY OF TIDE GAUGES

A simple correlation computation between actual tide gauge time series (from PSMSL) and nearby satellite altimetry gives the result shown in Figure 4. No detrending has been performed, giving an idea of the similarity of the two datasets.

7. CONCLUSIONS

A preliminary EOF-based reconstruction has been established, with an apparently reasonable ability to recreate the existing reconstruction of the SODA model. Since no regularization is done apart from truncating higher-order EOFs, it is rather sensitive to noise-like signals if the truncation is not chosen wisely. A full model in the style of Kaplan et al. would likely yield better results.

Some climate indices, including the Southern Oscillation Index (SOI) and the North Atlantic Oscillation (NAO) have been investigated as possible predictors for sea level. However, such indices are sometimes based on EOFs and therefore should be used cautiously in an EOF-based analysis.

It is intended to focus the reconstruction particularly on the Arctic area, and with retracked ERS and Envisat data hopefully available in the future, it should be possible to improve on existing models there.

Eventually, it is desired to investigate a variety of dimension reduction techniques, such as a temporal MAF or principal oscillation patterns (POP). Particularly interesting would be an approach for simultaneously identifying spatial and temporal interaction. Further interesting possibilities could include independent component analysis to identify "non-noise-like" signals, as well as tensor decomposition.
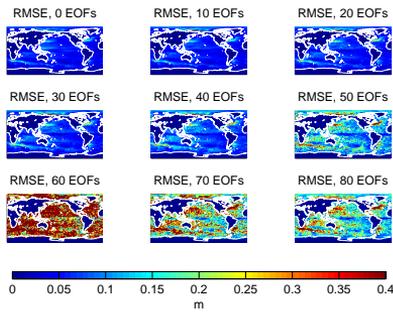
Figure 3. Standard deviations of reconstruction compared to SODA for the full 1949–2008 period. It is interesting that including higher-order EOFs does not necessarily improve quality when reconstructing historical data.
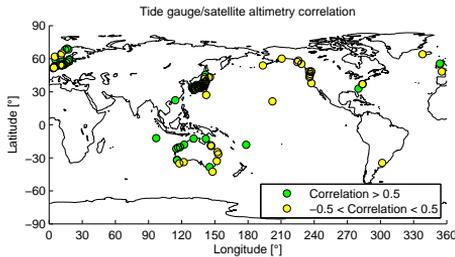

Figure 4. Correlation of tide gauge data with satellite altimetry for points in time where both are available. The satellite altimetry is sampled within a radius of 500 km from the tide gauges. Only 113 of the 1291 PSMSL stations have enough overlap with satellite altimetry to allow this analysis, and of those, only 52 have a correlation larger than 0.5. Only 3 have a correlation larger than 0.9.

REFERENCES

[1] B. Christiansen, T. Schmith and P. Thejll (2010): A surrogate ensemble study of sea level reconstructions, *Journal of Climate*, Volume 23, Issue 16, pp. 4306–4326.

[2] J. A. Church, N. J. White, R. Coleman, K. Lambeck, J. X. Mitrovica (2004). Estimates of the regional distribution of sea level rise over the 1950–2000 period. *Journal of Climate*, Volume 17, Issue 13, pp. 2609–2625.

[3] A. Kaplan, Y. Kushmir, M. A. Cane and M. B. Blumenthal (1997): Reduced space optimal analysis for historical data sets: 136 years of Atlantic sea surface temperatures, *Journal of Geophysical Research*, Volume 102, Issue C13, pp. 27835–27860.

[4] P. Switzer and A. A. Green (1984): *Min/max auto-correlation factors for multivariate spatial imagery*, Technical report no. 6, Department of Statistics, Stanford University.

A.4 Exploring methods for combining altimetry with other data to extend the 20-year altimetric record onto a 50 year timescale

Poster presented at AGU Fall Meeting 2012, San Francisco, United States.

Exploring methods for combining altimetry with other data to extend the 20-year altimetric record onto a 50 year timescale

Peter Limkilde Svendsen, Ole Baltazar Andersen and Allan Aasbjerg Nielsen

{plsv, oa, aa}@space.dtu.dk | DTU Space, Technical University of Denmark, Copenhagen, Denmark

DTU Technical University of Denmark

DTU Space
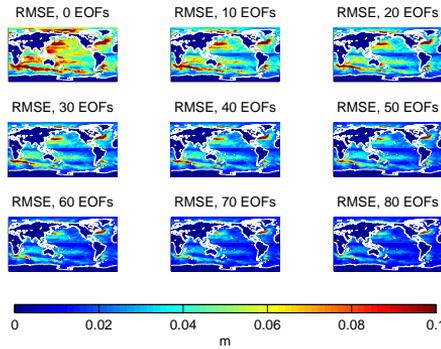National Space Institute

Introduction

For the last two decades, satellite altimetry has provided a near-global view of spatial and temporal patterns in sea surface height (SSH). When combined with records from tide gauges, a historical reconstruction of sea level can be obtained; while tide gauge records span up to 200 years back, their combined quality for reconstruction purposes is limited by the sparsity of their geographical distribution and other factors.

We examine both a traditional EOF analysis of sea surface height, and another method known as minimum/maximum autocorrelation factors (MAF).

The implementation is currently based on data from the Simple Ocean Data Assimilation (SODA) model, an existing reconstruction, where a calibration period can be easily extracted and our model's basic performance can be relatively easily assessed.

Data

For these initial experiments, data from the Simple Ocean Data Assimilation (SODA) model (v. 2.2.4) are used. This is an assimilated model covering the period 1949–2008. This way, we can extract both satellite altimetry and "pseudo-tide gauge" data to test reconstruction from a small spatial subset of the data.

The PSMSL database covers measurements from more than 1000 tide gauges, in some cases going 200 years back. These are spatially and temporally sparse in coverage, and have many issues regarding quality of data. Still, few other options exist when attempting a sea level reconstruction going back beyond the era of satellite altimetry.

Both the SODA and PSMSL data used in this case are monthly data.

EOF analysis

Empirical orthogonal functions (EOFs) try to explain the maximum amount of variance in the data, subject to mutual orthogonality. This of course allows for a minimization of model residuals with as few components as possible, though possibly at the cost of physical explicability.
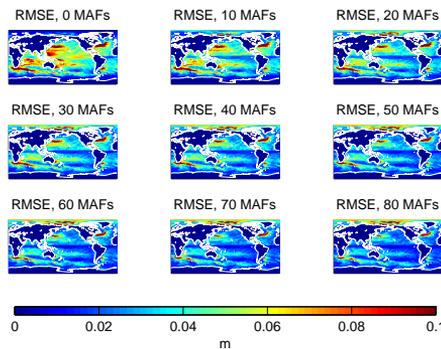

Residuals after removal of different numbers of EOFs. The EOFs have been applied after removal of a constant, a one-year and a half-year signal. Note how the first few EOFs readily describe the ENSO-like phenomena, while eddy signals are among the last to disappear.

MAF analysis

Minimum/maximum autocorrelation factors (MAF) [4] work by instead trying to maximize (or minimize) the autocorrelation in the data. This autocorrelation may be spatial, temporal or a combination. In this case, we consider spatial autocorrelation.
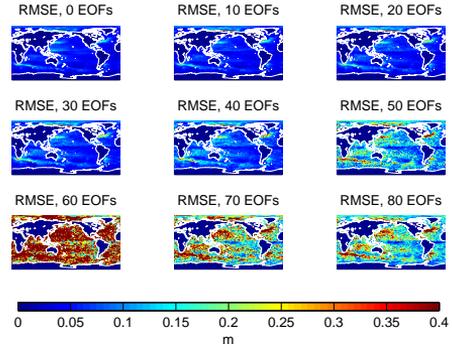
The MAF method, unlike the EOF, is not oblivious to the spatial structure of the data. Therefore, the method has here been adapted to work on a global grid with wraparound and land masks, as opposed to a simple rectangular image.

Residuals after removal of different numbers of MAFs, similar to the EOF plot above. While the method also captures ENSO phenomena relatively quickly, the results do not seem as good as with the EOFs. There seems to be some convergence problems, possibly due to errors in the adaptation to global datasets.
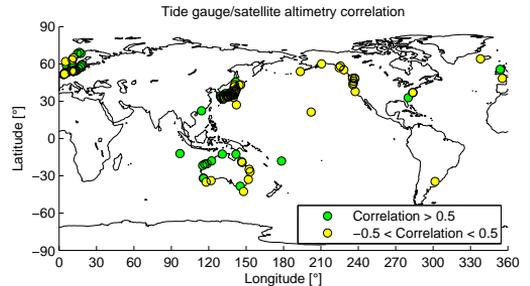
Reconstruction ability

A basic EOF-based reconstruction has been performed using the SODA data. Removing first a best-fit constant and whole- and half-year oscillations (based on patterns from the satellite altimetry era), a set of 59 pseudo-tide-gauge time series are then extracted from the SODA data. Expansion coefficients corresponding to the "tide gauge measurements" at these historical points in time are then determined and applied to the spatial EOF patterns found from the satellite altimetry era.

Standard deviations of reconstruction compared to SODA for the full 1949–2008 period. It is interesting that including higher-order EOFs does not necessarily improve quality when reconstructing historical data. Kaplan et al. (1997) [3] proposed a cost function approach to reconstruction, allowing simultaneous inclusion of higher-order EOFs and regularization. This is also followed by Church et al. [2] and Christiansen et al. [1].

Quality of tide gauges

A simple correlation computation between actual tide gauge time series (from PSMSL) and nearby satellite altimetry gives the result shown below. No detrending has been performed, giving an idea of the similarity of the two datasets.

Correlation of tide gauge data with satellite altimetry for points in time where both are available. The satellite altimetry is sampled within a radius of 500 km from the tide gauges. Only 113 of the 1291 PSMSL stations have enough overlap with satellite altimetry to allow this analysis, and of those, only 52 have a correlation larger than 0.5. Only 3 have a correlation larger than 0.9.

Conclusions

A preliminary EOF-based reconstruction has been established, with an apparently reasonable ability to recreate historical data from the SODA model. Since no regularization is done apart from truncating higher-order EOFs, it is rather sensitive to noise-like signals if the truncation is not chosen wisely. A full model in the style of Kaplan et al. would likely yield better results.

Some climate indices, including the Southern Oscillation Index (SOI) and the North Atlantic Oscillation (NAO) have been investigated as possible predictors for sea level. However, such indices are sometimes based on EOFs and therefore should be used cautiously in an EOF-based analysis.

It is intended to focus the reconstruction particularly on the Arctic area, and with retracked ERS and Envisat data hopefully available in the future, it should be possible to improve on existing models there.

Eventually, it is desired to investigate a variety of dimension reduction techniques, such as a temporal MAF or principal oscillation patterns (POP). Particularly interesting would be an approach for simultaneously identifying spatial and temporal interaction. Further interesting possibilities could include independent component analysis to identify "non-noise-like" signals, as well as tensor decomposition.

References

[1] B. Christiansen, T. Schmith and P. Thejll: A surrogate ensemble study of sea level reconstructions, *Journal of Climate*, Volume 23, Issue 16, pp. 4306–4326, 2004.

[2] J. A. Church, N. J. White, R. Coleman, K. Lambeck, J. X. Mitrovica: Estimates of the regional distribution of sea level rise over the 1950–2000 period, *Journal of Climate*, Volume 17, Issue 13, pp. 2609–2625, 2004.

[3] A. Kaplan, Y. Kushnir, M. A. Cane and M. B. Blumenthal: Reduced space optimal analysis for historical data sets: 136 years of Atlantic sea surface temperatures, *Journal of Geophysical Research*, Volume 102, Issue C13, pp. 27835–27860, 1997.

[4] P. Switzer and A. A. Green: *Min/max autocorrelation factors for multivariate spatial imagery*, Technical report no. 6, Department of Statistics, Stanford University, 1984.

A.5 Acceleration of the Greenland ice sheet mass loss as observed by GRACE: Confidence and sensitivity

The paper "Acceleration of the Greenland ice sheet mass loss as observed by GRACE: Confidence and sensitivity" was published in *Earth and Planetary Science Letters* in 2013.

While its subject is not fully within the scope of this PhD project, it was written entirely within the timespan of the project and is thus included here.

Acceleration of the Greenland ice sheet mass loss as observed by GRACE: Confidence and sensitivity

P.L. Svendsen*, O.B. Andersen, A.A. Nielsen

DTU Space, Technical University of Denmark, Kgs. Lyngby, Denmark

ARTICLE INFO

ABSTRACT

We examine the scale and spatial distribution of the mass change acceleration in Greenland and its statistical significance, using processed gravimetric data from the GRACE mission for the period 2002–2011. Three different data products – the CNES/GRGS, DMT-1b and GGFC GRACE solutions – have been used, all revealing an accelerating mass loss in Greenland, though with significant local differences between the three datasets. Compensating for leakage effects, we obtain acceleration values of -18.6 Gt/yr^2 for CNES/GRGS, -8.8 Gt/yr^2 for DMT-1b, and -14.8 Gt/yr^2 for GGFC.

We find considerable mass loss acceleration in the Canadian Arctic Archipelago, some of which will leak into the values for Greenland, depending on the approach used, and for our computations the leakage has been estimated at up to -4.7 Gt/yr^2.

The length of the time series of the GRACE data makes a huge difference in establishing an acceleration of the data. For both 10-day and monthly GRACE solutions, an observed acceleration on the order of $10-20$ Gt/yr^2 is shown to require more than 5 yrs of data to establish with statistical significance.

In order to provide an independent evaluation, ICESat laser altimetry data have been smoothed to match the resolution of the GRACE solutions. This gives us an estimated upper bound for the acceleration of about -29.7 Gt/yr^2 for the period 2003–2009, consistent with the acceleration values and corresponding confidence intervals found with GRACE data.

1. Introduction

In recent years, the mass loss of the Greenland Ice Sheet (GrIS) has been analysed in a variety of ways, including altimetry, gravimetry and mass budget calculations, establishing a continuing decrease in the ice mass, with a number of studies finding an acceleration in the mass loss, such as Rignot et al. (2008), or in glacial retreat, e.g. Howat and Eddy (2011).

Determination of acceleration in GRACE (Gravity Recovery and Climate Experiment) time series has been examined in previous studies using piecewise line fits (Chen et al., 2006), as well as line fits through a differenced time series for the entire ice sheet (Rignot et al., 2011). As noted by Wouters et al. (2008), the GRACE solutions contain enough data to allow regional estimation of trends, though assessing the mass loss to be dominated by summer events rather than a linear trend. We examine pointwise trend fits, though such trends should only be considered qualitatively.

The mass loss, previously mostly limited to the southeast part, has been spreading to northwest Greenland in recent years, as confirmed using GRACE and GPS data (Khan et al., 2010), Gardner

et al. (2011) have also found a rapidly increasing mass loss in the Canadian Arctic Archipelago (CAA) for the period 2004–2009, using both surface mass budget/discharge, GRACE and ICESat data.

While the GRACE mission provides a unique set of gravity data, the measurements need considerable processing to yield usable mass change data. Slobbe et al. (2009) compared four different GRACE solutions, obtaining mass change rates varying by almost a factor of two (between -128 and -218 Gt/yr) for the period 2002–2007. Sørensen and Forsberg (2010) also found substantial differences in Greenland mass change rates (between -67 and -189 Gt/yr for 2002–2008) depending on the GRACE solution used.

Velicogna (2009) fitted a quadratic trend to the GRACE data for Greenland (April 2002–February 2009), using a 13-month moving average and an *F*-test to conclude that it provides a better fit than a simple linear trend, and obtaining an acceleration for this period of -30 ± 11 Gt/yr^2.

We examine the variation in this mass loss acceleration within Greenland, with uncertainty estimation for both local and overall trends for three different datasets, with an additional three for reference. Since the time series for the GRACE data are relatively short for the purposes of determining secular trends, we have estimated a development of the size of the confidence intervals

* Corresponding author. Tel.: +45 45259742.
E-mail address: plsv@space.dtu.dk (P.L. Svendsen).

with increasing length of the observation period in order to determine the length of GRACE time series required to establish the presence of an acceleration.

2. Data

We consider three different GRACE data products, each giving mass changes as equivalent water height (EWH).

The CNES/GRGS (Groupe de Recherche de Géodésie Spatiale) 10-day solutions (release 02) used are $1° \times 1°$ grids based on spherical harmonics up to degree and order 50. They are stabilised (constrained) towards a time-variant mean field, EIGEN-GRGS.RL02.MEAN-FIELD (Bruinsma et al., 2010) and span from August 2002 to August 2011. A total of twenty 10-day solutions are missing, mostly at the beginning and end of the time series.

The DMT-1b monthly solutions from Delft Institute for Earth-Oriented Space research (DEOS) are $0.5° \times 0.5°$ grids, based on spherical harmonics up to degree and order 120. The timespan covered is from February 2003 to November 2010. While their temporal resolution is lower than the CNES/GRGS solution, their spatial resolution is considerably higher. The DMT-1b solutions are given as deviations from the mean field EIGEN-GL04C, and smoothed by post-processing using a Wiener filter (Ditmar et al., 2011). One monthly solution (June 2003) is missing.

The monthly solutions from Global Geophysical Fluids Center (GGFC) are $1° \times 1°$ grids, truncated at degree 60 and covering from April 2002 to September 2011. They are derived from the CSR RL04 solutions, and have decorrelation/destriping and 500 km Gaussian smoothing applied, consequently yielding generally smaller signals than the other solutions (Swenson and Wahr, 2006). Five monthly solutions are missing from the GGFC (June/July 2002, June 2003, and January/June 2011); they have been downloaded from http://www.csr.utexas.edu/research/ggfc/datar esources.html.

In order to test the effect of smoothing and processing of the GRACE data on establishing mass loss acceleration, three additional models were included in the analysis. These models were release 4 of the Center for Space Research (CSR) and Geo-ForschungsZentrum Potsdam (GFZ) for the period 2003–2011 (downloaded from (http://podaac.jpl.nasa.gov/grace) as well as the ITG-GRACE 2010 for the slightly shorter period 2003–2009. As the GGFC is basically a decorrelated version of the CSR solution, this gives a total of five independent models which were submitted to a common or identical computation of mass change for Greenland. Monthly solutions were used to compute EWH mass changes using the method by Andersen et al. (2005) and applying a Gaussian smoothing of 500 km. Gravity coefficients for degree and order 2–50 were used fora each model, as GRACE does not recover spherical harmonic coefficients 0 and 1. Furthermore the C_{20} time series was substituted by more accurate time series derived from satellite laser ranging (Cheng and Tapley, 2004). For consistency, the following monthly solutions have been set to be missing for all solutions: June/July 2002, June 2003, and January/June 2011.

3. Model

Our model is a simple ordinary least squares (OLS) regression model. Since we are testing for the presence of an acceleration, the predictors in the model include a constant term, time, and time squared (the latter normalised by 1/2). Also included, based on results from spectral analysis of the CNES/GRGS data, are harmonic oscillations of 1/1-, 1/2- and 1/3-yr wavelengths; the subannual frequencies are due to the somewhat sawtooth-shaped waveform of the annual signal, as the ice level each year takes
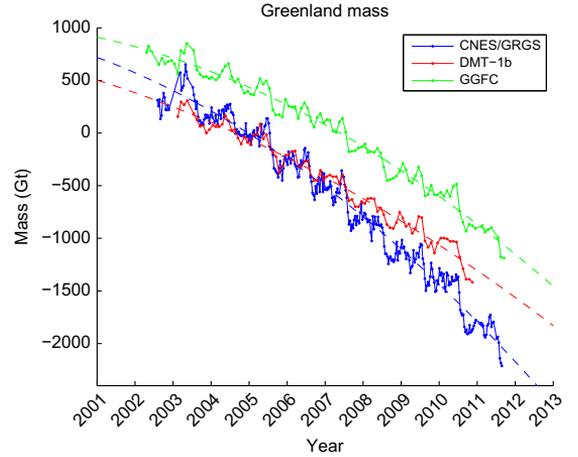
Fig. 1. Time series and OLS model fits for the Greenland mass for each of the GRACE solutions used (400 km mask extension applied); the mass values are relative to an arbitrary zero level. Only the nonseasonal (polynomial) parts of the model are shown.

more time to build up than to melt, which is also visible to some extent in Fig. 1. Velicogna (2009) also uses a quadratic model to examine the acceleration of the ice sheet, though with a smoothing procedure to filter out seasonal variation, then fits a quadratic trend; this should take into account the variability of the seasonal amplitude. However, variation in the seasonal amplitude and phase will still show up in the residuals from an OLS model, and we find that an OLS model with the three harmonic oscillations to provides a very good fit to the GRACE solutions used.

3.1. Parameter dispersion

Considering each pixel's EWH time series as a column vector $\boldsymbol{y}$, we can build a predictor matrix $\mathbf{X}$ containing the desired functions of time. For such an OLS model

$$\boldsymbol{y} = \mathbf{X}\boldsymbol{\theta} + \boldsymbol{e} \tag{1}$$

we can determine a dispersion matrix of the estimated coefficients $\hat{\boldsymbol{\theta}}$, $D(\hat{\boldsymbol{\theta}})$. This is given by the predictor and the mean squared error ($\hat{\sigma}^2 = \hat{\boldsymbol{e}}^\mathsf{T}\hat{\boldsymbol{e}}/(N-p)$) of the fit relative to the input data

$$D(\hat{\boldsymbol{\theta}}) = \hat{\sigma}^2 (\mathbf{X}^\mathsf{T}\mathbf{X})^{-1} \tag{2}$$

Then, using the diagonal elements $\hat{\sigma}_{\theta_i}^2 = D(\hat{\boldsymbol{\theta}})_{i,i}$ (i.e., the parameter variances), we can obtain a test statistic

$$z_i = \frac{\hat{\theta}_i - c_i}{\hat{\sigma}_{\theta_i}} \tag{3}$$

to test for equality of the coefficient $\hat{\theta}_i$ with a constant c_i. Assuming the residuals to be normally distributed and independent, z_i will then follow a t-distribution with $(N-p)$ degrees of freedom, where N is the number of data points in the time series, and p the number of parametres. The assumption about the residuals is key to the validity of the coefficient confidence intervals; if data uncertainties are not present as Gaussian noise of appropriate variance, the confidence intervals will generally not reflect the true sensitivity of the model.

4. Results

4.1. Mass trends for the entire Greenland ice sheet

Fitting to the area-integrated EWH values within the Greenland mask (as opposed to the pointwise data), all three GRACE solutions show an overall acceleration in the ice mass loss. The best-fit mass acceleration values for Greenland within a mask extended 400 km from the coast are shown in Table 1.

The OLS model provides a good fit to the Greenland mean EWH for all three datasets; all have $R^2 > 0.98$, and all have root mean squared errors (RMSE) of less than 80 Gt (or 2 cm EWH). Rignot et al. (2011) obtain a GRACE mass loss acceleration for Greenland of 17.0 ± 8 Gt/yr^2, with an additional estimate from the mass budget method of 19.3 ± 4 Gt/yr^2 (i.e., estimated from weather and glacial movement).

The DMT-1b solution yields a smaller RMSE than the other two solutions, though the coefficient of determination R^2 is the smallest of the three. This suggests that although the model provides a closer fit in absolute terms, it also generally exhibits less variation to explain. The differences between the GRACE products may be due to differences in the way the solutions are constrained; the Greenland mass values from DMT-1b are less prone to large, sudden jumps.

The CNES/GRGS and the GGFC solutions have roughly the same time span, and the acceleration integrated over Greenland are very similar and within the confidence intervals estimated. The DMT-1b solution provides a somewhat lower estimate due to the fact that data are missing for 2002 and 2011 and thus the time span is shorter; also, this solution sees a very large slowdown of the melting in Southeast Greenland, cf. Fig. 3. If the southeastern part of Greenland is not considered the three solutions agree to better than ± 3 Gt/yr^2 in acceleration.

The confidence intervals given in Table 1 are determined from the residuals of the model fit to the input data. Since the data products are very smooth, these errors may be artificially low. As an alternative, one could decide on a fixed estimate for $\hat{\sigma}^2$ if specific knowledge is available regarding the uncertainties in the data.

Because of the smoothness of the data, and because the mass loss is largely focused in coastal areas, the relevant mass changes affect pixel time series some distance outside Greenland, and a spatially extended mask must be applied when determining the total mass loss. In our investigation we used a spatial mask extension of half the maximum wavelength represented in each model (cf. Slobbe et al., 2009). Consequently the spatial mask extensions were 400 km for GRGS, 330 km for GGFC and 170 km for the DMT-1b model.

Note that we have not corrected the trends for glacial isostatic adjustment (GIA), which in Greenland may appear in the mass change rate as up to 1–2 cm/yr of water equivalent, mostly present in the northernmost part of Greenland, per the model by (Paulson et al., 2007). However, for the short time span considered, this rate may be considered constant, allowing us to

consider the acceleration without correcting for GIA. Velicogna (2009) also concluded that a change in the rate of the ice mass loss on this time scale would not be affected by GIA.

Change in the rate of ice mass loss might also be contaminated by leakage from change in mass loss rates from other geophysical signals. Velicogna (2009) estimated the contribution from a combination of the GLDAS land hydrology and ECCO general circulation model (Lee et al., 2002). In both cases it was found that the predicted oceanic and hydrological leakage is negligible.

The most notable leakage problem will be leakage from recently observed mass loss acceleration in the CAA region, as described by Gardner et al. (2011). A simulation was performed to study the impact of this mass loss. In this simulation, the observed mass acceleration of approximately -20 Gt/yr^2 by Gardner et al. (2011) was added to the northern CAA region and a spherical harmonic expansion to degree and order 50 was performed. Subsequently the contribution to this signal under the 400 km extended Greenland mask were computed. This gave a leakage of -4.7 Gt/yr^2 for the 400 km mask, -3.0 Gt/yr^2 for the 330 km GGFC mask and -1.2 Gt/yr^2 for the 170 km DMT-1b mask. Subsequently our estimates should be corrected for this contribution; the corrected acceleration values in Table 1 will thus be -18.6 Gt/yr^2 for the CNES/GRGS solutions, -8.8 Gt/yr^2 for DMT-1b, and -14.8 Gt/yr^2 for GGFC.

Table 2 confirms that all commonly used GRACE solutions show a clear acceleration of mass loss on Greenland. The CSR and GFZ both confirm an acceleration of the same magnitude as the original CNES/GRGS solutions as well as the CNES/GRGS solution processed using common or identical processing to the two other GRACE solutions. It is also notable that the CSR solution shows higher acceleration than the GGFC solution based on the same Release 4 CSR data, but decorrelated to remove the north-south striping in GRACE (Chen et al., 2006). The results found here are in agreement with the fact that this decorrelation removes part of the signal (Swenson and Wahr, 2006). Contrary to this both the DMT and the CNES/GRGS solutions computed using identical processing shows less acceleration. This can largely be explained by the fact that the manually processed solution is smoother and

Table 2
Acceleration values with 95% confidence intervals for all six models. In this case, the solutions have been processed in a common way—truncated at degree and order 50, smoothed with a 500 km Gaussian filter and computed with 400 km Greenland mask extension. Note that the GGFC solution thus becomes equal to the CSR product on which it is based.

GRACE product	Time span	d/o	Smoothing (km)	Acceleration (Gt/yr^2)	RMSE (Gt)
CSR (GGFC)	2003–2011	50	500	-22.1 ± 4.3	66.9
GFZ	2003–2011	50	500	-21.3 ± 3.9	59.1
CNES/GRGS	2002–2011	50	500	-18.9 ± 1.7	48.3
ITG	2002–2009	50	500	-12.8 ± 4.8	41.7
DMT	2003–2010	50	500	-14.2 ± 4.9	54.1

Table 1
Acceleration values with 95% confidence intervals, root mean squared error (RMSE, $\hat{\sigma}$), and coefficient of determination for OLS fits to the total Greenland mass level. The values are given for mask extensions calculated for the maximum degree and order of each individual dataset; as described in the text, the values include a leakage from the Canadian Arctic Archipelago, estimated as up to approximately -4.7 Gt/yr^2 for the largest extension. The acceleration value with this estimated leakage removed is also shown. Processing notes: (1) inversion, (2) optimal (Wiener) filtering, and (3) decorrelation and 500 km Gaussian smoothing.

GRACE product	Time span	Resolution	Proc.	Acc. (Gt/yr^2)	Acc. (no CAA) (Gt/yr^2)	RMSE (Gt)	R^2
CNES/GRGS	2002–2011	d/o 50	(1)	-23.3 ± 2.9	-18.6	76.6	0.9885
DMT-1b	2003–2010	d/o 120	(2)	-10.0 ± 3.8	-8.8	41.7	0.9856
GGFC	2002–2011	d/o 60	(3)	-17.8 ± 3.1	-14.8	51.3	0.9898

hence will be more contaminated by leakage from CAA as described previously.

The RMSE values of Table 2 show a slightly different picture compared to Table 1; for example, the CSR solution (on which the GGFC is based) now has the largest RMSE of all. Large values of the RMSE appear to be associated with large acceleration, and may thus be a reflection of a larger underlying signal variation in the GRACE solution, rather than a poorer model fit as such.

The DMT and ITG models (Mayer-Gürr et al., 2005) only cover the first 7 and 6 yrs of the time period, respectively. Both show accelerations that are roughly 8 Gt/yr^2 smaller than the longer periods except for the models computed over longer timeseries. This seems to agree well with the fact that Greenland experienced record-breaking summer melting during 2010 and 2011 which is not fully accounted for in this shorter time series.

4.2. Spatial distribution of trends

Applying the OLS model to the individual time series (i.e., each pixel), we can obtain an estimate for the EWH acceleration in each particular point. Since the datasets are spatially very smooth, the mass loss from any actual point will be smeared out across numerous pixels, but we may obtain a qualitative value for the acceleration. The best-fit local accelerations for the individual data products are shown in Figs. 2–4.

Regressions on the individual pixels of the datasets generally show highly statistically significant results, with p-values for zero acceleration down to the order of 10^{-81} (CNES/GRGS), 10^{-5} (DMT-1b) and 10^{-33} (GGFC) within the Greenland mask. The particularly low values for the CNES/GRGS and GGFC data are likely due to the processing, with any signals constrained and/or smoothed to lie closely around the mean field.

The three solutions agree on a clear accelerated mass loss in the northwestern part of Greenland and all GRACE solutions agree that the major acceleration is found around the Melville Bay/Thule region where several huge glaciers are found. The CNES/GRGS solution also identifies a secondary maximum in the Disko Bay right on the Jakobshavn Glacier. It is interesting that this maximum is not seen in the CNES/GRGS data if the timespan is limited to the time period for the DMT-1b solution. By excluding or including CNES/GRGS GRACE data for 2011, it is generally revealed that the acceleration computed for the 2002–2010 period is continued in 2011, but with an increased acceleration around the Jakobshavn Glacier.

The DMT-1b solution clearly stands out from the other two solutions in Southeast Greenland. Both the CNES/GRGS and the
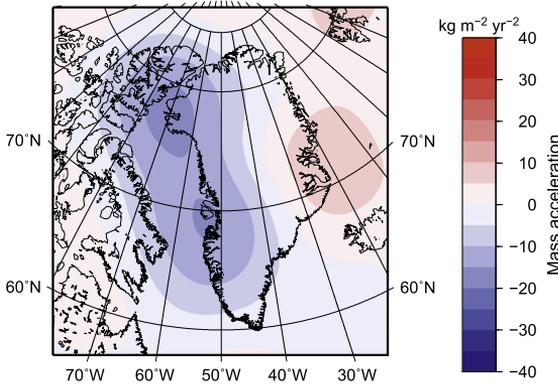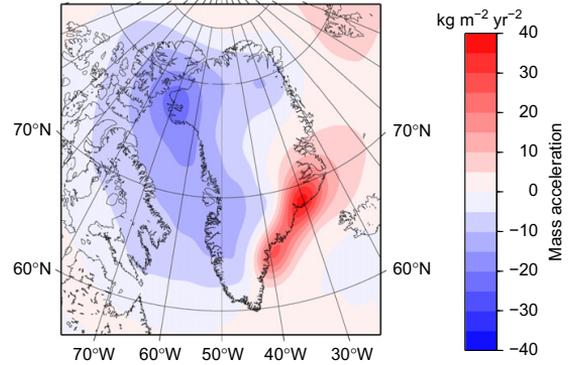

Fig. 3. Acceleration in the DMT-1b model over Greenland (February 2003–November 2010). Note the apparent strongly positive acceleration (slowing mass loss) in SE Greenland, which is not present in the CNES/GRGS and GGFC solutions.
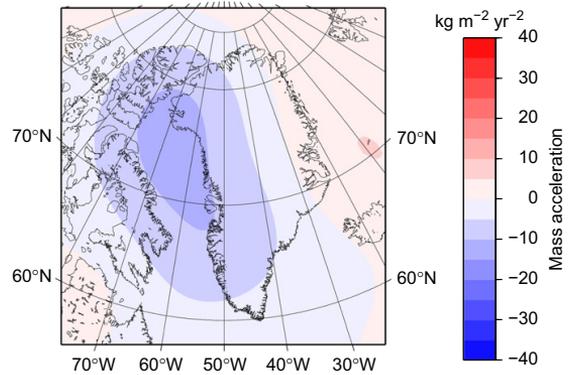

Fig. 4. Acceleration in the GGFC model over Greenland (April 2002–September 2011).

GGFC solutions show a positive acceleration in the eastern Greenland corresponding to a slowdown in the melting, but neither of the two solutions show the huge signal that is found in the DMT-1b solution.

The maximum in the DMT-1b solution is neatly located close to the Kangerdlugssuaq glacier around 68.5°N and 30.5°W, with a secondary maximum close to the Helheim glacier at 66.5°N and 37°W, which could support the physical nature of such a signal. Moreover, the DMT-1b solution is given up to degree and order 120, whereas the CNES/GRGS and GGFC are only given up to degree/order 50 and 60, respectively, and thus this model should be able to resolve much finer spatial signal. The six GRACE solutions processed as similarly as possible were studied to determine the effect of the processing (smoothing/inversion) on the result. Most GRACE solutions show a deceleration over southeast Greenland. However, for identical processing, the DMT solution clearly shows a much larger deceleration than any other solution.

In order to investigate this in more detail, Fig. 5 shows the time series of EWH development for the Kangerdlugssuaq glacier for the CNES/GRGS and DMT-1b solutions. The two models agree on the magnitude and rate of melting. However, a larger acceleration of the melting was seen during the 2005–2007 period and a corresponding deceleration in the 2007–2010 period is seen for the DMT-1b solution giving rise to a much larger overall positive acceleration for the 2002–2010 period. The huge acceleration of the melting during the first period have also been confirmed by GPS-observed uplift close to the two glaciers (Khan et al., 2010).

Fig. 2. Acceleration in the CNES/GRGS model over Greenland (July 2002–August 2011).
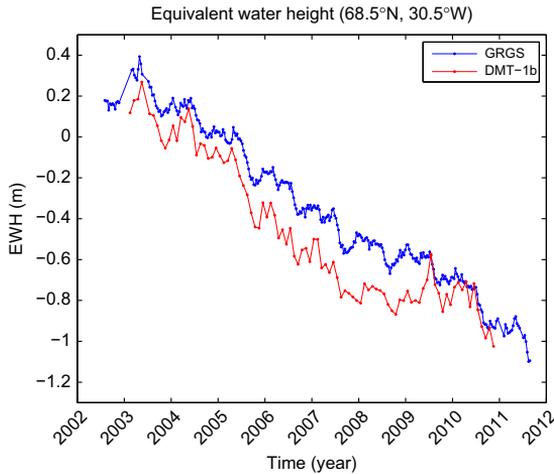
Fig. 5. EWH development for a point in southeast Greenland, where the DMT-1b model shows a large positive acceleration (see Fig. 3). It is clear that the positive acceleration is due to relatively low values in the period 2005–2009.

Fig. 6. Theoretical development of the standard deviation of the acceleration term with increasing time series length, taking into account the interval length and determined RMSE for each dataset.

4.3. Confidence intervals

The standard deviations of the acceleration terms are very much dependent on location, with larger dispersion generally occurring in areas containing any kind of signal (secular or seasonal variation). With the DMT-1b data, we obtain standard deviations of below 1 mm/yr^2 in the centre of the ice sheet to more than 4 mm/yr^2 in the southeast. In the southeast, a considerable seasonal signal is present, and the larger error is likely to be a reflection of the variations in seasonal changes.

The model RMS errors variy considerably for the local fits, with values of about 1.5 mm in central Greenland to 6 mm (CNES/GRGS) or 10 mm (DMT-1b) in the southeast, reflecting the spatially more well-defined phenomena in the DMT-1b solutions.

As the length of the GRACE time series increases, the acceleration term can be determined with improving precision. As Fig. 6 shows, the uncertainty is very similar for all three solutions, with slightly smaller confidence intervals for the CNES/GRGS solutions.

The standard deviations in Fig. 6 have been computed analytically, though (for ease of computation) without seasonal terms in the model, which we have empirically found to have a very small influence on the scale of these values.

The DMT-1b solutions yield a wider confidence interval for the total Greenland acceleration than the other two solutions, due to the time series being somewhat shorter than the other two (since the RMSE is virtually equal to that of the also monthly GGFC data).

Since the number of observations in each case is large compared to the number of model parameters, a $t(N-p)$ distribution will be approximately normal. Thus, the acceleration can be considered statistically significantly different from 0 when the term is more than 2–3 standard deviations from 0, assuming the RMSE to be an appropriate estimate of the uncertainty in the data.

The length of the time series of the GRACE data makes a huge difference in establishing the presence of an acceleration in the data. For example the monthly DMT-1b and GGFC an observed acceleration on the order of 10–20 Gt/yr^2 requires more than 5 yrs of data to establish. This period may naïvely be considered shorter for the 10-day GRGS data, but it should be noted that the shorter time averaging used for the GRGS data
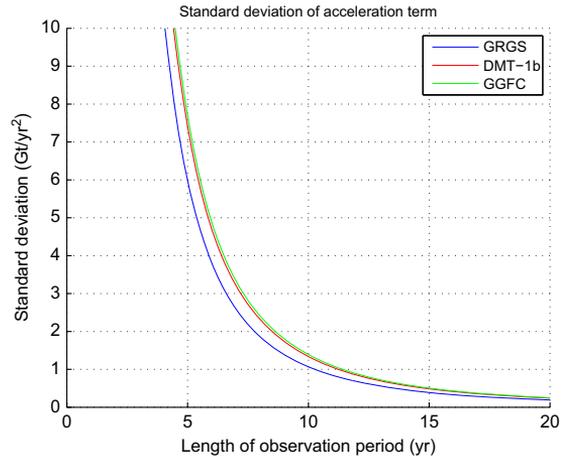
sacrifices some of the spatial resolution (and precision of each data point) of the data.

4.4. Comparison with ICESat results

The laser altimeter onboard ICESat can be used to provide an upper bound on the acceleration in ice mass loss of Greenland. ICESat observes the change in volume of the Greenland ice sheet. The laser pulse reflects from the uppermost surface of the snow, making it difficult to accurately estimate mass change from ICESat. However, assuming the entire volume to be solid ice and using the density of pure ice (917 kg/m^3), volume change from ICESat can be used to estimate an upper bound on the mass change. ICESat laser altimetry data for the 2003–2009 period were provided and prepared as in Sørensen et al. (2011) for comparison with the GRACE data. The estimated ICESat normal point acceleration parameters were then expanded into spherical harmonic functions to degree and order 50 to yield an upper bound on the acceleration of mass-loss of approximately −29.7 Gt/yr^2.

This compares well with the findings using CNES/GRGS and GGFC in this study. ICESat provides very high resolution data and the results by Sørensen et al. (2011) also confirm that the melting is primarily focused along the edges of the Greenland Ice Sheet. Unfortunately, due to the failure of the instrument onboard the satellite, the ICESat data are only available up to 2009.

5. Conclusions

We find a statistically significant acceleration in the Greenland Ice Sheet mass loss with all three data products used. There is variation in best-fit values between the data products and their respective uncertainties. For the CNES/GRGS and GGFC solutions spanning the entire 2002–2011 period, we find an acceleration of −18.6 Gt/yr^2 and −14.8 Gt/yr^2, whereas the DMT-1b solution spanning 2003–2010 gives a lower acceleration of −8.8 Gt/yr^2. These values are lower than the −30 ± 11 Gt/yr^2 by Velicogna (2009), though nearly consistent with the value of −17.0 ± 8 Gt/yr^2 by Rignot et al. (2011).

In addition to the mass loss in Greenland, we find a considerable contribution from the CAA of up to −4.7 Gt/yr^2. This is both apparent when plotting the local best-fit acceleration, and was

verified by simulating a mass loss at the CAA and computing the contribution under the Greenland mask. The findings are also supported by Gardner et al. (2011).

Despite local disagreement between the data products, all models agree that the acceleration in mass loss is largely confined to the west-northwestern part of Greenland. For southeast Greenland, the DMT-1b model indicates a significant deceleration which is not found by the two other models.

Establishing the presence of an acceleration on the order of magnitude found in the Greenland Ice Sheet requires more than 5 yrs of data, and we find that the GRACE time series available are now long enough to establish the presence of such an acceleration.

Acknowledgments

References

Andersen, Ole B., Seneviratne, S.I., Hinderer, J., Viterbo, P., 2005. GRACE-derived terrestrial water storage depletion associated with the 2003 European heatwave. Geophys. Res. Lett. 32, 18, http://dx.doi.org/10.1029/2005GL023574.

Bruinsma, S., Lemoine, J.-M., Biancale, R., Valès, N., 2010. CNES/GRGS 10-day gravity field models (release 2) and their evaluation. Adv. Space Res. 45, 587–601, http://dx.doi.org/10.1016/j.asr.2009.10.012.

Chen, J.L., Wilson, C.R., Tapley, B.D., 2006. Satellite gravity measurements confirm accelerated melting of Greenland Ice Sheet. Science 313, 1958–1960.

Cheng, M., Tapley, B., 2004. Variations in the Earth's oblateness during the past 28 years. J. Geophys. Res. 109, B0940.

Ditmar, P., Liu, X., Siemes, C., Hashemi Farahani, H., Klees, R., Revtova, E., Zhao, Q, 2011. DEOS Mass Transport Model Release 1 (DMT-1). Description Document.

Gardner, A.S., Moholdt, G., Wouters, B., Wolken, G.J., Burgess, D.O., Sharp, M.J., Cogley, J.G., Braun, C., Labine, C., 2011. Sharply increased mass loss from glaciers and ice caps in the Canadian Arctic Archipelago. Nature 473, 357–359, http://dx.doi.org/10.1038/nature10089.

Howat, I.M., Eddy, A., 2011. Multi-decadal retreat of Greenland's marine-terminating glaciers. J. Glaciol. 57, 389–396.

Khan, S.A., Wahr, J., Bevis, M., Velicogna, I., Kendrick, E., 2010. Spread of ice mass loss into northwest Greenland observed by GRACE and GPS. Geophys. Res. Lett. 37, L06501, http://dx.doi.org/10.1029/2010GL042460.

Lee, T., Fukumori, I., Menemenlis, D., Xing, Z., Fu, L.-L., 2002. Effects of the indonesian throughflow on the pacific and indian oceans. J. Phys. Oceanogr. 32, 1404.

Mayer-Gürr, T., Ilk, K.H., Eicker, A., Feuchtinger, M., 2005. ITG-CHAMP01: a CHAMP gravity field model from short kinematical arcs of a one-year observation period. J. Geod. (Springer-Verlag) 78, 462–480.

Paulson, A., Zhong, S., Wahr, J., 2007. Inference of mantle viscosity from GRACE and relative sea level data. Geophys. J. Int. 171, 497–508, http://dx.doi.org/10.1111/j.1365-246X.2007.03556.x.

Rignot, E., Box, J.E., Burgess, E., Hanna, E., 2008. Mass balance of the Greenland ice sheet from 1958 to 2007. Geophys. Res. Lett. 35, L20502, http://dx.doi.org/10.1029/2008GL035417.

Rignot, E., Velicogna, I., van den Broeke, M.R., Monaghan, A., Lenaerts, J.T.M., 2011. Acceleration of the contribution of the Greenland and Antarctic ice sheets to sea level rise. Geophys. Res. Lett. 38, L05503, http://dx.doi.org/10.1029/2011GL046583.

Slobbe, D.C., Ditmar, P., Lindenbergh, R.C., 2009. Estimating the rates of mass change, ice volume change and snow volume change in Greenland from ICESat and GRACE data. Geophys. J. Int. 176, 95–106, http://dx.doi.org/10.1111/j.1365-246X.2008.03978.x.

Sørensen, L.S., Forsberg, R., 2010. Greenland Ice Sheet mass loss from GRACE monthly models. Gravity Geoid Earth Obs., 527–532.

Sørensen, L.S., Simonsen, S.B., Nielsen, K., Lucas-Picher, P., Spada, G., Adalgeirs-dottir, G., Forsberg, R, Hvidberg, C.S., 2011. Mass balance of the Greenland ice sheet (2003–2008) from ICESat data: the impact of interpolation, sampling and firn density. Cryosphere 5, 173–186, http://dx.doi.org/10.5194/tc-5-173-2011.

Swenson, S., Wahr, J., 2006. Post-processing removal of correlated errors in GRACE data. Geophys. Res. Lett. 33, L08402, http://dx.doi.org/10.1029/2005GL025285.

Velicogna, I., 2009. Increasing rates of ice mass loss from the Greenland and Antarctic ice sheets revealed by GRACE. Geophys. Res. Lett. 36, L19503, http://dx.doi.org/10.1029/2009GL040222.

Wouters, B., Chambers, D., Schrama, E.J.O., 2008. GRACE observes small-scale mass loss in Greenland. Geophys. Res. Lett. 35, L20501, http://dx.doi.org/10.1029/2008GL034816.

A.6   Confidence and sensitivity of sea-level reconstructions

Proceedings from oral presentation given at CLIVAR WGOMD/SOP Workshop on Sea Level Rise, Hobart, Australia, 2013.

Confidence and sensitivity of sea-level reconstructions

P. Limkilde Svendsen[1], O. Baltazar Andersen[1] and A. Aasbjerg Nielsen[1]

1) **DTU Space, Technical University of Denmark, Kgs. Lyngby, Denmark**

Introduction

Reconstructions of historical sea level on the timescale of a few decades to slightly more than a century has been notably established, for example in Church et al. (2004) and Church and White (2011), using satellite altimetry from 1993 onwards to establish a calibration period for a model. From this calibration period, empirical orthogonal functions (EOFs) are obtained, the time-variable amplitudes of which are then constrained by tide gauge records. Thus, both historical mean sea level and regional distributions can be estimated. Minimum/maximum autocorrelation factors (MAF) (Switzer and Green, 1984) is a decomposition technique developed to isolate noise components from multivariate data, based on the assumption that the desired signal is spatially (or temporally) correlated with a shifted version of itself, while noise will generally be uncorrelated.

Model

As in Church et al. (2004), the amplitudes of each EOF are determined by employing a regularized optimal interpolation as described in Kaplan et al. (2000). However, in this preliminary analysis, the tide gauge data are represented by extracts from satellite altimetry, which allows the convenience of a vertical datum consistent between the calibration period and the "tide gauge" record. The unknown tide gauge datums are handled in Church et al. (2004) by using first differences of the time series, and in Ray and Douglas (2011) by solving for the datum of each gauge.

Analysis

For this analysis, 455 pre-selected tide gauge positions (from Church et al., 2004, selected for time series length and geodetic quality) have been used, in order to emulate a real reconstruction problem, though isolating the influences of tide gauge position and choice of calibration period. This analysis focuses on the influence of the character of the calibration period, and the resulting reconstruction error for various lengths of the calibration period. The influence of the prominent 1997/98 El Niño event has also been examined, showing a more Central Pacific El Niño-like pattern in the leading EOFs when excluding 1997/98 from the calibration period.

The error of the reconstruction with respect to known satellite altimetry for different lengths of the calibration period is shown in Figure 1. It appears that for calibration periods shorter than approximately 10 years, the error rapidly accumulates when moving away from the calibration, whereas the error seems largely stationary at a moderate level for longer calibration periods. This might be connected to the fact that all three reconstructions include 10 EOFs, and so may capture undesirable signals for the shortest period. To estimate the influence of geographical distribution, separate solutions have been made with only Northern Hemisphere and Southern Hemisphere gauges, respectively, see Figure 2. The MAF technique has been very preliminarily studied for this project, recovering some ENSO-like patterns, but with some work still needed to correctly handle masked-out areas in data grids.

Conclusions

The inclusion of a spatially uniform pattern (sometimes referred to as "EOF0") in the model basis has been found to be crucial in appropriately reconstructing global mean sea level, more so than the spatial distribution of tide gauges or the choice of the EOFs. This is in line with Christiansen et al. (2010), who also noted that the resulting performance is comparable to a simple arithmetic mean of the tide gauges; for improvement, they suggest using long-term climate simulations as an alternative way of obtaining the EOFs.

Regularization is of little concern for this preliminary analysis, since using actual altimetry data does not introduce the sparse coverage or possibly contradictory constraints of tide gauges. Indeed, it makes only a tiny difference in this study. In this case, limiting the choice of available to either hemisphere does not make much difference to the overall accuracy of the reconstruction; however, this study does not take into account the quality of the actual tide gauge data, only their spatial positions.

The MAF transform, while providing spatially "smooth" patterns, does not address the issue of missing data more than does the EOF. In addition, sea surface variability occurs on a variety of scales, including large-scale oscillation patterns like the ENSO and mesoscale phenomena, and any covariance across spatial scales may be poorly captured by the MAF transform.

References

Christiansen, B., T. Schmith, and P. Thejll, 2010: A surrogate ensemble study of sea level reconstructions.
Journal of Climate, 23 (16), 4306-4326.

Church, White, Coleman, Lambeck, and Mitrovica, 2004: Estimates of the regional distribution of sea level
rise over the 1950-2000 period. Journal of Climate, 17 (13), 2609-2625.

Church, J. A. and N. J. White, 2011: Sea-level rise from the late 19th to the early 21st century. Surv Geophys, 32 (4-5), 585_602.

Kaplan, A., Y. Kushnir, and M. A. Cane, 2000: Reduced space optimal interpolation of historical marine sea level pressure: 1854-1992. Journal of Climate, 13 (16), 2987-3002.

Ray, R. D. and B. C. Douglas, 2011: Experiments in reconstructing twentieth-century sea levels. Progress in Oceanography, 91 (4), 496-515.

Switzer, P. and A. A. Green, 1984: Min/max autocorrelation factors for multivariate spatial imagery. Technical Report 6, Department of Statistics, Stanford University, Stanford, California.
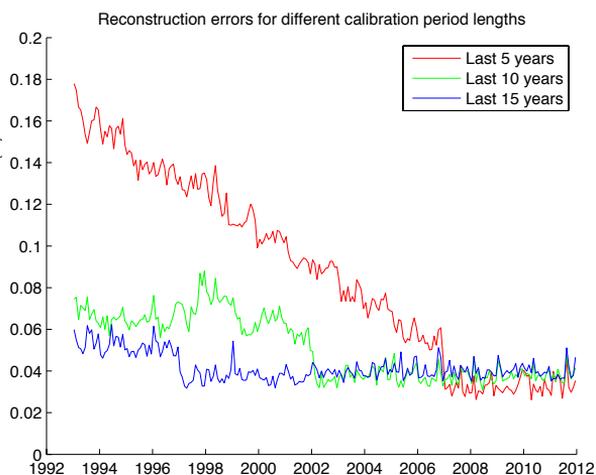
Figure 1: Global mean reconstruction error (with respect to satellite altimetry) for different calibration periods (shown in legend). All reconstructions shown include 10 EOFs in addition to an EOF0, and are fitted to the pseudo-tide gauges using an OLS fit. All tide gauge locations from the PSMSL database are used.
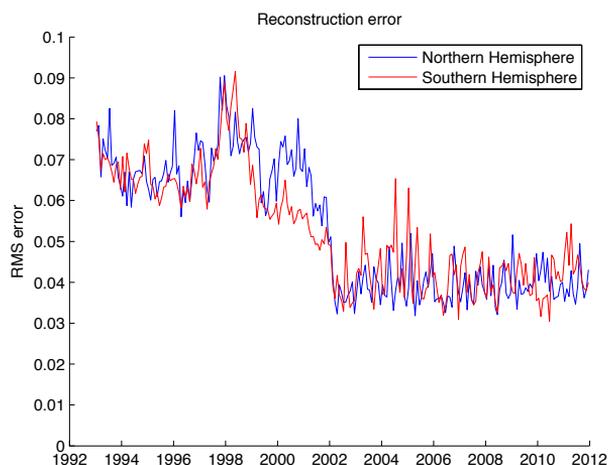

Figure 2: Global mean reconstruction error (with respect to satellite altimetry) for calibration patterns fitted to gauges only in the Northern or Southern Hemisphere, respectively. 364 of the 455 gauges used are in the Northern Hemisphere, while the remaining 91 are in the Southern Hemisphere. All reconstructions shown include 10 EOFs in addition to an EOF0, and are fitted to the pseudo-tide gauges using a Kaplan-based model.

Modeling Sea Level Rise and Ice Sheet Evolution using the Community Ice Sheet Model within the Community Earth System Model

Philip Jones[1], Stephen Price[1], William Lipscomb[1], Matthew Hoffman[1], Jeremy Fyke[1], Matthew Maltrud[1], Xylar Asay-Davis[1, 2, 3], Dan Martin[4]

1) **Los Alamos National Laboratory, Los Alamos, New Mexico**
2) **New York University, New York, New York**
3) **Potsdam Institute for Climate Impact Research, Potsdam, Germany**
4) **Lawrence Livermore National Laboratory, Livermore, California**

Introduction

Predicting future sea level rise requires comprehensive ice sheet models that can capture the important dynamics within the ice sheet. In addition, such an ice sheet model must be coupled with an Earth System Model to address the response of the ice sheets to future changes in forcing, including both the surface mass balance and melting due to ocean waters reaching the ocean-ice shelf interface. This brief note describes recent progress in developing the Community Ice Sheet Model (CISM) and coupling this model within the Community Earth System Model (CESM). A broad set of activities is described, including ice sheet dynamics, subglacial hydrology, surface mass balance and ocean-ice shelf coupling.

The Community Ice Sheet Model (CISM)
The CISM effort is focused on developing an ice sheet model suitable for use within coupled climate models for projections of future sea level rise. Initially, CISM started with the Glimmer model that simulated ice sheet dynamics based on the shallow ice approximation on uniform, rectilinear grids (Rutt et al. 2009). Initial development focused on coupling Glimmer with the CESM model (see below).

More recently, the dynamics of the model has been upgraded to a higher-order approximation to the full Stokes model, namely the first-order scheme of Blatter and Pattyn (2003). Improved solvers and domain-decomposition based parallelism were also implemented to allow for efficiency on larger computational grids and at higher resolution (Lemieux et al. 2011; Evans et al. 2012). This higher-order, parallel implementation of CISM formed the basis for simulations that were included in the SeaRISE (Bindschadler et al. 2013) and Ice2Sea (Edwards et al. 2013a; Edward et al. 2013b; Shannon et al. 2013) intercomparison efforts. Model output compares reasonably well with observed ice flow and, when perturbed with observational time series of changing ice flux, with observed ice sheet elevation changes (Price et al. 2011).

Current projects are developing new dynamical formulations on variable-resolution horizontal grids. Variable-resolution

A.7 Using leverages for objective analysis of PSMSL tide gauges in Arctic Ocean sea level reconstruction

Poster presented at PSMSL 80th Anniversary Workshop on Sea Level Science, Liverpool, United Kingdom, 2013.

Using leverages for objective analysis of PSMSL tide gauges in Arctic Ocean sea level reconstruction

Technical University of Denmark

Peter Limkilde Svendsen[1], Ole Baltazar Andersen[1] and Allan Aasbjerg Nielsen[2]
plsv@space.dtu.dk, oa@space.dtu.dk, alan@dtu.dk | [1]DTU Space, [2]DTU Compute
Technical University of Denmark, Kgs. Lyngby, Denmark

INTRODUCTION

For reconstructing historical sea levels in the Arctic area, lack of data presents a major challenge. We attempt to adapt the model by Church et al. (2004), examining inclusion criteria for tide gauges in the area.

The reconstruction model is based upon spatial, stationary patterns of variability extracted from a calibration period, usually satellite data. These patterns are determined as empirical orthogonal functions (EOFs). The model determines, for each point in time, an appropriately weighted sum of these, constrained locally by tide gauge records and regularized per Kaplan et al. (1997).

The *leverage* of each tide gauge is a statistical measure of its influence on the result. This way, we can readily identify possible outliers among the tide gauge records in a procedural, objective way.
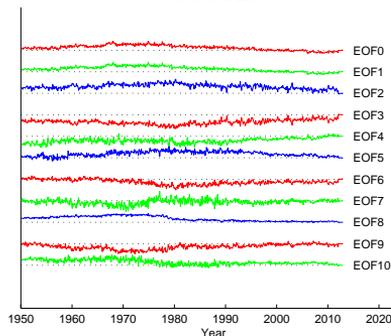
DATA

We use monthly PSMSL tide gauge data (RLR only) above approx. 60°N, allowing only records from stations with more than 5 years of data. We use the first differences of the time series to work around vertical datum considerations, then integrate the results, as in Church et al. (2004). GIA correction has been applied to the tide gauges, using the Peltier ICE-5G model (Peltier, 2004).

For this preliminary analysis, the EOFs have been extracted from the Drakkar ocean model (1949–2008).

EOFs

The reconstruction model incorporates a spatially uniform pattern (known as an "EOF0"), in addition to the leading ten EOFs. The first four of these are shown below.
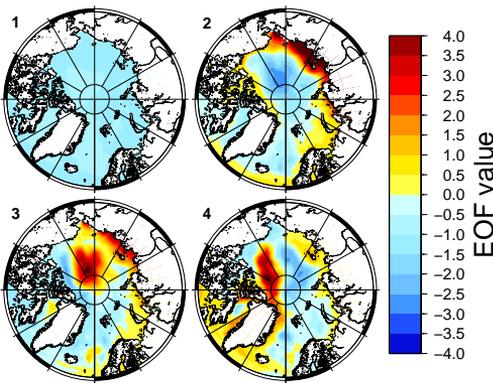

Time series of EOFs

EOF1 is fairly close to uniform and may capture a large amount of overall trend. It is by far the dominant mode in the Drakkar data, explaining almost 90% of the variance.

HIGH-LEVERAGE GAUGES

In least-squares regression, the leverage of each observation is given by the diagonal elements of the "hat matrix" that relates the response variable y (in this case, tide gauge records) to its estimate, $\hat{y}$. See e.g. Nielsen, 2013.

The map shows all tide gauges included in the reconstruction (green) and those rejected due to high leverage (red). Rejection criterion here is three times the mean gauge leverage.

The plot shows an example of rejected gauges, the three on Kotelny Island (75°N, 140°E). These gauges may simply not be sufficiently represented within the appropriate EOFs.

Example of rejected gauges (Kotelny Island)
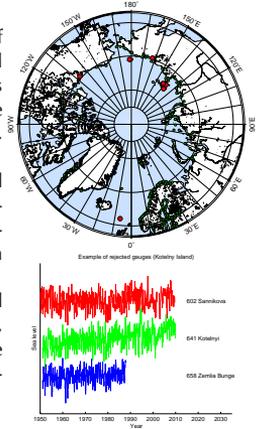
LOCAL RECONSTRUCTION ABILITY

To assess the validity of the results, the reconstructed sea-level time series in selected points have been plotted and compared with actual tide gauge data and the existing MONARCH-A reconstruction (by Henry et al.). The model has been applied both without regularization ("OLS") and with regularization ("Kaplan").
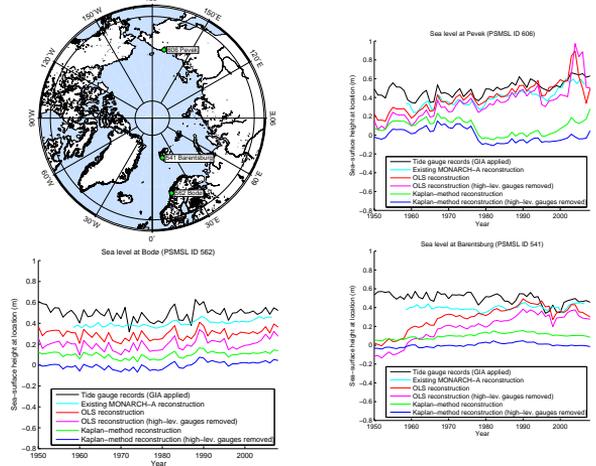
The unregularized reconstruction seems more prone to developing nonexistent trends in the time series, and not very appropriate for this purpose. Removing a handful of gauges of high leverage seems to dampen the oscillations near the coast considerably, while keeping almost the same behaviour in open ocean.

REFERENCES

- Church, J., White, N., Coleman, R., Lambeck, K. and Mitrovica, J. (2004). Estimates of the regional distribution of sea level rise over the 1950–2000 period. Journal of Climate, Volume 17, Issue 13, pp. 2609–2625.

- Kaplan, A., Kushnir, Y., Cane, M.A. and Blumenthal, M.B. (1997). Reduced space optimal analysis for historical data sets: 136 years of Atlantic sea surface temperatures. Journal of Geophysical Research, Volume 102, Issue C13, pp. 27,835–27,860.

- Nielsen, A.A. (2013). Least Squares Adjustment: Linear and Nonlinear Weighted Regression Analysis. Lecture note.

- Peltier, W.R. (2004). Global glacial isostasy and the surface of the ice-age Earth: The ICE-5G (VM2) model and GRACE. Annual Review of Earth and Planetary Sciences, Volume 32, pp. 111-149.

A.8   Analysis of sea-level reconstruction techniques for the Arctic Ocean

Poster presented at AGU Fall Meeting 2013, San Francisco, United States.

Analysis of sea-level reconstruction techniques for the Arctic Ocean

Abstract ID: 1814711 | Peter Limkilde Svendsen[1] | Ole Baltazar Andersen[1] and Allan Aasbjerg Nielsen[2]

plsv@space.dtu.dk, oa@space.dtu.dk, alan@dtu.dk | [1]DTU Space, [2]DTU Compute | Technical University of Denmark, Kgs. Lyngby, Denmark

Introduction

For reconstructing historical sea levels in the Arctic area, lack of data presents a major challenge. We attempt to adapt the model by Church et al. (2004), examining inclusion criteria for tide gauges in the area. The tide gauge records are taken from the PSMSL database.

The reconstruction model is based upon spatial, stationary patterns of variability extracted from a calibration period, usually satellite data; however, for this exercise, we are using data from the Drakkar ocean model, covering the period 1958–2008 with monthly data. These patterns are determined as empirical orthogonal functions (EOFs). The model determines, for each point in time, an appropriately weighted sum of these, constrained locally by tide gauge records and regularized per Kaplan et al. (1997).

The leverage of each tide gauge is a statistical measure of its influence on the result. This way, we can readily identify possible outliers among the tide gauge records in a procedural, objective way.

Model

We use the model described by Kaplan et al. (1997), i.e. minimizing the cost function

$$(\mathbf{H}E\alpha - \mathbf{G})^{\mathrm{T}} \mathbf{R}^{-1} (\mathbf{H}E\alpha - \mathbf{G}) + \alpha^{\mathrm{T}} \Lambda^{-1} \alpha$$

where **E** are the retained eigenfunctions from a calibration period, G are the tide gauge records, **H** an indicator matrix, **R** describes the error covariance, and Λ contains the retained eigenvalues. We solve for α, giving coefficients for the eigenfunctions at each time step.

To capture any overall trend in the data, the eigenfunction basis is augmented with an "EOF0" (a spatially uniform pattern).

As in Church et al. (2004), we use first differences of the tide gauge time series, avoiding the need for a consistent vertical datum for the tide gauges, something that is hard to provide in the Arctic.

Data

For this reconstruction, only PSMSL tide gauges above 68°N have been included. The differenced time series have had glacial isostatic adjustment (GIA) relative sea level predictions (Peltier ICE-5G) removed. The time series do not have inverse barometric (IB) correction applied in this case. All data are pre-processed to remove a constant term, a 12-month oscillation and a 6-month oscillation.

Only tide gauges with more than 5 years of data are included. At any point in time, the solution is enforced by the gauges with available data; this varies from 13 to 69 gauges over the record considered (out of the 106 gauges located at above 68°N). We reconstruct the period 1950–2010 as this is the only period where a reasonable amount of tide gauge data seems available. The calibration sea-level dataset is from the Drakkar ocean model (Barnier et al., 2006); it is intended to replace this with satellite altimetry in the long run.
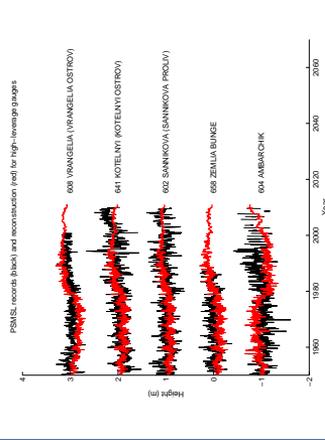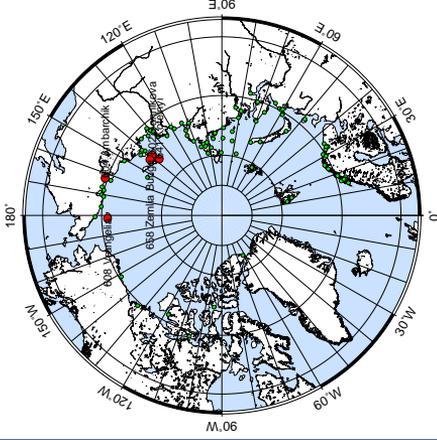
Reconstruction
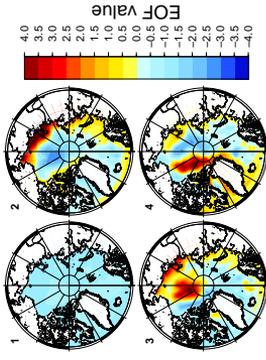
EOF1 is clearly near-uniform, and therefore the augmentation with "EOF0" may thus be superfluous; the corresponding solution time series are also virtually identical.

Time series of EOFs

Reconstructed Arctic MSL
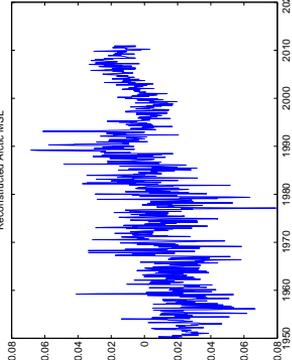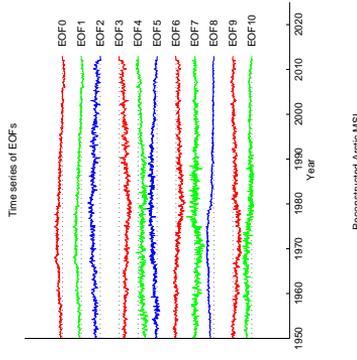
Reconstructed mean sea level for the entire Arctic Ocean above 68°N, using only tide gauges above 68°N, yielding a trend of approx. 0.8 to 1 mm/yr for the entire period. From 1995 to 2010, we obtain > 3 mm/yr.

Leverages

Among the tide gauges above 68°N (green), our analysis identifies five gauges (red) as having a leverage more than three times the mean leverage of all gauges.

The three gauges exhibit some of the highest leverages, statistically suggesting a large influence on the reconstruction. This may suggest removal could be appropriate, though they could also represent an important subpattern in the data. In this case, it seems that the high-leverage gauges may be singled out due to being the primary driver of the positive MSL trend. Some of the reconstructed time series have rather sudden vertical shifts, or the EOFs may not correspond very well with the tide gauge records, which could also play a role.

Conclusions

The reconstructed development in Arctic mean sea level (above 68°N) shows an increasing trend of about 0.9 mm/yr for the 1950–2010 period. Although this is somewhat lower coastal MSL findings by Henry et al. (2012) (1.6 ± 0.11 mm/yr for the Norwegian and Russian sectors), the qualitative development is very similar, with a positive trend of about 4 mm/yr between 1998 and 2010. Also, the lack of IB correction in our reconstruction (on the order of 0.3 mm/yr) may affect the results. While leverage is often used to identify dubious observations and outliers, in this case they might indicate appropriately influential gauges; by far the most variance in the area is explained by the uniform EOF0 and the practically uniform EOF1, and forcing these will introduce large changes to the reconstruction.

References

- Barnier B., G. Madec, T. Penduff, J.-M. Molines, A.-M. Treguier, J. Le Sommer, A. Beckmann, A. Biastoch, C. Böning, J. Dengg, C. Derval, E. Durand, S. Gulev, E. Remy, C. Talandier, S. Theetten, M. Maltrud, J. McClean, and B. De Cuevas (2006). Impact of partial steps and momentum advection schemes in a global ocean circulation model at eddy permitting resolution. Ocean Dynamics, Vol 4, DOI 10.1007/s10236-006-0082-1.
- Church, J., White, N., Coleman, R., Lambeck, K. and Mitrovica, J. (2004). Estimates of the regional distribution of sea level rise over the 1950–2000 period. Journal of Climate, Volume 17, Issue 13, pp. 2609–2625.
- Henry, O., Prandi, P., Llovel, W., Cazenave, A., Jevrejeva, S., Stammer, D., Meyssignac, B. and Koldunov, N. (2012). Tide gauge-based sea level variations since 1950 along the Norwegian and Russian coasts of the Arctic Ocean: Contribution of steric and mass components. Journal of Geophysical Research, Volume 117, C06023.
- Kaplan, A., Kushni, Y., Cane, M.A. and Blumenthal, M.B. (1997). Reduced space optimal analysis for historical data sets: 136 years of Atlantic sea surface temperatures. Journal of Geophysical Research, Volume 102, Issue C13, pp. 27,835–27,860.
- Nielsen, A.A. (2013). Least Squares Adjustment: Linear and Nonlinear Weighted Regression Analysis. Lecture note.
- Peltier, W.R. (2004). Global glacial isostasy and the surface of the ice-age Earth: The ICE-5G (VM2) model and GRACE. Annual Review of Earth and Planetary Sciences, Volume 32, pp. 111-149.
- Switzer, P. and Green, A.A. (1984). Min/max autocorrelation factors for multivariate spatial imagery. Technical report no. 6, Department of Statistics, Stanford University.

A.9   Influence analysis of Arctic tide gauges using leverages

Poster presented at EGU General Assembly 2014, Vienna, Austria.

Influence analysis of Arctic tide gauges using leverages

Peter Limkilde Svendsen[1], Ole Baltazar Andersen[1] and Allan Aasbjerg Nielsen[2]

plsv@space.dtu.dk, oa@space.dtu.dk, alan@dtu.dk | [1]DTU Space, [2]DTU Compute | Technical University of Denmark, Kgs. Lyngby, Denmark

INTRODUCTION

Reconstruction of sea level in the Arctic Ocean is a major challenge, owing to the sparsity of data available. To obtain a reconstruction covering 1950 to today, we adapt the EOF-based model by Church et al. (2004), using a calibration period based on the Drakkar ocean model (as a surrogate for satellite altimetry, using only data from the altimetry era), and using PSMSL tide gauge records to force the model.

The *leverage* of each tide gauge is a statistical measure of its influence on the result. This way, we can readily identify possible outliers among the tide gauge records in a procedural, objective way.
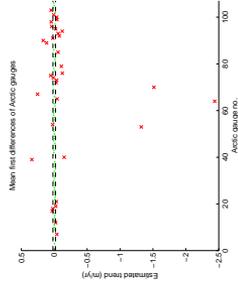
MODEL

We adapt the model by Church et al. (2004), which is in turn based on the model described by Kaplan et al. (1997), i.e. minimizing the cost function.

$$(\mathbf{H}\mathbf{E}\alpha - \mathbf{G})^{\mathsf{T}} \mathbf{R}^{-1} (\mathbf{H}\mathbf{E}\alpha - \mathbf{G}) + \alpha^{\mathsf{T}} \Lambda^{-1} \alpha$$

where $\mathbf{E}$ are the retained eigenfunctions from a calibration period, $\mathbf{G}$ are the tide gauge records, $\mathbf{H}$ an indicator matrix, $\mathbf{R}$ describes the error covariance, and Λ contains the retained eigenvalues. We solve for α, giving coefficients for the eigenfunctions at each time step. To capture any overall trend in the data, the eigenfunction basis is augmented with an "EOF0" (a spatially uniform pattern).
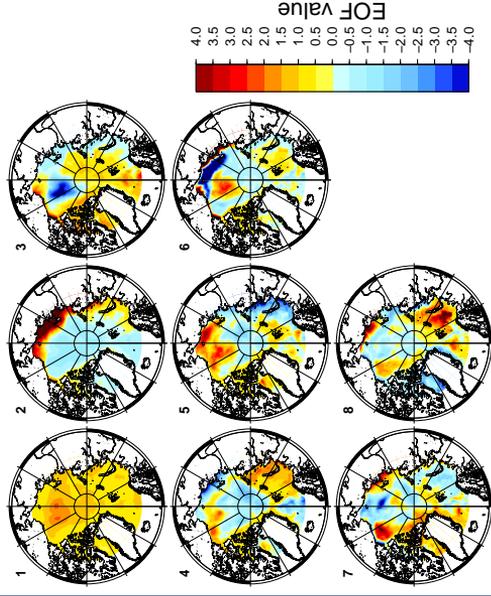
DATA

- Only data above 68°N
- Monthly Drakkar ocean model data (sea level height, monthly, 1993–2007)
- Monthly PSMSL tide gauge data (monthly, 1950–2010)
- GIA and IB corrections applied to tide gauge data (Peltier ICE-5G and HadSLP2, respectively)
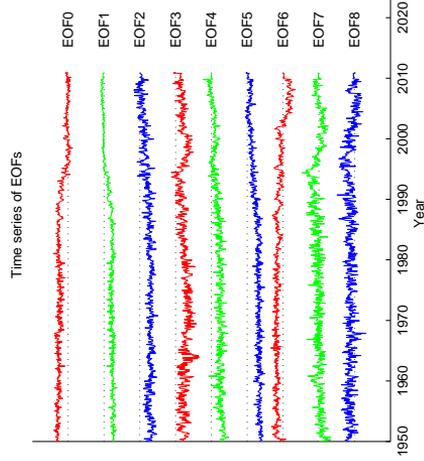
In order to obtain a good reconstruction, we find that it is crucial to perform an empirical pre-culling (based on rough trend estimates) of the gauges.
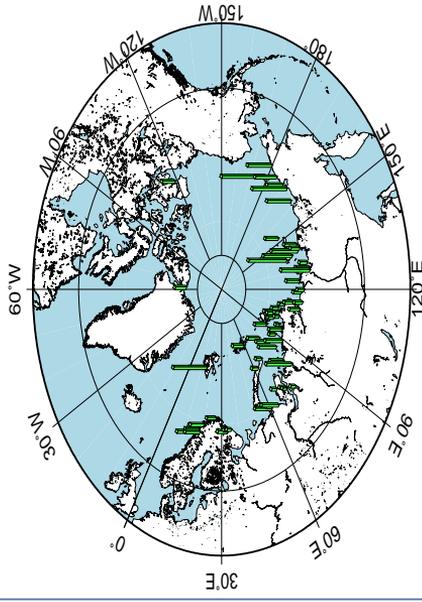

Mean first differences of Arctic gauges

EOFs

EOF value

Time series of EOFs

Note the near-uniform appearance of "EOF0" may thus be superfluous; the corresponding solution time series are also strongly correlated.
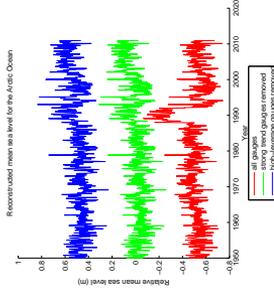
LEVERAGES

The computed leverages are illustrated in the figure below. Highly influential gauges can be identified using empirical criteria, e.g. more than three times the mean of all leverages.

Of the tide gauges above 68°N, we identify two gauges in the Russian sector as having particularly high leverage and omit them from the reconstruction.

The reconstructed mean sea level with all Arctic gauges, all gauges surviving empirical pre-culling, and those additionally having "moderate" leverage is shown on the right.

Reconstructed mean sea level for the Arctic Ocean

CONCLUSIONS

- Leverage useful to indicate trend mismatches (GIA inaccuracies?)
- Reasonable agreement with other sea level studies of the area

A.10 Analysis and robustness of Arctic sea level reconstructions

Poster presented at AGU Fall Meeting 2014, San Francisco, United States.

Analysis and robustness of Arctic sea level reconstructions

Abstract ID: 22237 | Peter Limkilde Svendsen[1], Ole Baltazar Andersen[1] and Allan Aasbjerg Nielsen[2]
plsv@space.dtu.dk, oa@space.dtu.dk, alan@dtu.dk | [1]DTU Space, [2]DTU Compute | Technical University of Denmark, Kgs. Lyngby, Denmark

Introduction

Reconstruction of sea level in the Arctic Ocean is a major challenge, owing to the sparsity of data available. To obtain a reconstruction covering 1950 to today, we adapt the EOF-based model by Church et al. (2004), using a calibration period based on the Drakkar ocean model (as a surrogate for satellite altimetry, using only data from the altimetry era), and using PSMSL tide gauge records to force the model.

The *leverage* of each tide gauge is a statistical measure of its influence on the result. This way, we can readily identify possible outliers among the tide gauge records in a procedural, objective way.

Model

We adapt the model by Church et al. (2004), which is in turn based on the model described by Kaplan et al. (1997), i.e. minimizing the cost function.
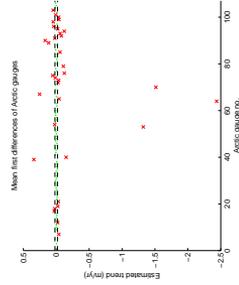
$$(\mathbf{H}\mathbf{E}\alpha - \mathbf{G})^{\mathrm{T}} \mathbf{R}^{-1} (\mathbf{H}\mathbf{E}\alpha - \mathbf{G}) + \alpha^{\mathrm{T}} \Lambda^{-1} \alpha$$

where $\mathbf{E}$ are the retained eigenfunctions from a calibration period, $\mathbf{G}$ are the tide gauge records, $\mathbf{H}$ an indicator matrix, $\mathbf{R}$ describes the error covariance, and Λ contains the retained eigenvalues. We solve for α, giving coefficients for the eigenfunctions at each time step. To capture any overall trend in the data, the eigenfunction basis is augmented with an "EOF0" (a spatially uniform pattern).
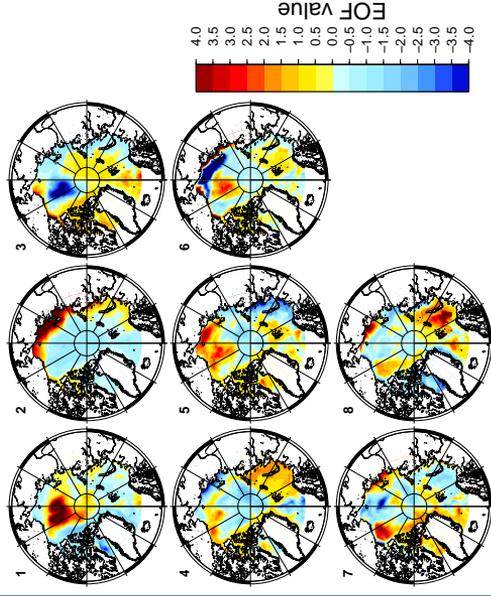
Data

- Only data above 68°N
- Monthly Drakkar ocean model data (sea level height, monthly, 1993–2007)
- Monthly PSMSL tide gauge data (monthly, 1950–2010)
- GIA and IB corrections applied to tide gauge data (Peltier ICE-5G and HadSLP2, respectively)

In order to obtain a good reconstruction, we find that it is crucial to perform an empirical pre-culling (based on rough trend estimates) of the gauges.
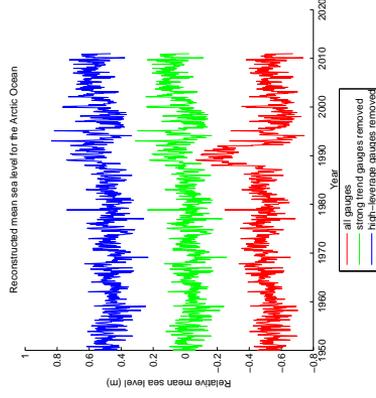
EOFs

Leverages

The computed leverages are illustrated in the figure below. Highly influential gauges can be identified using empirical criteria, e.g. more than three times the mean of all leverages.

Of the tide gauges above 68°N, we identify two gauges in the Russian sector as having particularly high leverage and omit them from the reconstruction.

As an alternative to cumulated differences, one can solve for the tide gauge datums and use the original tide gauge series as in Ray and Douglas (2011). This generally gives a robust reconstruction, though the sea level rise in the Beaufort Gyre still needs additional tweaks to be captured.
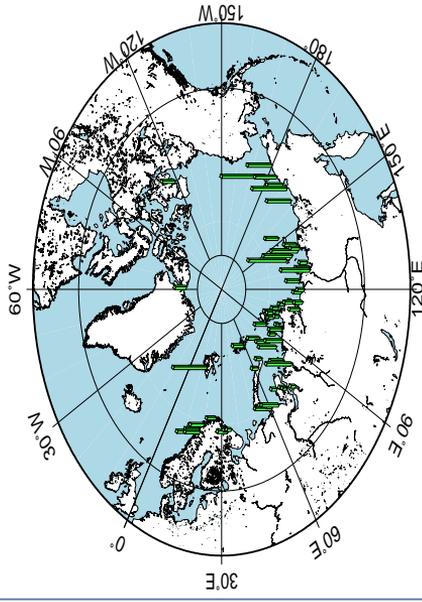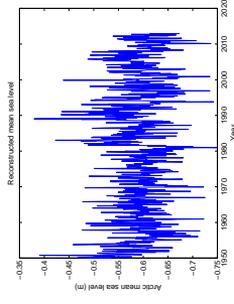
The EOF patterns are dominated by a strong sea level rise in the Beaufort Gyre area, which is difficult to control using only gauges located on the coastlines.

The reconstructed mean sea level with all Arctic gauges, all gauges surviving empirical pre-culling, and those additionally having "moderate" leverage is shown on the right.

Conclusions

- Leverage useful to indicate trend mismatches (GIA inaccuracies?)
- Reasonable agreement with other sea level studies of the area
- Difficult to capture changes in Beaufort Gyre

A.11 Statistical selection of tide gauges for Arctic sea level reconstruction

The paper "Statistical selection of tide gauges for Arctic sea level reconstruction" was published in *Advances in Space Research* in 2015.

Statistical selection of tide gauges for Arctic sea-level reconstruction

Peter Limkilde Svendsen [a,*], Ole Baltazar Andersen [a], Allan Aasbjerg Nielsen [b]

[a] *DTU Space, Technical University of Denmark, Elektrovej 328, 2800 Kgs. Lyngby, Denmark*
[b] *DTU Compute, Technical University of Denmark, Richard Petersens Plads 324, 2800 Kgs. Lyngby, Denmark*

Abstract

In this paper, we seek an appropriate selection of tide gauges for Arctic Ocean sea-level reconstruction based on a combination of empirical criteria and statistical properties (leverages). Tide gauges provide the only in situ observations of sea level prior to the altimetry era. However, tide gauges are sparse, of questionable quality, and occasionally contradictory in their sea-level estimates. Therefore, it is essential to select the gauges very carefully.

In this study, we have established a reconstruction based on empirical orthogonal functions (EOFs) of sea-level variations for the period 1950–2010 for the Arctic Ocean, constrained by tide gauge records, using the basic approach of Church et al. (2004). A major challenge is the sparsity of both satellite and tide gauge data beyond what can be covered with interpolation, necessitating a time-variable selection of tide gauges and the use of an ocean circulation model to provide gridded time series of sea level. As a surrogate for satellite altimetry, we have used the Drakkar ocean model to yield the EOFs.

We initially evaluate the tide gauges through empirical criteria to reject obvious outlier gauges. Subsequently, we evaluate the "influence" of each Arctic tide gauge on the EOF-based reconstruction through the use of statistical leverage and use this as an indication in selecting appropriate tide gauges, in order to procedurally identify poor-quality data while still including as much data as possible.

To accommodate sparse or contradictory tide gauge data, careful preprocessing and regularization of the reconstruction model are found to make a substantial difference to the quality of the reconstruction and the ability to select appropriate tide gauges for a reliable reconstruction. This is an especially important consideration for the Arctic, given the limited amount of data available. Thus, such a tide gauge selection study can be considered a precondition for further studies of Arctic sea-level reconstruction.
© 2015 COSPAR. Published by Elsevier Ltd. All rights reserved.

Keywords: Empirical orthogonal functions; Leverage; Principal component analysis

1. Introduction

Sea-level reconstructions spanning several decades have been examined in numerous studies (Church et al., 2004; Cazenave and Le Cozannet, 2008; Calafat et al., 2014; Jevrejeva et al., 2014), typically where satellite altimetry missions such as TOPEX/Poseidon and Jason-1 and Jason-2 have provided accurate measurements of variability and long-term changes in sea level. However, these dedicated oceanographic missions are limited in coverage to between ±66° latitude, and satellite data at higher latitudes are of a substantially lower quality.

For sea-level reconstructions in the Arctic Ocean region, especially careful consideration needs to be given to data preprocessing, as the tide gauge data available are very limited in extent, both spatially and temporally. We specifically look at the leverage, a statistical property describing the influence upon the solution, of each individual tide gauge. We examine the appropriateness of removing high-leverage gauges (gauges that have the highest influence) from the

* Corresponding author. Tel.: +45 45259742; fax: +45 45259575.
E-mail addresses: plsv@space.dtu.dk (P.L. Svendsen), oa@space.dtu.dk (O.B. Andersen), alan@dtu.dk (A.A. Nielsen).

data, and the qualitative consequences on the reconstruction.

For global sea-level reconstructions, a common procedure is to constrain the reconstruction using a limited number of high-quality gauges, under criteria such as length of time series and geodynamic stability; see, for example, Douglas (1997). To avoid manual editing of the data, and because there are so few gauges to choose from, we seek to establish appropriate criteria for tide gauge inclusion. We consider only per-gauge criteria, not assessment of individual observations.

Achieving full spatial coverage in the reconstruction is typically done by extracting the leading empirical orthogonal functions (EOFs) from an altimetry dataset, which then serves as calibration for the reconstruction. However, as Arctic altimetry data are limited in a spatial extent and has seasonally variable availability, we use data from the Drakkar ocean model (Barnier et al., 2006).

As this paper is intended as a preliminary study towards an altimetry-based reconstruction, we have used only the Drakkar data from within the altimetry era. This has a small effect on the appearance of the EOFs.

We derive and compare three sea-level reconstructions for the Arctic Ocean for the period 1950–2010: one including all available gauges above 68°N with at least 5 years of data in the reconstruction period 1950–2010 (excluding data flagged in the dataset as having poor quality), one with empirically conspicuous (high sea-level trend) gauges removed, and one in which high-leverage gauges are also removed. Additionally, comparison is made with a reconstruction using only a spatially uniform pattern (the "EOF0").

2. Data

The EOFs for the calibration period were obtained from the Drakkar ocean model (Barnier et al., 2006), spanning the period 1958–2007. Prior to EOF computation, the model grids have been spatially and temporally limited so as to only include data above 68°N, and to cover only the period from 1993 (in order to simulate the availability of satellite altimetry). We have chosen the cutoff latitude at 68°N to avoid artifacts from the Baltic Sea.

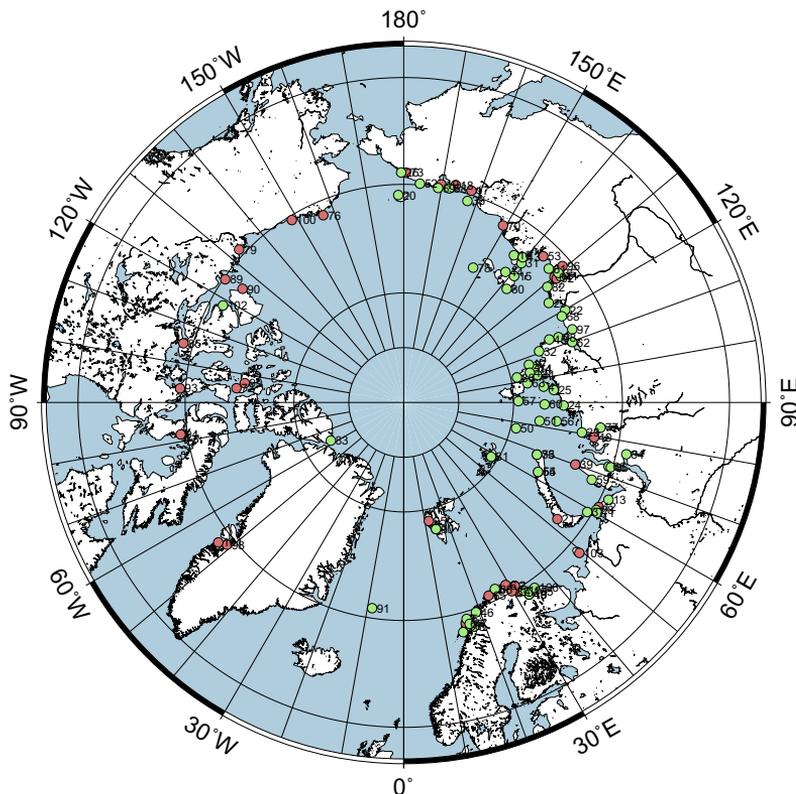

Fig. 1. All 106 PSMSL tide gauges above 68°N. Green dots mark the 69 gauges with at least 5 years of data and trends within ±2 cm/year, while red dots mark rejected gauges. The gauges are labelled with numbers 1–106, a numbering particular to this selection of Arctic gauges.

The reconstruction uses tide gauge data from the Permanent Service for Mean Sea Level (PSMSL) database (Holgate et al., 2012; Permanent Service for Mean Sea Level (PSMSL), 2014). The lengths of PSMSL records in the Arctic are substantially limited compared to those used in global reconstructions. For many gauges along the northern coast of Siberia, there are data records available only in the approximate period 1960–1990, unfortunately precluding an overlap with satellite data that would have aided in setting up and validating our reconstruction.

The PSMSL database contains both "metric-only" and, where a reasonable vertical reference can be determined, "Revised Local Reference" (RLR) records. In some cases, only metric data are available; in the case of the Arctic Ocean, gauges with only metric data are concentrated largely around Greenland and Canada. While great caution is advised when using metric-only data, we do allow it (as in Church et al., 2004) as we use height *changes* (first differences) in the time series. Gauges and observations with quality flags in the PSMSL records have been removed, which should eliminate the most substantial datum shifts.

There are a total of 106 PSMSL gauges above 68° N, the spatial distribution of which is shown in Fig. 1. The number of gauges fulfilling our various inclusion criteria are listed in Table 1. The availability of tide gauge data over time is shown in Fig. 2. It is readily apparent that there is a clear dominance of Russian and Norwegian gauges, and a very substantial loss of Russian gauges around 1990.

Correction for glacial isostatic adjustment (GIA) has been applied to the tide gauge data, using the Peltier dataset with ICE-5G deglaciation history (Peltier, 2004). Using 14 different GIA models, Huang et al., 2013 found a relatively large range of GIA trends for tide gauges, but a relatively small contribution range of between −0.24 and 0.11 mm/year to any potential altimeter-measured sea level between 66°N and 90°N.

Prior to the reconstruction, we apply an inverse barometer (IB) correction to the tide gauge records to make them comparable to the Drakkar data. The pressure data are obtained from the Hadley Centre Sea Level Pressure (HadSLP2) dataset ($5 \times 5°$ monthly grids; Allan and Ansell, 2006) and interpolated to the individual tide gauge locations. The pressure-driven contribution is applied using anomalies from the local pressure mean over the reconstruction period. It should be noted that the HadSLP2 data
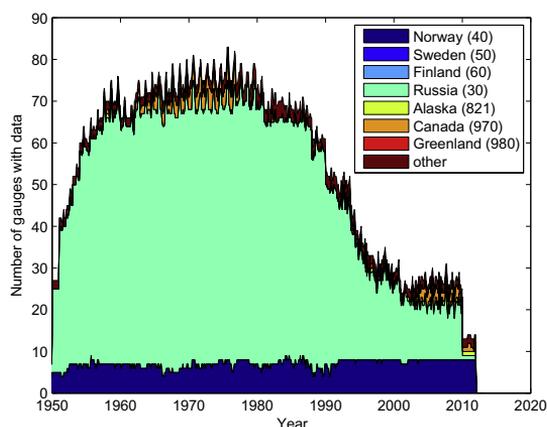

Fig. 2. Availability of data for the gauges above 68°N by coastline. Numbers in parentheses indicate PSMSL coastline IDs.

are themselves based on reduced-space optimal interpolation, and therefore include a substantial amount of reconstructed values.

Some Arctic gauges exhibit extraordinary trends, in some cases 0.5–1 m/year. Regional sea-level trends have been estimated to be in the range of approximately −2 cm/year to +2cm/year (Nerem et al., 2006). Therefore, to ensure basic plausibility, gauges with estimated trends outside a particular range have been removed in preprocessing. Based on the analysis in Section 4.1, we reject gauges with trends larger than ±2 cm/year (after GIA and IB correction). Gauges with <5 years of data available within our reconstruction period are also removed in this
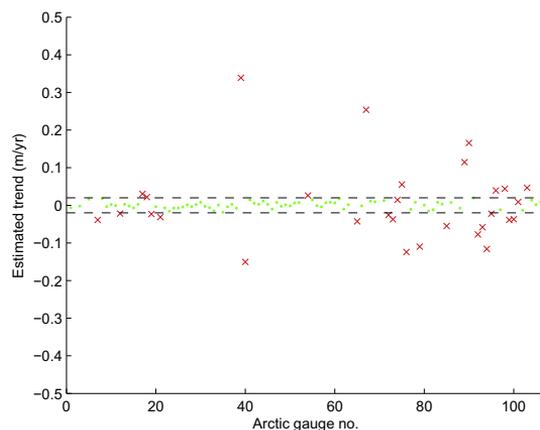

Fig. 3. Trends for each of the 106 Arctic tide gauges. The 69 gauges falling within ±2 cm/year and at least 5 years of data are shown in green, whereas those rejected on either criterion are shown in red. The gauges are numbered 1 through 106 as in Fig. 1. Note that three gauges are outside (below) the vertical range of the plot. (For interpretation of the references to colour in this figure legend, the reader is referred to the web version of this article.)

Table 1
Number of available gauges corresponding to different inclusion criteria.

Inclusion criteria	No. gauges
Above 68°N	106
At least 5 years of data in reconstruction period	90
Trend within ±2 cm/year and ⩾ 5 year data in reconstruction period	69
The above and "moderate" leverage	67

preprocessing. An overview of the trends of the gauges is shown in Fig. 3.

For comparison, Church et al., 2004 removed continuous sections shorter than 2 years and removed gauges deemed unsuitable (such as in estuaries and if contradicting nearby gauges, having noisy time series, or having a residual trend of >1 cm/year). However, for the sparse Arctic data, a fairly inclusive approach is needed.

In a Russian-sector study of tide gauge trends between 1954 and 1989, Proshutinsky et al. (2004) required near-completeness of the time series, allowing a maximum of 10 missing months from each time series in that period. However, we aim to reconstruct the largest spatial and temporal range possible for the Arctic Ocean, rather than achieving great robustness for a particular area.

In establishing a global sea-level reconstruction, Meyssignac et al. (2012) carefully picked 91 gauges across the globe. Those gauges were chosen using more elaborate (and stringent) criteria than have been applied here, including only RLR data, requiring at least 35 years of data in the time series, and omitting outlier gauges based on Rosner's test (Rosner, 1975), which is aimed at detecting outliers even when they may be masked by other outliers.

3. Reconstruction method

The reconstruction is based on the method from Church et al. (2004). That is, the spatial (EOF) patterns from a calibration period are used in conjunction with tide gauge records to yield a reconstruction covering the timespan of the tide gauges. In this case, the EOFs are obtained from Drakkar fields.

With this reconstruction method, the oceans are assumed to have a stationary covariance pattern, derived from the Drakkar model grids. From these, the first few EOFs are determined. The EOFs are amended with a spatially uniform pattern to capture any overall trend; this uniform pattern is commonly known as "EOF0." The first eight EOFs (in addition to the EOF0) are retained in the basis of our reconstruction; see the analysis section. Calafat et al. (2014) argued that regional variability is better captured in global sea-level reconstructions if the EOF0 is omitted; however, we are interested in obtaining MSL trends and therefore include the EOF0.

Both the calibration (Drakkar) and tide gauge data are preprocessed to remove a constant term, as well as whole- and half-year harmonic oscillation. Unlike Church et al. (2004), no trend is removed, as the tide gauge time series are often very short, and any trend should be reasonably captured by the EOF0. The oscillations are then added back to the solution after solving for the EOF coefficients. In order to handle the unknown vertical datum of the tide gauges, first differences of their time series are used (minus the estimated relative sea-level (RSL) contribution from the GIA model), and the subsequent EOF fit temporally cumulated to provide the actual sea-level reconstruction.

To accommodate sparse or contradictory tide gauge data, the problem is regularized as described by Kaplan et al. (2000). This involves damping the influence of EOFs with small corresponding eigenvalues. As EOF0 has no inherent eigenvalue, here, it is assigned the same "eigenvalue" as EOF1. The optimal interpolation requires an error estimate, and a standard deviation of 3 cm on the tide gauge data is assumed in this case. The model lets a gauge enforce the nearest (great-circle distance) pixel in the grid, with a cutoff threshold distance of 500 km. For their global sea-level reconstruction, Church et al. (2004) allowed a maximum of 250 km between the tide gauge and the nearest altimetry grid point.

Our reconstruction uses a time-variable selection of gauges. This causes the reconstruction to be less skillful than with a constant tide gauge selection (Calafat et al. (2014)), but the sparsity of Arctic tide gauge data leaves little choice.

3.1. Optimal interpolation

The reconstruction method in Church et al. (2004) and Christiansen et al. (2010) uses optimal interpolation (OI), minimizing the cost function (in the notation of Christiansen et al. (2010)):

$$(\mathbf{HE\boldsymbol{\alpha}} - \mathbf{G})^{\mathsf{T}}\mathbf{R}^{-1}(\mathbf{HE\boldsymbol{\alpha}} - \mathbf{G}) + \boldsymbol{\alpha}^{\mathsf{T}}\boldsymbol{\Lambda}^{-1}\boldsymbol{\alpha}$$

in which $\mathbf{E}$ is the retained eigenfunctions of the calibration period, $\mathbf{G}$ is the data matrix of tide gauge heights, $\mathbf{H}$ is an indicator matrix for the positions of the tide gauges, $\mathbf{R}$ is the error covariance matrix, $\boldsymbol{\Lambda}$ is the diagonal matrix of retained eigenvalues, and $\boldsymbol{\alpha}$ is the time series (for which we are solving) corresponding to each eigenfunction. The solution for $\boldsymbol{\alpha}$ is then given by

$$\boldsymbol{\alpha} = \mathbf{P}\mathbf{E}^{\mathsf{T}}\mathbf{H}^{\mathsf{T}}\mathbf{R}^{-1}\mathbf{G}$$

with $\mathbf{P} = \left(\mathbf{E}^{\mathsf{T}}\mathbf{H}^{\mathsf{T}}\mathbf{R}^{-1}\mathbf{HE} + \boldsymbol{\Lambda}^{-1}\right)^{-1}$.

3.2. Leverage

A multivariate least-squares regression is described by the equation

$$\mathsf{y} = \mathsf{X}\boldsymbol{\theta} + \mathsf{e}$$

where y is the response variable (here, tide gauge readings), X is our predictor, $\boldsymbol{\theta}$ the model parameters, and e the residuals. We solve for $\boldsymbol{\theta}$. The so-called "hat matrix" relates the y to its estimate, ŷ:

$$\hat{\mathsf{y}} = \mathsf{X}\hat{\boldsymbol{\theta}}_{OLS} = \mathsf{X}(\mathsf{X}^{\mathsf{T}}\mathsf{X})^{-1}\mathsf{X}^{\mathsf{T}}\mathsf{y}$$

The diagonal elements of $\mathsf{X}(\mathsf{X}^{\mathsf{T}}\mathsf{X})^{-1}\mathsf{X}^{\mathsf{T}}$ give the leverages of the respective observations.

For our OI fit, we estimate the leverage as the diagonal elements of the matrix

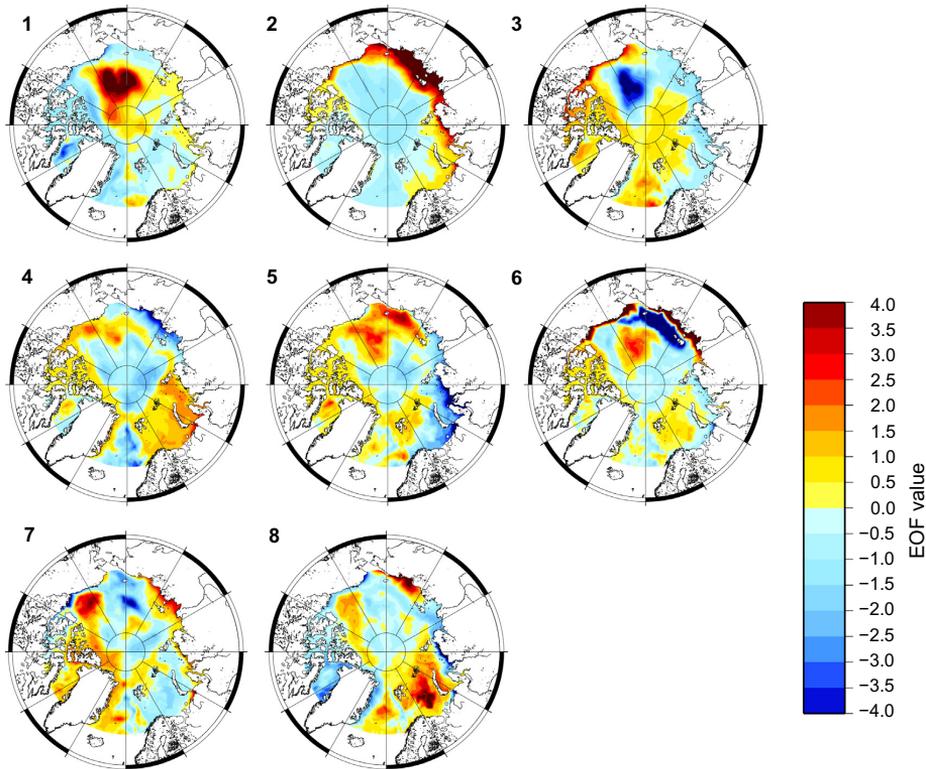$$\mathbf{HEPE}^{\mathsf{T}}\mathbf{H}^{\mathsf{T}}\mathbf{R}^{-1}$$

Fig. 4. The leading eight EOF patterns of the Drakkar data for the period 1993–2007 (arbitrary scaling). Note that the reconstruction includes an additional, uniform pattern, the EOF0.

Unlike in the ordinary least squares (OLS) case, the sum of the leverages will not generally equal the number of parameters. We normalize our leverage values in this case so that the leverage values for each time step sum to the same value. Note that as the normalized leverage for each gauge will vary with time and occasionally be missing (due to missing data), we estimate, for each gauge, a mean value based on the available data.

Systematic deviations from the fit can be identified using residual analysis.

4. Analysis

The leading EOF patterns of the Drakkar data are shown in Fig. 4. The dominant mode of variability (>75% explained variance) is a dipole of deep ocean versus coastal areas north of Siberia, as seen in EOF1. The corresponding time series for the patterns are shown in Fig. 5. The inclusion of eight EOFs (in addition to the EOF0) is chosen so that >95% of the Drakkar variance is explained, but only just (so as to avoid overfitting).

Including only altimetry-era data slightly affects the appearance of the EOFs, in particular the relative dominance of the Beaufort Gyre in EOF1. If using the full
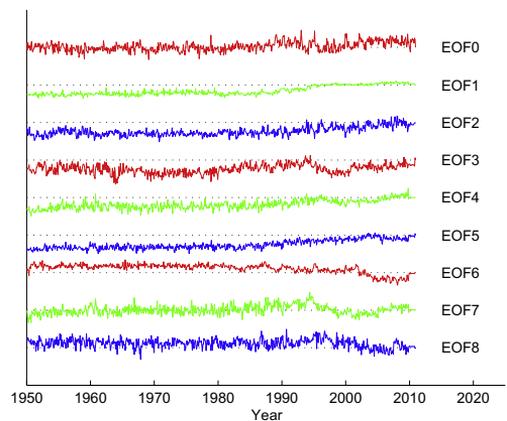

Fig. 5. Time series for the eight EOFs (and EOF0) as determined by the reconstruction including 69 gauges. The vertical scale is normalized to give them identical variance, showing in a qualitative way the nature of temporal variation.

Drakkar dataset (1958–2007), the EOF1 pattern will be more positive in the North Atlantic and the Baffin Bay.

Table 2
Reconstruction MSL trends and number of available gauges corresponding to different inclusion criteria. MSL trends are for the entire reconstruction period, 1950–2010.

Inclusion threshold	MSL trend (mm/year)	MSL trend, EOF0 only (mm/year)	Number of gauges
± 1 cm/year	3.8 ± 0.3	2.3 ± 0.3	49
± 2 cm/year	2.3 ± 0.3	1.0 ± 0.3	69
± 3 cm/year	-1.5 ± 0.4	0.5 ± 0.3	75

The choice not to detrend the calibration data prior to the EOF analysis affects the appearance of the EOFs; the prominent Beaufort Gyre feature in EOF1 is much less apparent in the patterns if the Drakkar data are detrended first, suggesting a fairly clear trend in this area. Apart from this, a Russian-sector coastal feature dominates the variability, whether the data are detrended or not. If detrending is applied, the EOF1 is less dominant, explaining only about 51% of the variance, while the Beaufort Gyre appears mostly in EOF3. This indicates that much of the trend occurs in the pattern described by EOF1.

4.1. Trend threshold for inclusion

As a simple sanity check of the tide gauges, we set a threshold for a tolerable trend in their time series. We compute this trend by taking the mean of the month-to-month differences. Specifically, when the trend threshold is set at ± 2 cm/year (see below for justification), we reject the gauge if the mean value of its month-to-month differences is larger than $\pm \frac{1}{6}$ cm.

The overall characteristic of the reconstructed mean sea level is sensitive to the choice of trend threshold in the pre-processing step, with dramatic consequences if the threshold is set larger than a few centimeters per year. To illustrate, we have performed the reconstruction with gauge mean trend threshold set at 1, 2, and 3 cm/year, respectively. From this, we obtain the number of gauges shown in Table 2, with a corresponding MSL trend for the reconstruction. While the trend is significantly lower with the threshold at $\pm 2 cm/year$ rather than ± 1 cm/year, the overall character of the MSL curve is still retained (see Fig. 6) while including 20 more gauges. Increasing the threshold to ± 3 cm/year introduces large vertical jumps around 1988 and 1992, and strongly disturbs the MSL trend, while only admitting six more gauges. On that basis, we have picked ± 2 cm/year as the threshold that provides the best compromise between including as much data as possible and retaining a stable reconstruction.

Using a simplified reconstruction including only the EOF0 avoids the vertical jumps around 1990 (see Fig. 7) and yields more moderate MSL trends (cf. Table 2). This suggests that the reconstruction is sensitive to the decline in the number of Russian gauges when using the full set of EOFs. Otherwise, the reconstructed MSL exhibits a similar peak in the early 1990s, and a subsequent rise, both with and without EOF1–8.
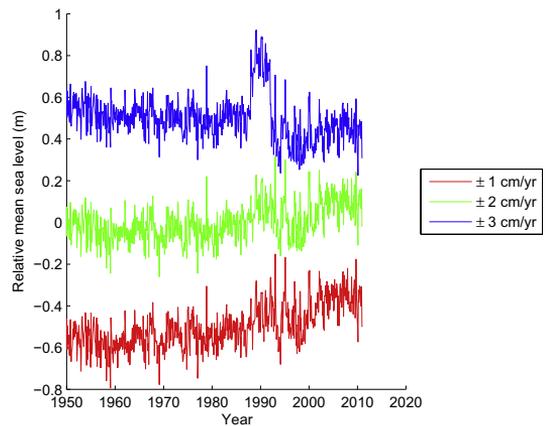

Fig. 6. Reconstructed mean sea level for the entire Arctic (above 68°N), with arbitrary vertical offsets, for different trend thresholds.
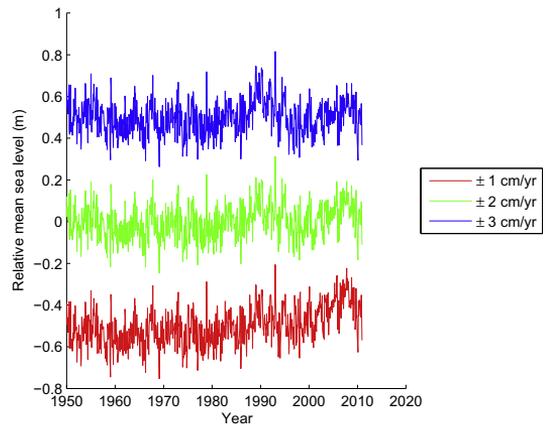

Fig. 7. Reconstructed mean sea level for the entire Arctic (above 68°N), with arbitrary vertical offsets, for different trend thresholds, using only EOF0.

4.2. Identification of influential tide gauges

The mean leverage for each included gauge is visualized in Fig. 8. It is seen that the high-leverage gauges are concentrated largely around the East Siberian Sea, although the Svalbard gauge (Barentsburg) is also estimated to be highly influential. The Barentsburg gauge is relatively geo-
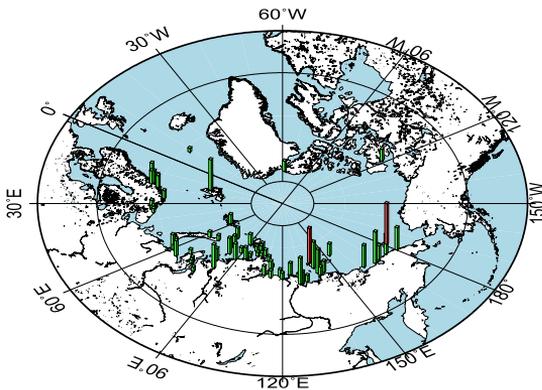
Fig. 8. Mean leverages of included gauges, shown as column height. The two highest-leverage gauges, PSMSL 608 (Vrangelia) and PSMSL 641 (Kotelnyi), are highlighted in red (right and left, respectively).

graphically isolated, and it may simply be an outlier because of that. Therefore, this gauge can be considered for inclusion despite having high leverage.

The leverage values given in this section are the mean leverages for the gauges, scaled so that 1 is equivalent to the mean "mean leverage" across the included gauges. As a rule of thumb, leverages of more than approximately three times the mean of all leverages may be considered suspicious (Nielsen, 2013), although not necessarily inappropriate for inclusion in the reconstruction. The highest and lowest leverage values for the gauges are shown in Tables 3 and 4, respectively.

The reconstructed sea level for the five highest-leverage gauges is shown in Fig. 9. It seems that there is a qualitatively reasonable agreement between the reconstruction and both tide gauge and calibration data; however, a rather large vertical gap seems to develop for the two first stations (Vrangelia and Kotelnyi, PSMSL codes 608 and 641, respectively) around 2000. Therefore, the high leverage could be due to a mismatch in trend between the tide gauge record and the reconstructed sea level at its location, which could possibly be attributed to GIA uncertainties. Based on the appearance of these two time series, and their leverage being around three times the gauge mean or higher (with a small downward jump between these two gauges and that of the third; see Fig. 10), we consider these two gauges to be rejectable. Their geographical locations are highlighted in Fig. 8.

Omission of the two high-leverage gauges very slightly increases the overall MSL trend for the Arctic in the period 1950–2010. However, the resulting trend is 2.3 mm/year, <0.1 mm/year different from a reconstruction with the gauges included, which is not statistically significant (see Table 2).

4.3. Correspondence with previous studies

Examining the Norwegian and Russian sectors from 1950, Henry et al., 2012 found no significant trend in coastal sea level for the period 1950–1980, but an increasing trend since 1980, and a post-1995 trend of approximately 4 mm/year. Our reconstructed (relative)

Table 3
Tide gauges having the highest leverage (strong-trend gauges having been rejected in preprocessing).

Rank	PSMSL ID	Arctic gauge No.	Name	Mean leverage (normalized)
1	608	20	VRANGELIA	3.54
2	641	30	KOTELNYI	3.03
3	730	58	AION	2.74
4	541	9	BARENTSBURG	2.66
5	569	11	TIKSI	2.29
6	602	15	SANNIKOVA	2.28
7	642	31	KIGILIAH	2.09
8	917	77	SOPOCHNAIA KARGA	2.02
9	616	26	MYS SHMIDTA	1.93
10	650	36	CHETYREHSTOLBOVOI	1.90

Table 4
Tide gauges having the lowest leverage (strong-trend gauges having been rejected in preprocessing).

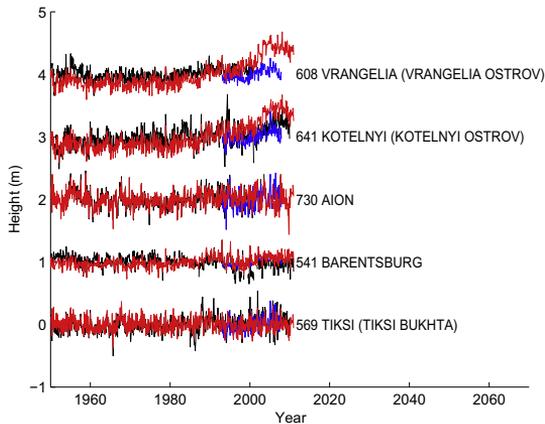| Rank	PSMSL ID	Arctic gauge No.	Name	Mean leverage (normalized)
60	1019	82	SAGYLLAH-ARY	0.36
61	2028	106	TERIBERKA	0.35
62	687	49	MURMANSK II	0.35
63	601	14	FEDOROVA	0.34
64	1200	86	SE-LAHA	0.33
65	1382	91	JAN MAYEN	0.32
66	531	8	EVENSKJAER	0.28
67	655	41	RUSSKII	0.25
68	2026	104	MYS PIKSHUEVA	0.24
69	667	45	MARII PRONCHISHEVOI	0.20

Fig. 9. Measured (black) and reconstructed (red) time series for the highest-leverage gauges, along with the corresponding Drakkar data (blue). (For interpretation of the references to colour in this figure legend, the reader is referred to the web version of this article.)
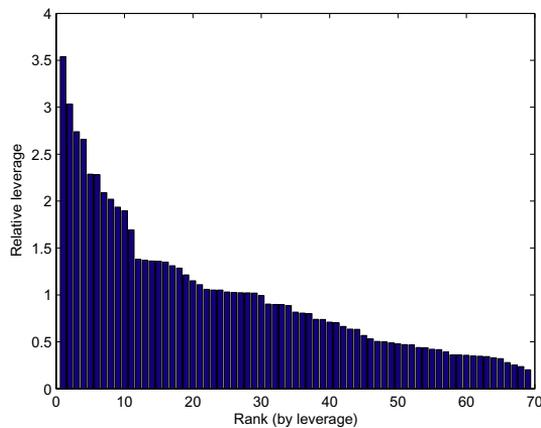

Fig. 10. Leverages of the 69 gauges that fulfil the empirical criteria (see Table 1), sorted by descending leverage.

Fig. 11. Reconstructed mean sea level for the Arctic Ocean (above 68°N), with arbitrary vertical offsets.

Table 5
Mean sea-level trends in the Arctic Ocean for reconstructions based on different selections of tide gauges.

Inclusion criteria	Trend 1950–1980 (mm/year)	Trend 1980–2010 (mm/year)
⩾ 5 years of data in time span	2.7 ± 0.8	−4.6 ± 1.4
Trend within ±2 cm/year and ⩾ 5 year data	−0.5 ± 0.8	4.0 ± 1.0
The above and "moderate" leverage	−0.6 ± 0.8	3.8 ± 1.0

mean sea level for the Arctic Ocean generally shows similar results (see Fig. 11 and Table 5), albeit with substantial high-frequency variation. It is notable that there is a clear, sudden rise around 1990 when including all gauges, which is virtually absent if the ±2 cm/year trend and record length criteria are applied.

Giles et al., 2012 found, using satellite measurements from the period 1995–2010, a distinct increasing trend in freshwater storage (and associated increase in sea surface height of 18.8 ± 0.9 mm/year) in the Western Arctic Ocean around the Beaufort Gyre, starting around 2002. Specifically, the study refers to an area between 180° and 130°W; our resulting trends for the same area are given in Table 6. While simply including all gauges with a reasonable amount of data yields a similar increase in trend around 2002, a sea-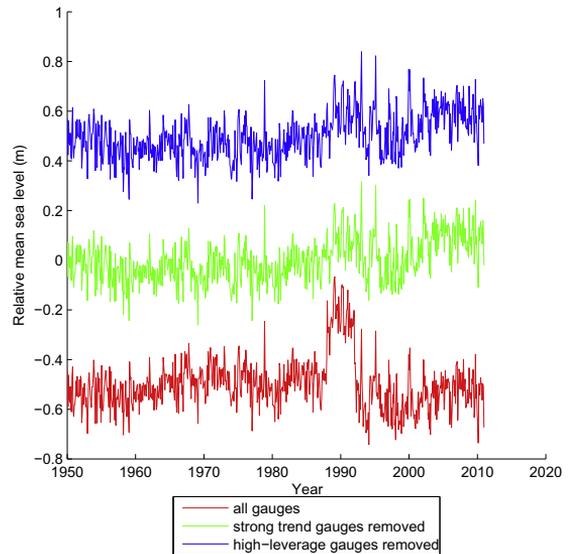level rise is also seen with our other selections of gauges; the increase merely happens earlier. It should be noted that the study by Giles et al. (2012) is based on altimetry, whereas our reconstructions use Drakkar model data and only a single Canadian-sector gauge. Our reconstructed MSL for the area is shown in Fig. 12; note the larger trend in 1950–1970 when empirical removal of gauges is not performed. A large sea-level increase in the Amerasian basin (comprising the Canada and Makarov Basins) in 2003–2009 has also been found by Koldunov et al. (2014).

The complete lack of tide gauge coverage of the deeper parts of the Arctic Ocean represents a major difficulty, and the sea level in the deep basins may not necessarily correlate well with that in shelf areas.

4.4. Correspondence between data and reconstruction

The root-mean-square error (RMSE) between reconstructed and observed sea level at the location of each of the 106 tide gauges above 68°N is shown in Fig. 13 (of which only 69 gauges have been determined as appropriate

Table 6
Mean sea-level trends in Western Arctic Ocean (130° W to 180° W) for reconstructions based on different selections of tide gauges.

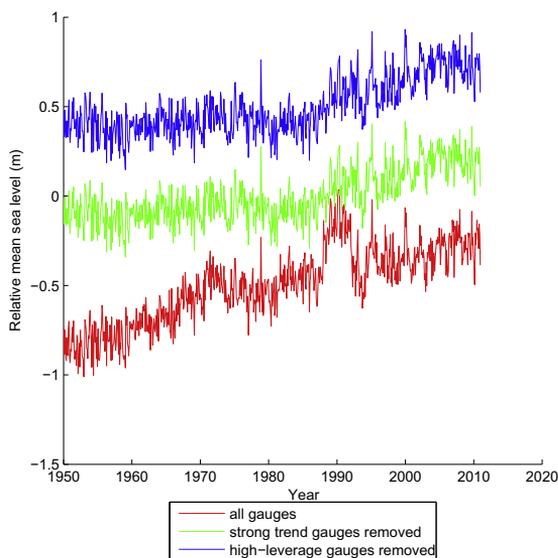| Inclusion criteria	Trend 1950–2010 (mm/year)	Trend 1996–2002 (mm/year)	Trend 2002–2010 (mm/year)
⩾ 5 years of data in time span	10.2 ± 0.5	5.3 ± 10.1	9.8 ± 6.4
Trend within ±2 cm/year and ⩾ 5 year data	5.8 ± 0.4	21.5 ± 10.1	−4.3 ± 5.8
The above and "moderate" leverage	6.5 ± 0.4	23.8 ± 10.1	−4.6 ± 5.8

Fig. 12. Reconstructed mean sea level for the Western Arctic Ocean (longitudes 130°W to 180°W), with arbitrary vertical offsets.
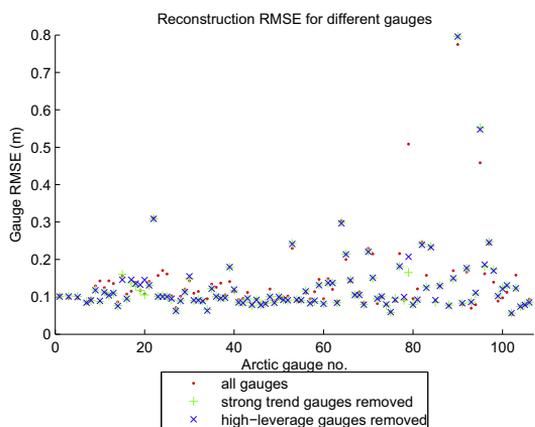

Fig. 13. RMSE for reconstruction versus tide gauge records for reconstructions based on different selections of tide gauges.

Fig. 14. Correlation coefficients for reconstruction versus tide gauge records for reconstructions based on different selections of tide gauges.

for driving the reconstruction). Four of the 106 gauges have insufficient data in the reconstruction period to compute an RMSE relative to the observed data, and the RMSE values are thus computed for only 102 gauges.

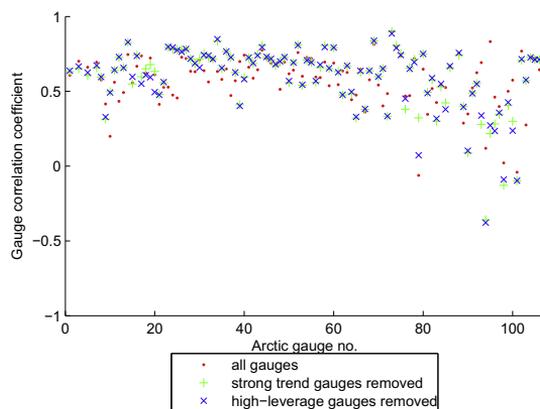The mean RMSE across the 102 Arctic gauges is 0.137 m when all gauges with at least 5 years of data are included, 0.128 m when an empirical gauge removal has been done, and 0.129 m when the two high-leverage gauges are removed. Although the RMSE increases slightly on average by omitting these two gauges, it must be noted that the empirical gauge removal lowers the RMSE for 63 of the 102 gauges, and omitting the two gauges further lowers the RMSE for 60 gauges.

The correlation coefficients for the reconstructed time series versus the recorded time series of the Arctic gauges are shown in Fig. 14. The mean of the correlation coefficients across the gauges is 0.575 when all gauges with enough data, 0.592 when removing high-trend gauges, and 0.588 when removing the two high-leverage gauges.

The fit is slightly poorer on average when omitting the high-leverage gauges. However, removing the high-trend gauges improves correlation for 62 of the 102 gauges and removing the high-leverage gauges further improves it for 61 gauges.

When performing the reconstruction with the high-trend gauges removed, three gauges (1419 Igloolik, 1820 Ilulissat and 1900 Aasiaat) exhibit a negative correlation coefficient; all of these are metric-only gauges.

5. Conclusions

Our reconstruction approach allows tide gauges with substantial gaps in their time series to be used in the reconstruction, in contrast to requiring near-complete records throughout the reconstruction time span. This is an impor-

tant necessary difference with global sea-level reconstructions, where such demands can more easily be made. The reconstruction is very sensitive to tide gauge selection, as small changes to inclusion criteria can result in large changes to reconstructed sea-level trends.

We estimate the overall trend for the Arctic MSL at approximately 2.3 ± 0.3 mm/year for the period 1950–2010, with a post-1980 trend of approximately 3.8 ± 1.0 mm/year. However, these values are highly sensitive to the inclusion criteria applied to the gauges, and also whether the reconstruction is based the full set of EOFs or only the EOF0.

Using only the EOF0 in the reconstruction appears to improve the robustness of the reconstruction. However, much of the expected sea-level rise is confined to the Beaufort Gyre, and inclusion of EOFs to capture this local trend is attractive, assuming it can be adequately controlled. This is a difficult issue as this mode of variability (captured in EOF1) has little expression in the coastal areas where the tide gauges are located.

While the selection of tide gauges seems to be key in providing a good reconstruction, statistical leverage appears useful in identifying outlier gauges, allowing further refinement of the reconstruction. Based on the present study, leverage seems to help in identifying data where trend estimates are inconsistent with the surrounding area, although less useful in identifying poor-quality data. Trend inconsistencies are an important phenomenon in the Arctic, where GIA is generally not well constrained. Removing the high-leverage gauges also results in better correspondence between reconstruction and tide gauge records for the vast majority of tide gauges.

Our reconstruction appears consistent with previous studies, including a distinctive increase in sea-level trend around 1980 as found by Henry et al., 2012, and an increase in sea level for the western Arctic Ocean since the early 1990s as described by Giles et al., 2012, although the timing of the latter is rather dependent on the gauge inclusion criteria.

Acknowledgments

References

Allan, R., Ansell, T., 2006. A new globally complete monthly historical gridded mean sea level pressure dataset (HadSLP2): 1850-2004.

Barnier, B., Madec, G., Penduff, T., Molines, J.-M., Treguier, A.-M., Le Sommer, J., Beckmann, A., Biastoch, A., Boening, C., Dengg, J., Derval, C., Durand, E., Gulev, S., Remy, E., Talandier, C., Theetten, S., Maltrud, M., McClean, J., De Cuevas, B., 2006. Impact of partial steps and momentum advection schemes in a global ocean circulation model at eddy-permitting resolution. Ocean Dyn. 56 (5–6), 543–567.

Calafat, F.M., Chambers, D.P., Tsimplis, M.N., 2014. On the ability of global sea level reconstructions to determine trends and variability. J. Geophys. Res. Oceans 119, 1572–1592. http://dx.doi.org/10.1002/2013JC009298.

Cazenave, A., Le Cozannet, G., 2008. Sea level rise and its coastal impacts. Earth's Future 2 (2), 15–34. http://dx.doi.org/10.1002/2013EF000188.

Christiansen, B., Schmith, T., Thejll, P., 2010. A surrogate ensemble study of sea level reconstructions. J. Clim. 23 (16), 4306–4326.

Church, White, Coleman, Lambeck, Mitrovica, 2004. Estimates of the regional distribution of sea level rise over the 1950-2000 period. J. Clim. 17 (13), 2609–2625.

Douglas, B.C., 1997. Global sea rise: a redetermination. Surv. Geophys. 18 (2–3), 279–292.

Giles, K.A., Laxon, S.W., Ridout, A.L., Wingham, D.J., Bacon, S., 2012. Western arctic ocean freshwater storage increased by wind-driven spin-up of the Beaufort Gyre. Nat. Geosci. 5 (3), 194–197.

Henry, O., Prandi, P., Llovel, W., Cazenave, A., Jevrejeva, S., Stammer, D., Meyssignac, B., Koldunov, N., 2012. Tide gauge-based sea level variations since 1950 along the Norwegian and Russian coasts of the Arctic Ocean: contribution of the steric and mass components. J. Geophys. Res.: Oceans, 117.

Holgate, S.J., Matthews, A., Woodworth, P.L., Rickards, L.J., Tamisiea, M.E., Bradshaw, E., Foden, P.R., Gordon, K.M., Jevrejeva, S., Pugh, J., 2012. New data systems and products at the permanent service for mean sea level. J. Coastal Res. 29 (3), 493.

Huang, Z., Guo, J.-Y., Shum, C.K., Wan, J., Duan, J., Fok, H.S., Kuo, C.-Y., 2013. On the accuracy of glacial isostatic adjustment models for geodetic observations to estimate Arctic Ocean sea-level change. Terr. Atmos. Oceanic Sci. 24 (4), 471–490. http://dx.doi.org/10.3319/TAO.2012.08.28.01(TibXS.

Jevrejeva, S., Moore, J., Grinsted, A., 2014. Trends and acceleration in global and regional sea levels since 1807. Global Planet. Change 113, 11–22.

Kaplan, A., Kushnir, Y., Cane, M.A., 2000. Reduced space optimal interpolation of historical marine sea level pressure: 1854–1992. J. Clim. 13 (16), 2987–3002.

Koldunov, N.V., Serra, N., Köhl, A., Stammer, D., Henry, O., Cazenave, A., Prandi, P., Knudsen, P., Andersen, O.B., Gao, Y., Johannessen, J., 2014. Multimodel simulations of Arctic Ocean sea surface height variability in the period 1970–2009. J. Geophys. Res. Oceans 119. http://dx.doi.org/10.1002/2014JC010170.

Meyssignac, B., Becker, M., Llovel, W., Cazenave, A., 2012. An assessment of two-dimensional past sea level reconstructions over 1950–2009 based on tide-gauge data and different input sea level grids. Surv. Geophys. 33 (5), 945–972. http://dx.doi.org/10.1007/s10712-011-9171-x.

Nerem, R.S., Leuliette, E., Cazenave, A., 2006. Present-day sea-level change: a review. C.R. Geosci. 338 (14–15), 1077–1083. http://dx.doi.org/10.1016/j.crte.2006.09.001.

Nielsen, A.A. (2013). Least squares adjustment: linear and nonlinear weighted regression analysis. Lecture note, pp. 13–14. <http://www2.imm.dtu.dk/pubdb/views/publicationdetails.php?id=2804>

Peltier, W., 2004. Global glacial isostasy and the surface of the ice-age earth: the ICE-5G (VM2) model and GRACE. Annu. Rev. Earth Planet. Sci. 32, 111–149.

Proshutinsky, A., Ashik, I.M., Dvorkin, E.N., Häkkinen, S., Krishfield, R.A., Peltier, W.R., 2004. Secular sea level change in the Russian sector of the Arctic Ocean. J. Geophys. Res. 109, C03042. http://dx.doi.org/10.1029/2003JC002007.

Permanent Service for Mean Sea Level (PSMSL), 2014, Tide Gauge Data, Retrieved 27 Feb 2013 from <http://www.psmsl.org/data/obtaining/>.

Rosner, B., 1975. On the detection of many outliers. Technometrics 17 (2), 221–227.

A.12 60-year Nordic and Arctic sea level reconstruction based on a reprocessed two-decade altimetric sea-level record and tide gauges

Poster presented at EGU General Assembly 2014, Vienna, Austria.

60-year Nordic and Arctic sea level reconstruction based on a reprocessed two-decade altimetric sea-level record and tide gauges

Peter Limkilde Svendsen[1], Ole Baltazar Andersen[1] and Allan Aasbjerg Nielsen[2]

plsv@space.dtu.dk, oa@space.dtu.dk, alan@dtu.dk | [1]DTU Space, [2]DTU Compute | Technical University of Denmark, Kgs. Lyngby, Denmark

Introduction

Due to the sparsity and often poor quality of data, reconstructing Arctic sea level is highly challenging. We present a reconstruction of Arctic sea level covering 1950 to 2010, using the approaches from Church et al. (2004) and Ray and Douglas (2011). This involves decomposition of an altimetry calibration record into EOFs, and fitting these patterns to a historical tide gauge record.

Model

As in Church et al. (2004), we use an EOF decomposition of available altimetry data and minimize the cost function

$$(\mathbf{H}\mathbf{E}\alpha - \mathbf{G})^{\mathsf{T}}\,\mathbf{R}^{-1}\,(\mathbf{H}\mathbf{E}\alpha - \mathbf{G}) + \alpha^{\mathsf{T}}\Lambda^{-1}\alpha$$

where $\mathbf{E}$ are the retained eigenfunctions from a calibration period, $\mathbf{G}$ are the tide gauge records, $\mathbf{H}$ an indicator matrix, $\mathbf{R}$ describes the error covariance, and Λ contains the retained eigenvalues.

We perform the reconstruction using cumulated differences between timesteps as in Church et al. (2004), as well as using the approach from Ray and Douglas (2011), which solves for the vertical datum of each tide gauge as part of the solution. The latter approach handles gaps in data relatively well, without allowing errors to accumulate over time.

Data

- Only data above 68°N
- Monthly DTU altimetry data fields used (ERS-1/2 and Envisat, 1993–2012)
- Monthly PSMSL tide gauge data (1950–2010)
- GIA and IB corrections applied to tide gauge data (Peltier ICE-5G and HadSLP2, respectively)
- Use EOF0 and 8 leading altimetry EOFs (explains ≥ 95% variance)
- Optionally use "virtual tide gauges" (altimetry time series at random locations used as if they were tide gauge data) to help cover post-1990 period

References

- Church, J., White, N., Coleman, R., Lambeck, K. and Mitrovica, J. (2004). Estimates of the regional distribution of sea level rise over the 1950–2000 period. *Journal of Climate*, Volume 17, Issue 13, pp. 2609–2625.
- Ray, R. D., Douglas, B. C., Experiments in reconstructing twentieth-century sea levels, *Progress in Oceanography*, Volume 91, Issue 4, December 2011, pp. 496–515, ISSN 0079-6611, http://dx.doi.org/10.1016/j.pocean.2011.07.021
- Svendsen, P. L., Andersen, O. B., Nielsen, A. A., Statistical selection of tide gauges for Arctic sea-level reconstruction, *Advances in Space Research*, Volume 55, Issue 9, 1 May 2015, Pages 2305-2314, ISSN 0273-1177, http://dx.doi.org/10.1016/j.asr.2015.01.017

Trends

The trend in the reconstruction for the period 1960–2010, using the Ray and Douglas-based reconstruction, appears generally in line with the development in other GMSL reconstructions. There is a particular positive trend in the Beaufort Gyre area and in the East Siberian Sea. The cumulated differences approach yields locally extreme trends due to the patchy coverage of tide gauge data.
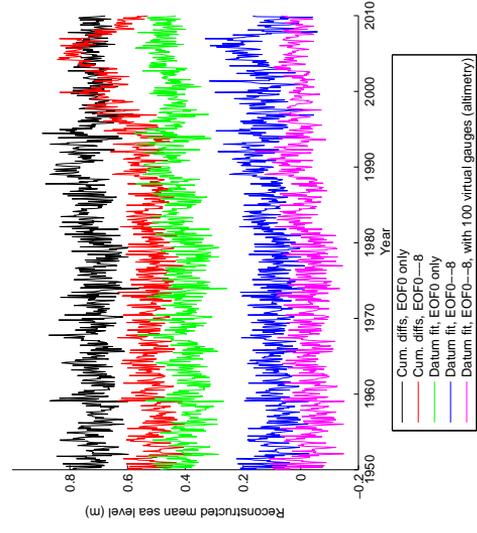

Cumulated differences (Church et al.)
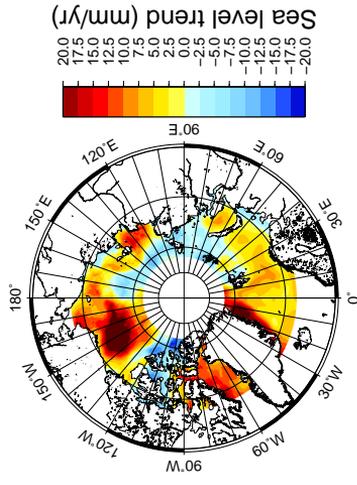
Datum fit (Ray/Douglas)
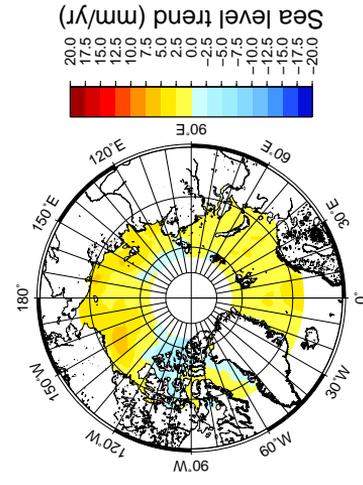
Different reconstructions

The reconstruction can take on a variety of developments depending on the method chosen. The Ray and Douglas approach appears to be generally robust and able to handle the patchy data coverage in the Arctic.

Method	Trend (mm/yr) 1960–2010	Trend (mm/yr) 1995–2010
Cum. diffs, EOF0 only	0.4 ± 0.3	0.9 ± 1.4
Cum. diffs, EOF0–EOF8	4.3 ± 0.4	5.0 ± 2.6
Datum fit, EOF0 only	2.0 ± 0.3	3.7 ± 1.4
Datum fit, EOF0–EOF8	1.5 ± 0.3	2.0 ± 2.4
Datum fit, EOF0–8, 100 virt.	1.5 ± 0.3	1.8 ± 1.1

Conclusions

- Ray and Douglas method (datum fit) appears able to provide a robust basis for Arctic sea-level reconstruction
- Further refinement may be obtained using "virtual tide gauges" in the altimetry era, seems to even out MSL peak in 2004–08
- Trends and characteristics otherwise quite sensitive to method choice
- Beaufort Gyre area variation apparently overestimated when using tide gauge data and EOFs. May be controlled by using only EOF0 or introducing virtual tide gauges.